AD-A125 135 COMPUTATIONAL STUDY OF NONADIABATIC EFFECTS IN ATOM-MOLECULE REACTIVE SCATTERING(U) CHEMICAL DYNAMICS CORP COLUMBUS OH B C GARRETT ET AL. 15 NOV 82 1/2

UNCLASSIFIED AFOSR-TR-83-0002 F49620-81-C-0046 F/G 7/4 NL

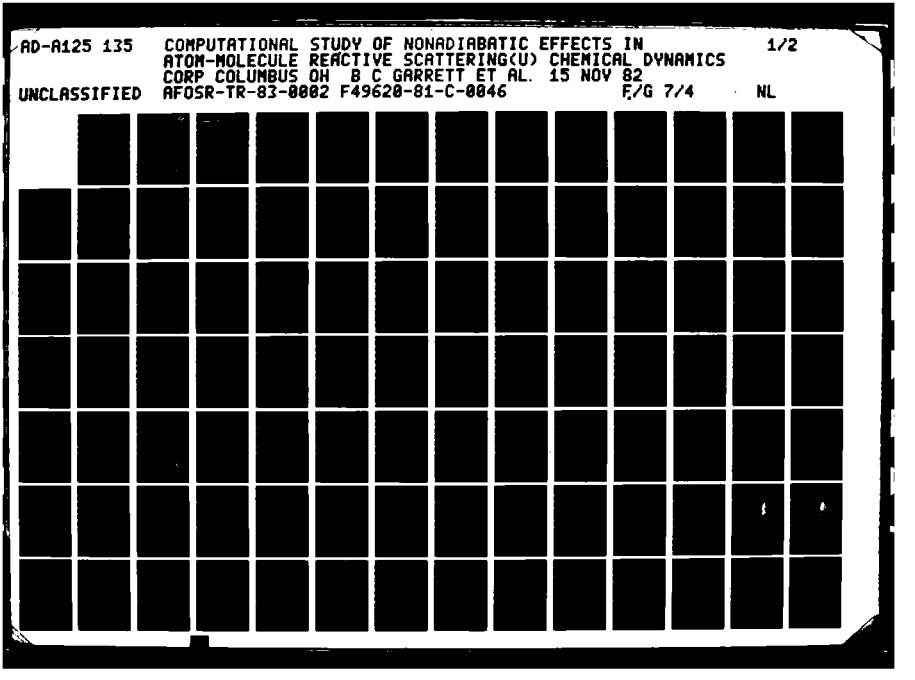

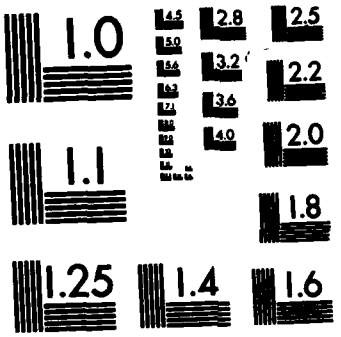

AFOSR-TR- 83-0002

(12)

FINAL TECHNICAL REPORT

AD A125135

COMPUTATIONAL STUDY OF NONADIABATIC EFFECTS IN ATOM-MOLECULE REACTIVE SCATTERING

TO

AIR FORCE OFFICE OF SCIENTIFIC RESEARCH
CONTRACT NO. F49620-81-C-0046

NOVEMBER 15, 1982

DTIC
ELECTE
S MAR 2 1983 D

D

CHEMICAL DYNAMICS CORPORATION
1550 WEST HENDERSON ROAD
COLUMBUS, OH 43220

DTIC FILE COPY

Unclassified

SECURITY CLASSIFICATION OF THIS PAGE (When Data Entered)

REPORT DOCUMENTATION PAGE	READ INSTRUCTIONS BEFORE COMPLETING FORM
1. REPORT NUMBER AFOSR-TR- 83-0002	2. GOVT ACCESSION NO. AD-A125 135
3. RECIPIENT'S CATALOG NUMBER	
4. TITLE (and Subtitle) COMPUTATIONAL STUDY OF NONADIABATIC EFFECTS IN ATOM-MOLECULE REACTIVE SCATTERING	5. TYPE OF REPORT & PERIOD COVERED Final Technical Report
	6. PERFORMING ORG. REPORT NUMBER
7. AUTHOR(s) Dr. Bruce C. Garrett, Dr. Michael J. Redmon, Dr. Lowell D. Thomas	8. CONTRACT OR GRANT NUMBER(s) F49620-81-C-0046
9. PERFORMING ORGANIZATION NAME AND ADDRESS Chemical Dynamics Corporation, 1550 West Henderson Road, Columbus, OH 43220	10. PROGRAM ELEMENT, PROJECT, TASK AREA & WORK UNIT NUMBERS 61102F, 2303/B1
11. CONTROLLING OFFICE NAME AND ADDRESS Air Force Office of Scientific Research/NC, Directorate of Chemical and Atmospheric Sciences, Bolling AFB, DC 20332	12. REPORT DATE 15 Nov 82
	13. NUMBER OF PAGES 119
14. MONITORING AGENCY NAME & ADDRESS(if different from Controlling Office)	15. SECURITY CLASS. (of this report) Unclassified
	15a. DECLASSIFICATION/DOWNGRADING SCHEDULE

16. DISTRIBUTION STATEMENT (of this Report)

Approved for public release - distribution unlimited

17. DISTRIBUTION STATEMENT (of the abstract entered in Block 20, if different from Report)

18. SUPPLEMENTARY NOTES

The views and conclusions contained in this document are those of the authors and should not be interpreted as necessarily representing the official policies and endorsement, either expressed or implied, of the Air Force Office of Scientific Research of the US Government.

19. KEY WORDS (Continue on reverse side if necessary and identify by block number)

quantum mechanics	chemical reactions	potential energy surfaces
scattering theory	combustion	plume technology
chemical dynamics	chemical lasers	gas dynamics
kinetics	state-to-state chemistry	finite element method
nonadiabatic	electronic transitions	decoupling approximations

20. ABSTRACT (Continue on reverse side if necessary and identify by block number)

This report describes an eighteen month research program designed to develop theoretical methods for studying nonadiabatic effects in atom-diatomic molecule collisions. A method for computing accurate three-dimensional reactive scattering wavefunctions has been developed. A method for including several electronic states in a molecular scattering calculation has been implemented. An iterative formulation of the exchange kernal approach to reactive scattering has been examined, and is found to have features that warrant its development for problems involving large numbers of coupled

DD FORM 1 JAN 73 1473

Unclassified

SECURITY CLASSIFICATION OF THIS PAGE (When Data Entered)

equations. A version of the method incorporating finite element techniques has been programmed and preliminary testing has begun on HF-HF self-relaxation. The current code needs refinement and is presently not programmed to allow for reaction. It is anticipated that this approach will allow treatment of several thousand coupled equations on the new generation of supercomputers.

Applications of these numerical methods are being made to several molecular systems, including collisions of atomic sodium, oxygen and fluorine with molecular hydrogen. Angular distributions have been obtained for the fluorine-hydrogen reaction. Quenching probabilities for sodium by hydrogen are providing information on electronic to vibrational energy transfer. Analysis of reactive scattering wavefunctions provides a method for analyzing energy flow during a chemical reaction.

TABLE OF CONTENTS

FINAL TECHNICAL REPORT

on

Contract No. F49620-81-C-0046

COMPUTATIONAL STUDY OF NONADIABATIC EFFECTS
IN ATOM-MOLECULE REACTIVE SCATTERING

to

AIR FORCE OFFICE OF SCIENTIFIC RESEARCH

NOVEMBER 15, 1982

I. STATEMENT OF WORK

Conduct a theoretical research program to develop quantum mechanical methods for studying nonadiabatic effects in three-dimensional atom-molecule interactive collisions.

II. TECHNICAL DISCUSSION

The traditional role of theory in chemistry has been to develop models that help to correlate large amounts of experimental data. However, because of the difficulty in obtaining state-to-state data on many systems, there is growing interest in using the computational methods of ab initio theoretical chemistry to predict kinetic data. Due to the increase in sophistication and accuracy of the computational methods available for calculating potential surfaces and obtaining dynamical information, theoretical studies specifically designed to predict kinetic data are appearing.[1]

Many areas of military technology are affected by the new developments in both experimental and theoretical kinetics. The collisional mechanisms of importance in chemical lasers include the conversion of vibrational energy into rotational energy (V-RT), conversion of rotational energy into translational energy (R-RT), exchange of vibrational energy (V-V), intramolecular conversion of rotational energy into vibrational energy (R-V),

translational to internal energy conversion (T-RV), and the conversion of electronic energy to vibrational, rotational, and translational energy (E-VRT). Also of importance is the transfer of electronic energy from one species to another. For example, the transfer of electronic energy from $O_2(^1\Delta)$ to atomic and molecular iodine is important in iodine lasers. In interhalogen lasers such as IF the production of electronically excited IF from F, I_2, and $O_2(^1\Delta)$ is poorly understood.

In the area of plume technology, an important problem is the prediction of the radiant intensity of rocket exhaust plumes in the upper atmosphere. These plume signatures are driven by collisional excitation of exhaust gas molecules by ambient atmospheric species, and standard models that predict plume radiation require state-to-state cross sections for collisional excitation[2] as input. The necessary cross-sections potentially involve all of the energetic processes which are also of importance in chemical lasers. Theoretical methods provide a cost effective and timely means of obtaining data of this type. For systems which are inaccessible to current experimental techniques, theoretical methods provide a complementary tool to the experimental determination of kinetic data.

The dynamical method most widely used for studies of complex systems is the quasiclassical trajectory method.[3] However, many phenomena cannot be accurately described by a classical approach, and quantal methods are required. Present quantum theoretical methods for obtaining transition probabilities are difficult to apply to problems such as the vibrational excitation of HF (or even H_2) because of the large number of internal states that must be included to converge the calculations.[4] There have been several exact close-coupling calculations reported for inelastic collisions involving light three-atom systems at relatively low energies, mostly involving rigid-

rotor models, but exact close-coupling studies of bimolecular reactions have been limited to $H+H_2$. Because of the importance of obtaining quantum mechanical results for collision processes, approximate decoupling methods have been developed.[5,6] Besides greatly enlarging the scope of inelastic quantum mechanical calculations to include vibrational excitation processes, implementation of decoupling methods is allowing three dimensional reactive scattering calculations for systems more complex and of greater interest than $H+H_2$.[7]

One area of current research that has received considerable attention is the development of methods for including electronic degrees of freedom in scattering calculations.[8] The usual difficulties of the coupled channel approach are magnified not only because of the many more states introduced, but due to complicated angular momentum coupling schemes not present in studies on a single adiabatic electronic surface. Thus there are few instances where actual applications to three dimensional atom-molecule systems have been made. Progress in this area will involve improvements in techniques for treating the large number of equations involved, particularly for reactive systems, where the further complications of difficult coordinate systems appear.

This report summarizes the progress at Chemical Dynamics to extend the quantum mechanical approach to molecular dynamics to systems of greater complexity than previously possible. The emphasis is on obtaining detailed information on vibrational and rotational nonadiabatic processes in atom-molecule reactions, and in developing methods for including electronic degrees of freedom in three-dimensional quantum scattering theory.

III. RESEARCH OBJECTIVES

The overall objectives of this research program are as follows:

- Extend current technology to treat the nonreactive, electronically nonadiabatic collisions of an atom with a diatomic molecule. This involves the development of a code for incorporating the appropriate electronic basis sets and decoupling schemes.

- Investigate decoupling approximations suitable for studying vibronic transitions. Such processes are very important in understanding the physical processes occurring in many areas of technology.

- Develop strategies for incorporating electronic angular momentum in molecular collisions.

- Conduct computational applications to the systems $O+H_2$ and $Na+H_2$, and other systems appropriate for the development of the computational methods. The calculations will involve both nonreactive and reactive studies.

- Continue the development of quantum scattering codes to enable more systems of chemical relevance to be amenable to study by quantum mechanical means. This development is an important component of research at Chemical Dynamics, where a major goal is the development of state-of-the-art methods capable of providing the best theoretical data for problems of current interest in chemical kinetics.

In addition to progress in computational techniques, the goals of this program involve furthering our understanding of fundamental processes in molecular collisions, such as resonance phenomena and energy pathways. Recent developments in quantum chemistry permit the calculation of accurate potential energy surfaces for both ground and excited molecular states, and provide new justification for the search for more powerful methods for studying dynamical processes.

IV. RESEARCH ACCOMPLISHMENTS

During this eighteen month research program, there has been progress in several areas. These include the development of a computational method for analyzing three-dimensional reactive scattering wavefunctions as a function of reaction path and for generating wavefunctions of sufficient accuracy to permit the computation of angular distributions for direct comparison with experiment. Applications to the $F+H_2$ reaction are providing new insight into energy disposal during exothermic reactions and into the nature of resonance phenomena (see Appendix A). The quantal angular distributions show features that appear in experimental data, and that are not predicted by classical theoretical methods (see Appendix B). Preliminary close-coupling probabilities have been obtained for this reaction for $J \geq 0$. These results are presently not sufficiently converged, even with the 180 channels so far included, but there is encouraging agreement between these results and the J_z-conserving probabilities that have formed the basis for our previous studies of this system. We should point out that these results, obtained under AFOSR sponsorship, are by far the most sophisticated quantum mechanical studies of chemical reactions to date.

Previous work on this contract included the development of techniques for treating electronic transitions in molecular collisions using both adiabatic and diabatic representations.[9] These new methods have been applied to the problem of the quenching of the resonance state of potassium by hydrogen and muonium.[9,10] Muonium (Mu) is an electron-muon pair which behaves as a light isotope of hydrogen. Because of the extremely light mass of muonium (one-ninth that of hydrogen) the validity of the Born-Oppenheimer adiabatic separation of nuclear and electronic motion has been questioned.[11] The comparison of cross sections for the quenching of K by H and Mu has given insight into the applicability of the Born-Oppenheimer approximation in systems containing Mu.

Work is currently in progress to examine the rich resonance features in this relatively simple atom-atom collision. Plots of the cross sections versus translational energy for the K + Mu collision show sharp peaks which are attributed to shape type resonances at low translational energies. This characterization of the low energy resonances has been confirmed by showing that the energies at which the resonances occur correspond to quasibound states of the effective potential for the first excited electronic state of KMu. Similar resonance features are expected for the KH system; however, these resonances are expected to be much more narrow because of the heavier mass of hydrogen. Resonances provide a very detailed probe of the potential energy surface. Comparisons of calculations of these types with spectroscopic observations of the resonance states of the "bound" molecule can provided information about the potential curves in regions previously undefined by tools such as RKR analysis.

An improved Diatomics-in-Molecules (DIM) representation for the lowest electronic surfaces of $Na+H_2$ has been obtained for use in scattering calculations.[12,13] These surfaces are being used in our current dynamical studies of this system (see Appendix C).

Significant improvements have been made in the iterative-variational method for heavy particle scattering (see Appendix D).[14] These include the use of finite-element techniques for greatly reducing the amount of I/O required by the previous implementation, and the development of a scheme for allowing for chemical reaction through an efficient implementation of Miller's exchange-kernal formalism.[15,16] To date, development of an inelastic code has been started, with the implementation of the finite element method complete. Implementation of an initial iterative scheme has been completed, and testing on the problem of HF-HF self-relaxation begun but not finished. This development was suspended due to lack of funds. However, we feel that this approach holds

promise for significantly expanding the number of channels that can be included in quantum scattering calculations and warrants further development. It is, in our opinion, the approach most likely to succeed in overcoming the limitation of coupled-channel methods imposed by the mass-dependence of many molecular systems, particularly those with small skew-angles in standard reaction coordinate theories. The current reaction coordinate methods are intractable for molecular systems involving masses other than hydrogen, except in a few cases where decoupling approximations work to an acceptable degree. This computational method, installed on one of the new generation of supercomputers, could open new horizons for accurate computation. With their very large memories and, more importantly for the present application, very rapid and large mass storage, these computers will possess the capacity to apply such algorithms to scattering problems on the order of thousands of channels. This will enable the accurate methods of quantum scattering theory to be applied to situations that are presently tractable only to classical methods.

V. RESEARCH IN PROGRESS

During this program, computational applications to several important collision collision problems, including studies of nonadiabatic processes in $Na+H_2$ collisions have been initiated. These calculations incorporate the Infinite-Order Sudden (IOS) approximation and a new approach to including electronic coupling. This method allows the economical study of electronic-to-vibrational energy processes by eliminating the explicit treatment of rotational degrees of freedom.

Reactive calculations on $O(^3P)+H_2$ are in progress, and, when sufficient computer time is available, converged cross sections will be obtained. This system is of interest because of the previous classical trajectory and transition state theory treatments, the availability of a reasonable ab-initio surface, and the existence of experimental rate data. The present three-dimensional treatment is tractable because of the relatively small endothermicity of the system and the presence of hydrogen atoms in both reagent and product molecules.

Work is also continuing on the problem of obtaining converged close-coupling probabilities for the $F+H_2$ reaction. This is an important problem, for these probabilities are necessary to fully evaluate the reliability of the decoupling methods that are essential for obtaining complete cross sections. As of the present time, we have made close-coupling calculations for $J = 2$ that involve approximately 180 coupled channels. The basis of rotor functions has been varied among the lower vibrational states to study convergence. The results compare reasonably well with the converged J_z-conserving calculations at low energies. The latter include up to 140 channels. The total probability for the process $F+H_2(v=0,j=0) \rightarrow H+FH(v=2,\Sigma j)$ is 0.39 in the J_z-conserving calculation compared with 0.43 in the close-coupling calculation. The close-

coupling result is still unconverged. We are presently in the process of rewriting the scattering code, using a new partitioning of the Hamiltonian, to allow many more channels to be included so that the close-coupling calculations can be converged at least for small J.

VI. SCIENTIFIC PERSONNEL SUPPORTED THIS PERIOD

The following scientists were supported on this contract:

M.J. Redmon

B.C. Garrett

L.D. Thomas

The following scientist supported in part by the prior phase of this research program received a degree during the period of this contract:

J.F. McNutt Ph.D. Univ. of Texas at Austin, 1981

Thesis: Quantum Dynamics of the Three-Dimensional $F+H_2$ reaction: Wavefunction Analysis and Energy Distribution in the Transition State

VII. CURRENT AND PLANNED PUBLICATIONS

1. B. C. Garrett, D. G. Truhlar, and C. F. Melius, "Quenching of the Resonance State of Potassium by Muonium", Phys. Rev. A 24, 2853 (1981).

2. L. D. Thomas, "Solution of the Coupled Equations of Inelastic Atom-Molecule Scattering for a Single Initial State.II. Use of Nondiagonal Matrix Green Functions.", J. Chem. Phys.76, 4925(1982).

3. R. E. Wyatt, J. F. McNutt, and M. J. Redmon, "Analysis of the Resonance in the Three-Dimensional F + H_2 Reaction", Ber. Bunsenges. Phys. Chem. 86, 437(1982).

4. D. G. Truhlar, J. W. Duff, N. C. Blais, J. C. Tully, and B. C. Garrett, "The Quenching of Na(3^2P) by H_2: Interactions and Dynamics", J. Chem. Phys. 77, 764 (1982).

5. J. F. McNutt, R. E. Wyatt, and M. J. Redmon, "Quantum Dynamics of the Three-Dimensional F+H_2 Reaction I. Energy Distribution and Entropy in the Transition State." Submitted to J. Phys. Chem.

6. J. F. McNutt, R. E. Wyatt, and M. J. Redmon, "Quantum Dynamics of the Three-Dimensional F+H_2 Reaction II. Density and Flux Analysis." Submitted to J. Phys. Chem.

7. N. C. Blais, D. G. Truhlar, and B. C. Garrett, "Improved Parameterization of Diatomics-in-Molecules Potential Energy Surface for Na($3p^2P$) + H_2 --> Na($3s^2S$) + H_2", submitted to J. Chem. Phys.

8. R. E. Wyatt and M. J. Redmon, "Quantum Mechanical Differential Reaction Cross Sections for the F+H_2(v=0) --> FH(v'=2)+H Reaction." Submitted to Chem. Phys. Lett.

9. J. F. McNutt, M. J. Redmon, and R. E. Wyatt, "Scattering Matrices for Reactive Three-Body Collisions".

10. B. C. Garrett, M. J. Redmon, and D. G. Truhlar, "The Quenching of Na(3^2P) by H_2: A Quantal IOS Calculation of Electronic-to-Vibrational Energy Transfer".

11. B. C. Garrett, M. J. Redmon, C. W. McCurdy, D. G. Truhlar, and C. F. Melius,"Analysis of the Resonance Structure and Quenching Cross Sections for Collisions of Atomic Potassium with Atomic Hydrogen and Muonium".

12. B. C. Garrett and M. J. Redmon, "Collisional Excitation of HF by O(^3P)".

13. M. J. Redmon, "A Quantal Study of Reactive Scattering for O(^3P) + H_2".

14. M. J. Redmon and B. C. Garrett," A Quantum Mechanical Study of Electronic Quenching of Na(3^2P) by H_2 in The Presence of Reaction".

VIII. INTERACTIONS

A. MEETINGS

The following meetings were attended, providing valuable interaction with other scientists and DoD personnel:

Austin Conference on Theoretical Chemistry, March 1981 (M.J. Redmon and B.C. Garrett)

12th ICPEAC, Gatlinburg, July 1981 (B.C. Garrett)

Gordon Conference on Atomic and Molecular Collisions, Plymouth, N.H., July 1981 (B.C. Garrett).

AFOSR Dynamics Contractors Meeting, Albuquerque, October 1981 (M.J. Redmon)

DoD Plume Visibility Workshop, Huntsville, November 1981 (M.J. Redmon)

AFRPL/AFSD Plume Technology Workshop, Los Angeles, February 1982 (M.J. Redmon)

American Chemical Society Annual Meeting, Las Vegas, Nevada, March 1982 (L.D. Thomas)

Symposium on Theoretical Aspects of Gas Phase Kinetics, University of Reading, England, March 1982 (B.C. Garrett)

Faraday Disussions on Van der Waals Molecules, Oxford, England, April 1982 (B.C. Garrett)

Workshop on the fundamentals of initiation of chemical decomposition of energetic materials, Chester, Maryland, May 1982 (B.C. Garrett)

American Chemical Society Meeting, Kansas City, Missouri, September 1982 (B.C. Garrett)

B. SUPPORT OF OTHER DOD PROGRAMS

The techniques investigated under the current program have application to many areas of DoD interest involving gas-phase chemistry. We have recently received support form the Rocket Propulsion Laboratory at Edwards Air Force Base to study collisional excitation of various high-altitude exhaust gas species by atomic oxygen. The quantum scattering calculations will be performed with methods developed under the current program. The computer codes developed under the current contract are to our knowledge the only existent codes capable of performing these calculations.

We have also submitted a proposal to perform a theoretical study of rotational relaxation in HF-HF collisions, a subject of enormous practical importance to the Air Force HF laser program. This study would involve application of the iterative-variational method in a close-coupling mode for the low-lying v=1 states decaying to the v=0 manifold, with decoupling applied to higher states. There is excellent experimental data available for the low-lying transitions, allowing a validation of the theoretical methods for low v,j states that could then be extrapolated to high v,j states. This extrapolation could provide reliable data for the prediction of parasitic lasing processes that can limit the scaling of high-power lasers.

IX. REFERENCES

1. Potential Energy Surfaces and Dynamics Calculations, D. G. Truhlar, ed., (Plenum, New York, 1981).
2. T. J. Rieger, K. S. Tait, and H. R. Baum, J. Quant. Spectrosc. Radiat. Transfer 15, 1117 (1975).
3. D. G. Truhlar and J. T. Muckerman, in Atom-Molecule Collision Theory, A Guide for the Experimentalist, R. B. Bernstein, ed., (Plenum, New York, 1979).
4. L. D. Thomas, M. H. Alexander, B. R. Johnson, W. A. Lester Jr., J. C. Light, K. D. McLenithan, G. A. Parker, M. J. Redmon, T. G. Schmalz, D. Secrest, and R. B. Walker, J. Comp. Phys. 41, 407 (1981).
5. R. T Pack, J. Chem. Phys. 60, 633 (1974).
6. P. McGuire and D. J. Kouri, J. Chem. Phys. 60, 2488 (1974).
7. M. J. Redmon, Int. J. Quantum Chem. S13, 559 (1979).
8. B. C. Garrett and D. G. Truhlar, in Theoretical Chemistry: Advances and Perspectives, Vol. 6A, edited by D. Henderson (Academic Press, New York, 1981), p. 215.
9. B. C. Garrett, M. J. Redmon, D. G. Truhlar, and C. F. Melius, J. Chem. Phys. 74, 412 (1981).
10. B. C. Garrett, D. G. Truhlar, and C. F. Melius, Phys. Rev. A 24, 2853 (1981).
11. J.N.L. Connor, Hyper. Inter. 8, 434 (1981).
12. D. G. Truhlar, J. W. Duff, N. C. Blais, J. C. Tully, and B. C. Garrett, J. Chem. Phys. 77, 764 (1982).
13. N. C. Blais, D. G. Truhlar, and B. C. Garrett, submitted to J. Chem. Phys.
14. L. D. Thomas, J. Chem. Phys. 70, 2979 (1979).
15. W. H. Miller, J. Chem. Phys. 50, 407 (1969).
16. B. C. Garrett and W. H. Miller, J. Chem. Phys. 68, 4051 (1978).

APPENDIX A

Quantum Dynamics of the Three-Dimensional F+H_2 Reaction I. Energy Partitioning and Entropy Analysis in the Collision Complex

Quantum Dynamics of the Three-Dimensional $F+H_2$ Reaction I. Energy Partitioning and Entropy Analysis in the Collision Complex*

by

Joe F. McNutt# and Robert E. Wyatt
Institute for Theoretical Chemistry
and
Department of Chemistry
University of Texas at Austin
Austin, Texas 78712

and

Michael J. Redmon
Chemical Dynamics Corporation
1550 West Henderson Road
Columbus, Ohio 43220

Abstract

Analysis is presented of the quantum dynamics of the three-dimensional $F+H_2 \rightarrow FH+H$ reaction for total angular momentum J=0. First, the method (coordinates, Hamiltonian, basis sets, close-coupling method, and boundary conditions) of solving the Schrodinger equation is reviewed, with emphasis on numerical construction of the scattering wavefunction in the region of the collision complex. Then, four types of analysis of the collision complex are presented: (1) translational wavefunctions for the dynamically significant channels, (2) vibration-rotation energy partitioning, (3) vibration-rotation entropies, (4) variation with position along the reaction coordinate of the total scattering wavefunction density. Emphasis is placed upon variations in these quantities as the system passes through a quantum resonance (near total energy 0.36 eV). In part II of this series, the total scattering wavefunction density and flux are analyzed in the region of the collision complex.

* Supported in part by grants from the Robert A. Welch Foundation and the National Science Foundation, and by the Air Force Office of Scientific Research, U.S. Air Force (AFSC), under contract No. F49620-81-C-0046.

Current address: Physics Division, Northern Kentucky University, Highland Heights, KY 41076.

Three-dimensional studies of this reaction are necessary to provide a realistic basis for comparison with experiment. Quantum studies using the Born[11], distorted-wave Born[12-14], and infinite-order-sudden[15-17] approximations have generated energy-dependent cross sections and relative probabilities for forming HF products in v′j′ states. Coupled channel studies (within the J_z-conserving approximation) have been presented by Redmon and Wyatt.[18-24] Reaction probability surfaces P(E,J) were obtained in these calculations for populating v′=2 and v′=3 from H_2 in its ground state (v=0,j=0). These probability surfaces were summed over final rotational states, and plotted as functions of total angular momentum J and total system energy E. The v′=2 surface has a maximum near 0.36 eV (for j=0, hence a classical impact parameter of b=0 for j=0). For fixed E below this energy, P(E,J) shows a monotonic decrease with increasing J. However, at energies only slightly above 0.36 eV, a maximum appears in the probability cuts at non-zero J. This maximum appears at increasing values of J as the value of E increases. The locus of these probability maxima forms a three-dimensional "resonance ridge" on the probability surface.[21] In contrast, the v=0 v′=1 and v=0 v′=3 reaction probability surfaces show slow post-threshold growth with maximum reactivity at J=0 for all energies studied (up to 0.5 eV). The shapes of the curves for higher J are similar, but the threshold energies are shifted to higher E. Recently, Bowman, Lee and Ju developed a method for generating three-dimensional probabilities for this reaction from collinear quantum probabilities.[25] These approximate probabilities show features in good agreement with the explicit three-dimensional calculations, and in particular, the presence of the resonance ridge for the v′=2 surface. This feature is completely absent in results obtained within a classical framework.

Quantum Dynamics of the Three-Dimensional $F+H_2$ Reaction I. Energy Partitioning and Entropy Analysis in the Collision Complex*

by

Joe F. McNutt# and Robert E. Wyatt
Institute for Theoretical Chemistry
and
Department of Chemistry
University of Texas at Austin
Austin, Texas 78712

and

Michael J. Redmon
Chemical Dynamics Corporation
1550 West Henderson Road
Columbus, Ohio 43220

Abstract

Analysis is presented of the quantum dynamics of the three-dimensional $F+H_2 \rightarrow FH+H$ reaction for total angular momentum J=0. First, the method (coordinates, Hamiltonian, basis sets, close-coupling method, and boundary conditions) of solving the Schrodinger equation is reviewed, with emphasis on numerical construction of the scattering wavefunction in the region of the collision complex. Then, four types of analysis of the collision complex are presented: (1) translational wavefunctions for the dynamically significant channels, (2) vibration-rotation energy partitioning, (3) vibration-rotation entropies, (4) variation with position along the reaction coordinate of the total scattering wavefunction density. Emphasis is placed upon variations in these quantities as the system passes through a quantum resonance (near total energy 0.36 eV). In part II of this series, the total scattering wavefunction density and flux are analyzed in the region of the collision complex.

* Supported in part by grants from the Robert A. Welch Foundation and the National Science Foundation, and by the Air Force Office of Scientific Research, U.S. Air Force (AFSC), under contract No. F49620-81-C-0046.

Current address: Physics Division, Northern Kentucky University, Highland Heights, KY 41076.

I. INTRODUCTION

During recent years, interest in state-to-state processes involved in elementary chemical reactions has continued to expand, and many new and informative results have appeared. The reaction $F+H_2(v,j)$ $FH(v',j')+H$ has been the reaction of greatest experimental and theoretical effort, primarily because it is a simple reaction with numerous dynamical features that can be studied with reasonable accuracy.[1-3] On the theoretical side, quasiclassical trajectory studies on a variety of potential energy surfaces have generated a wealth of dynamical information.[2,3] Quantum collinear calculations show a number of striking features not predicted by the classical results.[4-6] The quantum v=0 v'=2 reaction probability curve exhibits a sharp resonance peak (0.01 eV half-width) slightly above the threshold for reaction, while the v=0 v'=3 probability curve exhibits slow but monotonic growth after threshold. Subsequent collinear studies substantiate and extend these studies,[7,8] in particular to investigations of the effect of variations in the topology of the potential energy surface on the calculated resonance features.[9]

In a study of the collinear reaction, we graphically displayed the scattering wavefunction, nodal patterns, the scattering probability density, and the flux distribution as functions of the reaction coordinate.[8] In that study, we showed that wells in the adiabatic vibrational correlation curves and the completness of the vibrational basis dramatically influence the resonance shape. Recently, Walker and Hayes[10] have shown that the v=0 v'=2 collinear resonance can be destroyed by removing the entrance channel potential barrier (0.05 eV on the Muckermann surface V). These results illustrate the importance of potential surface features on these resonance effects, and provide a measure of the accuracy desired in <u>ab initio</u> potential energy surfaces.

Three-dimensional studies of this reaction are necessary to provide a realistic basis for comparison with experiment. Quantum studies using the Born[11], distorted-wave Born[12-14], and infinite-order-sudden[15-17] approximations have generated energy-dependent cross sections and relative probabilities for forming HF products in v′j′ states. Coupled channel studies (within the J_z-conserving approximation) have been presented by Redmon and Wyatt.[18-24] Reaction probability surfaces P(E,J) were obtained in these calculations for populating v′=2 and v′=3 from H_2 in its ground state (v=0,j=0). These probability surfaces were summed over final rotational states, and plotted as functions of total angular momentum J and total system energy E. The v′=2 surface has a maximum near 0.36 eV (for j=0, hence a classical impact parameter of b=0 for j=0). For fixed E below this energy, P(E,J) shows a monotonic decrease with increasing J. However, at energies only slightly above 0.36 eV, a maximum appears in the probability cuts at non-zero J. This maximum appears at increasing values of J as the value of E increases. The locus of these probability maxima forms a three-dimensional "resonance ridge" on the probability surface.[21] In contrast, the v=0 v′=1 and v=0 v′=3 reaction probability surfaces show slow post-threshold growth with maximum reactivity at J=0 for all energies studied (up to 0.5 eV). The shapes of the curves for higher J are similar, but the threshold energies are shifted to higher E. Recently, Bowman, Lee and Ju developed a method for generating three-dimensional probabilities for this reaction from collinear quantum probabilities.[25] These approximate probabilities show features in good agreement with the explicit three-dimensional calculations, and in particular, the presence of the resonance ridge for the v′=2 surface. This feature is completely absent in results obtained within a classical framework.

New results from crossed molecular beam experiments carried out at Berkeley,[26] when displayed on polar velocity-angle maps, support the resonance interpretation of the quantum mechanical calculations. At a center-of-mass energy near 0.08 eV, the product intensity for $v'=1,2,3$ maximizes at $\theta = \pi$ (in the direction of the incoming Fluorine atom). However, when the relative energy is increased to 0.12 eV, the $v'=2$ intensity maximizes near $\theta = 100^{o}$, while the $v'=1,3$ components remain predominately backscattered. This sideways peaking corresponds to nonzero impact parameter collisions, and directly correlates with the quantum mechanical prediction that a resonance ridge forms for $J>0$ when the collision energy exceeds about 0.1 eV.

Differential reaction cross sections computed from three-dimensional reactive scattering in the J_z-conserving approximation agree very well[27] with recent high-resolution beam data.[28] However, both the quantum mechanical and experimental results are quite different than the predictions of classical trajectory calculations.[29] Classically, the $v=0$ $v'=2$ differential reaction cross section remains backwards peaked, even up to 0.5 eV total energy.

The work presented in this and the following paper[30] (II) provides the first detailed analysis of the three-dimensional $F+H_2$ reaction in the transition state region. In addition to asymptotic information such as reaction probabilities and cross sections, we examine the total scattering wavefunction and quantities calculated with this wavefunction, as a function of the reaction coordinate. In the present paper, by examining average vibrational and rotational energies, we follow the partitioning of the available energy as the system proceeds from reactants to products. To gain additional insight into the population inversion and resonance phenomena, we present in II an analysis of the scattering wavefunction probability density

and flux at three total energies: 0.33, 0.36, and 0.40 eV.

In the following section we discuss the coordinates, Hamiltonian, and the numerical solution of the coupled equations. In section III, we discuss the method used to construct the three-dimensional scattering wavefunction. In section IV, the methods used to analyze internal energy disposal are presented, and in the final section the insights gained into the fundamental processes that dominate the dynamics of this important reaction are summarized.

II. Formulation of the Reactive Scattering Problem

A. Coordinates

For atom-diatom reactions at subdissociative energies there are three arrangement channels which lead to separated A+BC (channel α), AC+B (product channel β), or AB+C (product channel γ). After removing the center-of-mass motion, two mass-scaled relative separation vectors describe the three-atom configuration in each arrangement channel; for example, in the α-channel:

$$\begin{aligned} R_\alpha &= c_\alpha^{-1}(r_c - (M_a r_a + M_b r_b)/(M_a+M_b)) \\ r_\alpha &= c_\alpha\,(r_b - r_c); \quad c_\alpha = (\mu_{bc}/\mu_{abc})^{\frac{1}{2}} \end{aligned} \tag{1}$$

Similar expressions apply to the other two arrangement channels. In these coordinates a single reduced mass

$$\mu = M_a M_b M_c/(M_a+M_b+M_c) \tag{2}$$

applies to all three arrangement channels. We now introduce a body-fixed frame, in each arrangement channel λ, with axes oriented relative to the space-fixed axes with three Euler angles $(\theta_\lambda,\phi_\lambda,\chi_\lambda)$. The BF frame is chosen so that the BF Z-axis is parallel to R_α for large reactant separations, but changes smoothly during the course of the reaction so that it is parallel to $-R_\beta$ for the product configuration channel β. This reorientation of the BF axes is accomplished with a switching angle $\alpha(s)$ whose value depends upon the extent of the reaction as measured by the reaction coordinate s. In order to specify the instantaneous size and shape of the nuclear triangle within the BF frame, natural collision coordinates (NCC) are used.[31-33] The translational coordinate s varies from $-\infty$ to $+\infty$ as the reaction progresses. In planes of constant s perpendicular to a reference curve (RC), usually taken to be a circular arc in the reaction zone, ρ and γ represent generalized vibrational and bending motion. Asymptotically, ρ and γ

correspond to simple diatomic molecule vibration and rotation. Fig. 1 illustrates the NCC for the α and β channels, and shows a plane of constant s.

Another useful set of orthogonal internal coordinates, (Z,z,m), is constructed in the following manner. By forcing the BF X-axis to be perpendicular to the nuclear plane, $\vec{r}_\alpha$ and $\vec{R}_\beta$ have BF components $(0,y_\alpha,z_\alpha)$ and $(0,Y_\alpha,Z_\alpha)$. Then, by replacing (y_α,Y_α) with polar coordinates (m,α), where $m = r \sin\gamma$, $y = -m\cos\alpha$, and $Y = m\sin\alpha$, we obtain the set (Z,z,m) shown earlier in Fig. 1... The m-axis is perpendicular to the collinear plane (m=0) and measures the deviation of the nuclear triangle from collinearity.

Because H_2 is a homonuclear molecule, only two of the three possible arrangement channels discussed above need be considered. The α and β channels join at s=0 (by definition), forming a surface on which the wavefunction and derivative for reactant and product channels must match.[32] The γ channel must also be considered in completely specifying the boundary conditions, but not in the integration of the coupled equations (for $A+B_2$ systems).

B. Hamiltonian and Wavefunction Expansion

The NCC Hamiltonian operator can be partitioned into operators representing pure translation, vibration, and rotation, plus the remaining coupling terms.[32]

$$\hat{H} = \hat{H}_{tr} + \hat{H}_{vib} + \hat{H}_{rot} + \hat{H}_{coup} \qquad (3)$$

The $\hat{H}_{coup}$ operator includes terms coupling translation, vibration, and rotation which vanish at large s. Many of these terms are small in systems for which the reaction passes through a linear intermediate. These terms are neglected in the present and previous NCC treatments, and this approximation

prevents this approach from consideration as an "exact" method.

In a similar manner, the electronic potential energy is decomposed as

$$V(s,\rho,\gamma) = V_{tr} + V_{vib} + V_{bend} + V_{coup} \quad (4)$$

In this representation, V_{tr} is the translational potential along the locus of local vibrational minima (defined for straight-line cuts perpendicular to the collinear RC), V_{vib} is the local vibrational potential along the cuts, and V_{bend} is the bending potential for variations in γ away from the local vibrational minima along a circular arc of radius r_0 in a plane of constant s (see Fig. 1).

Vibration-rotation coupling is small for points near the RP for the present surface, and has been neglected in our work on the $F+H_2$ system. This coupling could, of course, be included without much difficulty.

The empirical surface V of Muckermann[34] is used in this and our previous studies to obtain the translational and vibrational potentials, with a simple functional form fit to the M5 bending potential for small deviations from linearity. The bending potential is represented with the function

$$V_{bend}(\gamma;s) = (V_0(s)/2)[1 - \cos 2\gamma] \quad (5)$$

where $V_0(s)$ is adjusted to represent the original M5 surface for small deviations from linearity.

The vibrational Hamiltonian is used to construct locally adiabatic vibrational eigenvalues and basis functions:

$$H_{vib}\,\chi_v(\rho;s) = E_v(s)\,\chi_v(\rho;s) \quad (6)$$

The vibrational potential in Eq. 4 is usually fit to a Morse potential so that the basis functions $\chi_v(\rho;s)$ are Morse oscillators and E_v are Morse energies. The lowest twelve vibrational energies and the sums $E_v(s) + V_{tr}(s)$ are shown in Fig. 2. The wells in these curves near s=0 are produced by expansion and contraction of the potential valley.

The rotational Hamiltonian is partitioned into terms representing a symmetric top, an asymmetry term, a Coriolis term (coupling bending motion to tumbling of the nuclear triangle), and a bending term:[32-33,35]

$$\hat{H}_{rot} = \hat{H}_{st} + \hat{H}_{asym} + \hat{H}_{cor} + \hat{H}_{bend} \tag{7}$$

Anticipating the use of locally adiabatic rotational functions, we form a symmetric top free-rotor diabatic basis by taking products of normalized symmetric top functions and normalized associated Legendre polynomials, $N^J_{MK}(\theta\phi\chi)\ P^K_j(\cos\gamma)$. These product basis functions are eigenfunctions of $\hat{H}_{st} + \hat{H}_{bend}$ (when $V_{bend} = 0$), for total angular momentum J with projection K on the BF Z-axis. Diagonalization of the representation of $\hat{H}_{asym} + \hat{H}_{cor}$ in the free-rotor basis leads to eigenfunctions $\tilde{\Omega}^{JM}_{j\ell}$ that mix free-rotor functions differing in K but not j:

$$\tilde{\Omega}^{JM}_{j\ell} = \sum_{K=-J}^{+J} N^J_{MK}\ \Phi^{JK}_{j\ell} \tag{8}$$

The free internal rotor function $\Phi^{JK}_{j\ell}$ are Legendre polynomials multiplied by terms dependent on ℓ, j, and J.[35] Asymptotically, the $\tilde{\Omega}^{JM}_{j\ell}$ are eigenfunctions of $\hat{H}_{rot}$, and j and ℓ are good quantum numbers. However, for $V_{bend} \neq 0$ the matrix representation of V_{bend} in the $\tilde{\Omega}^{JM}_{j\ell}$ basis must be diagonalized. The equation

$$\hat{H}_{rot}\tilde{\Omega}^{JM}_{j\ell}(\theta\phi\chi\gamma;s) = W^J_{j\ell}(s)\tilde{\Omega}^{JM}_{j\ell}(\theta\phi\chi\gamma;s) \tag{9}$$

defines the hindered asymmetric top functions and energies. The adiabatic hindered asymmetric top states are[36]

$$\Omega^{JM}_{j\ell}(\theta\phi\chi\gamma;s) = \sum_{j'\ell'} d^{J}_{j'\ell'j\ell}\,\tilde{\Omega}^{JM}_{j'\ell'} = \sum_{K} N^{J}_{MK}\,R^{JK}_{j\ell}(\gamma;s) \qquad (10)$$

where $R^{JK}_{j\ell}(\gamma;s)$ are hindered internal rotor functions. The j and ℓ values no longer remain good quantum numbers, but are used to label the rotor states at all values of s.

In the present study, analysis is restricted to collisions with total angular momentum $J=0$. Thus, the orbital angular momentum has only the value $\ell=j$. Since $M=K=0$ for these collisions, the symmetric top functions are independent of the orientation of the three-body triangle. Thus, the local asymmetric top function $\tilde{\Omega}^{JM}_{j\ell}(\theta\phi\chi\gamma;s)$ depends only on the bending angle γ, and is proportional to $R^{00}_{jj}(\gamma;s)$. It can therefore be represented as a simple expansion over Legendre polynomials

$$R_j(\gamma;s) = \sum C_{j'j}(s)\,P_{j'}(\cos\gamma) \qquad (11)$$

The total scattering wavefunction for input channel $v\ell j$ can be expanded as:

$$\Psi^{JM}_{vj\ell}(\theta\phi\chi s\rho\gamma) = (\eta^{\frac{1}{2}}/\omega^{\frac{1}{2}}r)\sum_{v'j'\ell'} f^{J}_{v'j'\ell'\,vj\ell}(s)\,\chi_{v'}(\rho;s)\,R_{j'}(\gamma;s) \qquad (12)$$

The coordinate dependent scale factor $\eta^{\frac{1}{2}}/\omega^{\frac{1}{2}}r$ simplifies the coupled equations. The factor $\eta^{\frac{1}{2}}$ preserves Hermiticity[37], and the factor $\omega^{-\frac{1}{2}}$ equals the scaled atom-molecule separation for large s. The expansion coefficients $f_{v'j'\ell'vj\ell}(s)$, the translational wavefunctions (TW), measure the amplitude

for occupying state $v'j'\ell'$ when the reaction was initiated in state v,j,ℓ.

C. Solution of the Coupled Equations

Having defined the expansion of the wavefunction, the next step is to numerically integrate a set of coupled differential equations for the TW. By the usual separation of coordinates into translational s and internal degrees of freedom, we can obtain the close-coupled equations for the $f^J_{v'j'\ell'vj\ell}(s)$. The set of N simultaneous second-order differential equations is solved by assuming that, within a small interval, the locally adiabatic basis sets are independent of s; this eliminates from explicit consideration the first-derivative term in the equations. The actual distortions of the basis sets with s are included by suitable transformations at the boundaries between adjacent intervals, or "sectors". Within one sector the coupled equations are

$$\frac{d^2}{ds^2} f^J_{v'j'\ell'vj\ell} = \sum_{v''j''\ell''} D^J_{v'j'\ell'v''j''\ell''} f^J_{v''j''\ell''vj\ell} \tag{13}$$

where the coupling matrix D^J has elements

$$D^J_{vj\ell v'j'\ell'} = -\delta_{jj'}\delta_{\ell\ell'}\left\{\langle\chi_v|\hat{V}_{eff}|\chi_{v'}\rangle + \frac{2\mu}{\hbar^2}\left[E - (E_v+E_{v'})/2 - W^J_{j\ell} - V_{tr}(s)\right]\langle\chi_v|\eta^2|\chi_{v'}\rangle\right\} \tag{14}$$

Note that the couping matrix is diagonal in the rotational indices.

The solution of Eq. (13) via the R-matrix method[38], followed by the determination of the scattering matrix and the TW can be viewed as a three-step procedure. First, one solves Eq. (13) as a boundary-value problem (R-matrix method). Second, asymptotic boundary conditions are applied to define the scattering matrix S. Finally, the local TW are constructed from the correct asymptotic conditions defining the appropriate scattering states, by

repeating the propagation with appropriate initial conditions using propagators assembled and saved during the R-matrix integration. This process is a new application of the R-matrix method to reactive scattering, and details will be more fully presented in this and the following sections.

In discussing the method of solution of the coupled equations within an arrangement channel (tube), we will focus on the even-j channels in the reactant α-tube. The α-tube is partitioned into two regions: one, represented in polar coordinates, lies between s=0 (which locates the α-β tube match surface) and a cartesian (large-s) region that is separated from the interior polar region by another match surface, the polar-cartesian boundary (PC_α). These two regions are further subdivided into small sectors of width h_i. Sector 1 lies between s_0 (s=0) and s_1, sector 2 between s_1 and s_2, ... sector m between s_{m-1} and s_m , with s_m taken to be some sufficiently large value of s. At the center of sector i, a unitary transformation of $\underline{\underline{D}}^{(i)}$ produces a diagonal energy-dependent eigenvalue matrix $\lambda^{2(i)}(E)$:

$$\underline{\underline{\tilde{T}}}^{(i)}\underline{\underline{D}}^{(i)}\underline{\underline{T}}^{(i)} = \underline{\underline{\lambda}}^{2(i)}(E) \tag{15}$$

The coupled equations in the new (adiabatic) representation can now be written as 2N first-order equations

$$\frac{d}{ds}\begin{bmatrix} \underline{g}^{(i)} \\ \frac{d\underline{g}}{ds}^{(i)} \end{bmatrix} = \begin{bmatrix} \underline{\underline{0}} & \underline{\underline{1}} \\ \underline{\underline{\lambda}}^{2(i)} & \underline{\underline{0}} \end{bmatrix}\begin{bmatrix} \underline{g}^{(i)} \\ \frac{d\underline{g}}{ds}^{(i)} \end{bmatrix} \tag{16}$$

where the adiabatic TW, $\underline{g}$, are related to the "diabatic" TW, $\underline{f}$, through the equation

$$\underline{g}^{(i)} = \underline{\underline{\tilde{T}}}^{(i)}\,\underline{f}^{(i)} \tag{17}$$

A Taylor series expansion of $\underline{g}$ on the LHS of sector i in terms of $\underline{g}$ on the RHS of the sector permits us to rewrite Eq. (16) as

$$\begin{bmatrix} \underline{g}^{(i)} \\ \frac{d\underline{g}}{ds}^{(i)} \end{bmatrix}_L = \begin{bmatrix} \underline{\underline{P}}_1^{(i)} & \underline{\underline{P}}_2^{(i)} \\ \underline{\underline{P}}_3^{(i)} & \underline{\underline{P}}_4^{(i)} \end{bmatrix} \begin{bmatrix} \underline{g}^{(i)} \\ \frac{d\underline{g}}{ds}^{(i)} \end{bmatrix}_R \tag{18}$$

The local propagators $\underline{\underline{P}}_q^{(i)}$ are given by analytical formulas[38] involving the sector width h and the eigenvalues λ_p.

Continuity of the total wavefunction and its derivative along s requires that at sector boundaries the <u>adiabatic</u> TW meet the following conditions:

$$\begin{aligned} \underline{g}_R^{(i-1)} &= \underline{\underline{\tilde{T}}}^{(i-1)} \underline{\underline{O}}^{(i-1,i)} \underline{\underline{T}}^{(i)} \underline{g}_L^{(i)} = \underline{\underline{F}}^{(i-1,i)} \underline{g}_L^{(i)} \\ \frac{d\underline{g}}{ds}_R^{(i-1)} &= \underline{\underline{\tilde{T}}}^{(i-1)} \underline{\underline{O}}^{(i-1,i)} \underline{\underline{T}}^{(i)} \frac{d\underline{g}}{ds}_L^{(i)} = \underline{\underline{F}}^{(i-1,i)} \frac{d\underline{g}}{ds}_L^{(i)} \end{aligned} \tag{19}$$

The diabatic overlap $\underline{\underline{O}}^{(i-1,i)}$ has elements generated from overlap integrals involving the basis functions,

$$O_{v'j'vj}^{(i-1,i)} = \langle \chi_{v'}^{(i-1)} R_{j'}^{(i-1)} \mid \chi_v^{(i)} R_j^{(i)} \rangle \tag{20}$$

Although the adiabatic TW are uncoupled within each sector, they mix at the sector boundaries.

Conservation of flux requires that the matrix product $\underline{\underline{\tilde{T}}}^{(i-1)} \underline{\underline{O}}^{(i-1,i)} \underline{\underline{T}}^{(i)}$ connecting adjacent sectors be orthogonal; in practice $\underline{\underline{O}}$ is not orthogonal, but it is still diagonally dominant. To insure the required orthogonality, we use a Gram-Schmidt procedure[39] at each sector boundary. The combination of propagation across a sector with matching at the sector boundary can be expressed as a matrix equation that integrates the coupled equations from the RHS of sector i to the RHS of sector i-1:

$$\begin{bmatrix} \underline{g}^{(i-1)} \\ \frac{d\underline{g}}{ds}^{(i-1)} \end{bmatrix}_R = \begin{bmatrix} \underline{\underline{F}}^{(i-1,i)} & \underline{\underline{O}} \\ \underline{\underline{O}} & \underline{\underline{F}}^{(i-1,i)} \end{bmatrix} \begin{bmatrix} \underline{\underline{P}}_1^{(i)} & \underline{\underline{P}}_2^{(i)} \\ \underline{\underline{P}}_3^{(i)} & \underline{\underline{P}}_4^{(i)} \end{bmatrix} \begin{bmatrix} \underline{g}^{(i)} \\ \frac{d\underline{g}}{ds}^{(i)} \end{bmatrix}_R \tag{21}$$

In addition to the sector matching requirements, there are three additional matchings, in addition to the arrangement channel matching, that

need to be mentioned. As discussed elsewhere,[40] at the boundary between the polar and cartesian (asymptotic) regions, a transformation accounting for the differences in coordinates must be performed. In addition, at s=0, the $\underline{\underline{F}}^{(0,1)}$ matrix connecting the reactant and product channel adiabatic TW is set equal to $\underline{\underline{T}}^{(1)}$ in order to initiate the propagation sequence at the LES of reactant sector 1. (In our notation, the "zero" sector in the reactant channel corresponds to sector 1 in the product channel). This means that we begin with <u>diabatic</u> TW at the match surface, which facilitates application of the matching conditions. The $\underline{\underline{O}}^{(0,1)}$ matrix connecting the diabatic TW at the matching surface is neglected at this step, but is incorporated into the S-matrix equations. The third matching is required to map the scattering wavefunction onto the asymptotic channels, and is incorporated explicitly by propagation to sufficiently large s such that all off-diagonal elements of $\underline{\underline{D}}$ vanish and the diagonal elements become independent of s; then $\underline{g}^{(m)} = \underline{f}^{(m)}$.

Assembly of the local propagators and $\underline{\underline{F}}$ matrices advances the diabatic $\underline{f}$ at s=0 to the asymptotic $\underline{f}$ at $s=s_m$. This arrangement channel propagator is formed by sequentially multiplying the F and P matrices:

$$\begin{bmatrix} \underline{f}^{(1)} \\ \underline{\frac{df}{ds}}^{(1)} \end{bmatrix} = \begin{bmatrix} \prod_{i=1}^{m} \underline{\underline{F}}^{(i-1,i)} \, \underline{\underline{P}}^{(i)} \end{bmatrix} \begin{bmatrix} \underline{f}^{(m)} \\ \underline{\frac{df}{ds}}^{(m)} \end{bmatrix} \tag{22}$$

Although this accumulation of local propagators is straightforward, this method suffers from numerical instabilities due to the closed channels that must be included in the basis. The R-matrix integration method can be used to circumvent these problems, because it is inherently stable to the inclusion of closed channels.

The R-matrix propagation equations may be obtained by rearrangement of the propagator equations[38] into the form,

$$\begin{bmatrix} \underline{g}^{(i-1)} \\ \underline{g}^{(i)} \end{bmatrix} = \begin{bmatrix} \underline{\underline{r}}_1^{(i)} & \underline{\underline{r}}_2^{(i)} \\ \underline{\underline{r}}_3^{(i)} & \underline{\underline{r}}_4^{(i)} \end{bmatrix} \begin{bmatrix} \frac{d\underline{g}}{ds}^{(i-1)} \\ -\frac{d\underline{g}}{ds}^{(i)} \end{bmatrix} \tag{23}$$

The $\underline{\underline{r}}_p^{(i)}$ matrices contain matrix products of the $\underline{\underline{P}}_q^{(i)}$ and $\underline{\underline{F}}^{(i-1,i)}$, and it is easy to show that $\underline{\underline{r}}_1^{(i)}$ and $\underline{\underline{r}}_4^{(i)}$ are symmetric, and that $\underline{\underline{r}}_2^{(i)} = \underline{\underline{r}}_3^{(i)}$, provided $\underline{\underline{F}}^{(i-1,i)}$ is orthogonal. Collecting the local $\underline{\underline{r}}$-matrices into an arrangement channel $\underline{\underline{R}}$-matrix is accomplished not by successive matrix multiplications, as with the propagator method, but by recursion formulas developed by Zvijac and Light.[41] The $\underline{\underline{r}}_p^{(i)}$ are accumulated for each sector beginning with sector 1 and ending with sector m. At sector m we have obtained an arrangement channel $\underline{\underline{R}}$-matrix that relates the TW $\underline{f}$ and their derivatives at s=0 and s=s_m:

$$\begin{bmatrix} \underline{f}^{(1)} \\ \underline{f}^{(m)} \end{bmatrix} = \underline{\underline{R}}^{\alpha} \begin{bmatrix} \frac{d\underline{f}}{ds}^{(1)} \\ -\frac{d\underline{f}}{ds}^{(m)} \end{bmatrix} \tag{24}$$

When these $\underline{\underline{R}}$-matrices are obtained for each arrangement channel, they are combined with the appropriate asymptotic boundary conditions to allow determination of the scattering matrix. For the initial channel v,j, the boundary conditions take the form:

$$f_{vj}(s) = k_{vj}^{(-)^{-\frac{1}{2}}} \left[h_\ell(k_{vj}^{(-)}s) - S_{vj}^{(-)} h_\ell^*(k_{vj}^{(-)}s) \right] \tag{25}$$

For the inelastic channels, the appropriate form is

$$f_{v'j'}(s) = -k_{v'j'}^{(-)^{-\frac{1}{2}}} S_{v'j'}^{(-)} h_\ell^*(k_{v'j'}^{(-)}s) \tag{26}$$

while for the reactive product channels the form is

$$f_{v'j'}(s) = -k_{v'j'}^{(+)^{-\frac{1}{2}}} S_{v'j'}^{(+)} h_\ell(k_{v'j'}^{(+)}s) \tag{27}$$

The Riccati-Hankel functions have the asymptotic forms

$$h_\ell(k_{vj}^{(\pm)}s) \sim \begin{cases} \exp\{i(k_{vj}^{(\pm)}s - \ell\pi/2)\}, & k_{vj}^2 \geq 0 \\ \exp\{-|k_{vj}^{(\pm)}s| - i\ell\pi/2\}, & k_{vj}^2 < 0 \end{cases} \tag{28}$$

while the channel wavenumbers are expressed as

$$k_{vj}^{(\pm)} = \left[\frac{2\mu}{\hbar^2}\left(E - E_v(\pm\infty) - W_{j\ell}^J(\pm\infty) - V_{tr}(\pm\infty)\right)\right]^{\frac{1}{2}} \tag{29}$$

The superscripts (+) and (-) denote reactive and nonreactive scattering, respectively.

In summary, the coupled equations are integrated with the R-matrix propagation technique to obtain an S-matrix. Then, a second propagation is performed to obtain the desired TW by using local propagators saved during the initial integration. These TW are used in the analysis of the reacton dynamics discussed in the remaining sections of this paper and in II.

III. The Scattering Wavefunction

A. Translational Wavefunction Assembly

In this section we consider the propagation of the TW and assembly of the 3-D wavefunction at each step. To initiate propagation of the TW in the asymptotic reactant or product regions, the correct initial amplitudes are obtained by substituting the appropriate S-matrix elements into Eqs. (25) through (27). With these initial conditions, the propagation sequence in Eq.(22) is used to generate the adiabatic TW at each s, using local information saved at each s during the initial R-matrix integration. Eq.(17) is then used to convert the adiabatic $\underline{g}$ into the diabatic $\underline{\underline{f}}$. For example, at the m^{th} sector we begin with the equation for the even-j $\underline{g}$ in the α-tube (odd-j construction proceeds in an analogous manner):

$$\begin{bmatrix} \underline{g}^{(m-1)} \\ \underline{g}'^{(m-1)} \end{bmatrix}_R = \begin{bmatrix} \underline{\underline{F}}^{(m-1,m)}\underline{\underline{P}}_1^{(m)} & \underline{\underline{F}}^{(m-1,m)}\underline{\underline{P}}_2^{(m)} \\ \underline{\underline{F}}^{(m-1,m)}\underline{\underline{P}}_3^{(m)} & \underline{\underline{F}}^{(m-1,m)}\underline{\underline{P}}_4^{(m)} \end{bmatrix} \begin{bmatrix} \underline{g}^{(m)} \\ \underline{g}'^{(m)} \end{bmatrix}_R \tag{30}$$

which takes the adiabatic TW and derivatives in sector m and propagates them to sector m-1, where they are transformed into the diabatic representation:

$$\underline{f}^{(m-1)} = \underline{\underline{T}}^{(m-1)}\,\underline{g}^{(m-1)}, \quad \underline{f}'^{(m-1)} = \underline{\underline{T}}^{(m-1)}\,\underline{g}'^{(m-1)} \tag{31}$$

Similarly, to calculate $\underline{g}^{(m-2)}$ and $\underline{g}'^{(m-2)}$ in sector (m-2) we simply relabel Eq.(30) by changing the superscripts m-1 to m-2 and m to m-1, substitute in the $\underline{g}^{(m-1)}$ and $\underline{g}'^{(m-1)}$ just obtained with Eq.(30), and perform the matrix multiplication. Successive application of this procedure generates both the adiabatic and diabatic TW throughout all arrangement tubes. If the numerical technique remains stable (remember, this is now an initial value method), $\underline{f}(0)$ and $\underline{f}'(0)$ will satisfy the proper rotor-partitioning (bifurcation)

conditions at s=0.[24]

In the present applications to $F+H_2$ linear dependencies did arise in the reactant tube in attempts to integrate large basis sets inward form large values of -s. The source of the linear dependence of the columns of $\underline{f}$ are the highly closed channels, with corresponding small asymptotic amplitudes and large propagator elements. Due to the finite machine precision, the matrix multiplications at each step introduce local errors that grow and eventually make the value of $\underline{f}$ meaningless. Because of this, the vibrational basis was limited to 10 states in these calculations, and the reactant tube propagation was started at a modest value of -s. The R-matrix propagation does not suffer from this problem, and for simply obtaining an S-matrix the number of vibratonal states and the range of s need not be restricted.

For the results reported here, a 60 channel basis with 10 vibratonal states and a rotor basis distributed 12/12/12/8/6/2/2/2/2 was employed. The rotationally averaged results using this basis agree reasonably well with results obtained using much larger basis sets,[23] and they are adequately converged for the graphical analysis of the present work. In the actual propagation, the even-j and odd-j states are propagated separately. Propagation in reactants is initiated at $-1.6a_0$; at this value of s the interaction matrix is essentially diagonal.

B. Assigning Quantum Numbers to the TW

One feature of the TW that we have not discussed is the labeling of the rows of $\underline{f}$ and $\underline{g}$ by quantum number. Considering only J=0 (ℓ=j), this means associating quantum numbers v,j with the elements of the TW. For the diabatic TW, $\underline{f}$, the assignment is straightforward; one simply takes the assignment used in filling the interaction matrix $\underline{\underline{D}}$. If, for example, $(\underline{\underline{D}})_{mm}$ corresponds to channel (vj), then $(\underline{f})_m$ corresponds to $\underline{f}_{vj}$, since $\underline{\underline{D}}$ retains

the same row and column labeling at each s in all tubes. For the adiabatic $\underline{g}$, the diagonalization of $\underline{\underline{D}}$ in the R-matrix propagation results in an energetic ordering of the locally uncoupled $\underline{g}$. Thus, even asymptotically, it is not immediately true that $(\underline{g})_m = (\underline{f})_m$, because the diagonal elements of D are not in energetic order. Therefore, to assign quantum numbers to $\underline{g}$, we use information contained in the transformation matrix at the last sector, $\underline{\underline{T}}^{(m)}$. This matrix contains only ones and zeros, where the relative position of the ones identifies the vj label.

C. TW Phasing Techniques

Our early attempts at generating $\underline{f}$ produced inconsistently phased TW; that is, from sector to sector an element $(\underline{f})_m$ might change sign many times over a single wavelength. This arbitrary sign switching was due to the phase of the eigenvector matrix in sector i being independent of the phase in sector i-1; there was no translational phase coherence. To overcome this difficulty, a phasing procedure previously employed to phase rotor functions[35] was used to phase the TW. Since the asymptotic phase of each eigenvector is arbitrary, we initially multiply each vector by +1 or -1 so that the largest (in magnitude) component of the vector is positive. Then at every subsequent step, we again require the largest component of the vector to have the same sign as in the previous sector, multiplying the vector by -1 as necessary to achieve this. In phasing the rotor functions used in assembling the TW, a similar procedure is employed, but account is taken of the asymptotic phasing of R_j being <u>not</u> arbitrary, but by the fact that $R_j(\gamma;s) \rightarrow P_j(\gamma)$; thus the columns of the rotor eigenvectors are multiplied by -1 as necessary to achieve this. This phasing is not necessary during the R-matrix propagation since all information on absolute phasing is lost in forming the rotor overlaps.

IV. Translational Wavefunction Analysis and Internal Energy Disposal

A. Diabatic Translational Wavefunctions

This section begins our analysis of the scattering wavefunction by first examining the diabatic TW and then discussing several quantities that illustrate the partitioning of internal energy among the channels during the reaction. Recall that the TW amplitudes squared are interpreted as local measures of the probability density for the individual channels. The TW can reveal many detailed facets of the collision process and they serve as a basis for understanding features of the full 3-D wavefunction. Of the 60 channels in these calculations, we will present the real part of $\underline{f}$ for j=0,2,4, and 6 in the three lowest vibrational levels for each tube. However, we should mention that the TW amplitudes in the closed vibrational levels do reach moderate magnitudes in the reaction zone, although they rapidly decay as the system moves out of this region.

We first examine the α -tube TW, which are shown in Fig. 3(a-c) at three total energies. For purposes of illustration, we have scaled the α -tube TW f_{00} by 0.25 and f_{02} by 0.50. This scaling amplifies the contrast between these two dominant channels and the rest of the reactant tube functions. There are several characteristics common to the TW for all three energies shown. With input flux in f_{00} and with $|S_{00}|^2 = 0.40$, we expect this channel to have the largest amplitude of all. This input channel couples strongest with f_{02} and consequently f_{02} has the next largest average amplitude. Within a given vibrational level in the α -tube, the TW tend to decrease in magnitude as j increases, and as v increases from 0 to 2 the amplitude of a given j level becomes smaller. Since only the j=0 and 2 states are asymptotically open in reactants, the wavefunction will show interference

effects caused by coupling in these two channels, the other TW amplitudes becoming vanishingly small.

The next region we will consider is the match surface between the α and β tubes. The rotor bifurcation constraints[24] require that at s=0 the α-tube f^{α}_{vj} split into the β-tube f^{β}_{vj+1} and f^{β}_{vj}, with $f^{\beta}_{vj+1} = f^{\beta}_{vj}$, and $f^{\alpha}_{vj} = f^{\beta}_{vj+1} + f^{\beta}_{vj}$. Comparing Figs. 3a, 3b, and 3c with 3d, 3e, and 3f respectively confirms that these conditions are satisfied. We do not present any of the f^{β}_{vj+1} functions because they appear nearly identical to the f^{β}_{vj}, which are plotted in Fig.3. Because of the difference in axis scales between the α and β tube plots and because of the small size of some of the TW at s=0, it is difficult to visually check the accuracy of the amplitude partitioning; numerically the agreement is to one part in ten thousand. Note that the phasing remains smooth across the s=0 match surface.

It is in the β-tube that we find dramatic evidence of the vibrational population inversion and rotational excitation of the HF product molecules. At the three energies studied here, all of the channels shown in Fig.6(d-f) are asymptotically open, so that at large H-HF separations the f^{β}_{vj} wavelengths vary inversely with the channel translational wavenumber. Focusing on Fig. 3e for the resonance energy 0.36 eV, we can see how dramatically the f_{00} amplitude declines from the very large value it has in reactants, so that by s=+1.5 a_0 it is negligable. Similar comments hold for the other v=0 rotor states.

Examination of the v=1 manifold in Fig. 3e,we see the beginning of the extensive rotational and vibrational excitation of the product HF molecule. It is f^{β}_{16} that shows the largest excitation in this figure. The lower rotors in this manifold build amplitude in the region between s=+0.5 and s=+1.5, but begin to die out for larger s values. It should be remembered

that all of these channels are energetically open in HF at these total energies. An interesting feature of f^{β}_{16}, f^{β}_{24} and f^{β}_{26} is that they suddenly switch on at about s=0.5. From Fig. 3e we can see the population inversion process occuring, and we can determine the FHH configurations where this process begins to dominate the dynamics of the reaction.

Comparing the f^{β}_{vj} functions channel by channel in fig. 3(d-f) we observe that the magnitudes of the TW for the 0.36 eV resonant energy (again interpreted as measures of the probability density) are substantially larger than those at 0.33 eV, while the j′=4 and 6 functions have nearly double the amplitude of the corresponding 0.40 eV TW. Thus, from an analysis of the TW, we have gained insight into the characteristics of the vibrational population inversion process, and of the amplitude growth in v′=2 at the resonance energy.

B. Vibrational and Rotational Energies in the Collision Complex

A very interesting aspect of chemical reactions concerns the disposal of energy into the various available channels as the collision proceeds from reactants to products. Of particular interest are quantities such as average vibrational and rotational energies and entropies as functions of the translational coordinate s. One method of calculating the average energies is to operate on the total scattering wavefunction at each s; however, this direct approach produces equations that are cumbersome.[8] The complications of this approach arise because of the curvature of the coordinates. As an alternative approach, we recast the wavefunction of Eq.(12) in terms of curvature free TW expansion coefficients that eliminate the $\eta^{\frac{1}{2}}$ scale factor:

$$\Psi_{vj} = \frac{1}{\omega^{\frac{1}{2}} r} \sum_{v'j'} U_{v'j'vj}(s) \chi_{v'}(\rho;s)\, R_{j'}(\gamma;s) \qquad (32)$$

where

$$U_{v'j'vj}(s) = \sum_{v''j''} \langle \chi_{v'} | n^{\frac{1}{2}} | \chi_{v''} \rangle \, \delta_{j''j'} \, f_{v''j''vj}(s) \tag{33}$$

The expansion of a single U_i mixes all of the diabatic f_i functions with the same rotational index, each weighted by the vibrationally averaged curvature factor. The overlap of Ψ with itself becomes

$$\langle \Psi_{vj} \mid \Psi_{vj} \rangle_{\theta\phi\chi\rho\gamma} = \frac{1}{\omega} \sum_{v'j'} |U_{v'j'vj}(s)|^2 \tag{34}$$

since the 3-D normalization of the vibrational functions requires

$$\int \left(\frac{\chi_{v'}}{r}\right)\left(\frac{\chi_{v}}{r}\right) r^2 \, dr = \delta_{v'v} \tag{35}$$

The $\underline{U}(s)$ functions can be utilized to define the local normalized probabilities $P_{vj}(s) = |U_{vj}(s)|^2 / \sum |U_{vj}(s)|^2$, where the channels are again labeled by vj. This set of $P_{vj}(s)$ allows us to obtain average values without explicitly operating on the wavefunction. Thus the average vibrational energy is obtained from the expression

$$\langle E_v \rangle = \sum_{vj} E_v(s) \, P_{vj}(s) \tag{36}$$

and the average rovibrational energy is obtained from

$$\langle E_v + E_R \rangle = \sum_{vj} \left(E_v(s) + W_j(s) \right) P_{vj}(s) \tag{37}$$

Figure 4 illustrates these quantities for total energies 0.33, 0.36, and 0.40 eV.

Looking first at the average vibrational energies in Fig. 4a, we notice that in the asymptotic reactant tube the average vibrational energy is predominately in v=0, as expected since it is the only open vibrational level. Approaching s=0, the average energies oscillate, with the frequency increasing as the total energy increases. As the vibrational energies plunge

in energy just before s=0, so do the average vibrational energies. However, the average vibrational energy grows relative to the bottom of the potential valley (the translational potential $V_{tr}(s)$ has been added to the average vibrational and rovibrational energies before plotting). Between s=0 and s=+2.0, the oscillations in the average energies still reflect the mixing of the upper vibrational levels, but in contrast to the reactant tube, at all three energies the oscillating pattern is similar; one minimum occurs very close to s=0, another minimum occurs at approximately s=+0.4, and a final minimum occurs near s=+1.0. The amplitude of these oscillations is however quite different for the three levels because of the increase in the $v'=3$ transition probability as the total energy rises from 0.33 to 0.40 eV. This is why at 0.33 eV the asymptotic product average vibrational energy lies close to the v=2 energy level, while at 0.36 eV more $v'=3$ component mixes in, so that by 0.40 eV the contribution from $v'=3$ is sufficiently large that $\langle E_v \rangle$ is approximately halfway between the v=2 and v=3 levels.

The average rovibrational energy plotted in Fig. 4 b combines the features contained in Fig. 4a with the effects of local rotational excitation. These curves have a similar interpretation to those in Fig. 4a, with the rotational effects most evident in the reactant tube (due to the mixing of the two open rotor states). An interesting feature of $\langle E_v + E_R \rangle$, excitation into the closed channels just prior to s=0, is indicative of the quantum nature of this reaction. Here, $\langle E_v + E_R \rangle$ rises <u>above</u> the system energy. The main contributor to the tunneling is $\langle E_v \rangle$. This is not surprising since quantum effects dominate the collinear reaction as well.

C. Vibrational and Rotational Entropies in the Collision Complex

By studying the local entropies, we can gain a better understanding of the distribution of probabilities and of the rovibrational disorder during the reaction. The total entropy at location s (in units of Boltzman's constant, k) is defined by:

$$S_T(s) = -\sum_{vj} P_{vj}(s)\, \ell n(P_{vj}(s)) \tag{38}$$

Two other entropies, the rotationally averaged vibrational entropy, $\langle S_V \rangle_R$, and the vibrationally averaged rotational entropy, $\langle S_R \rangle_V$ require averaging the P_{vj} functions in the following manner:

$$\begin{aligned} \langle S_V \rangle_R &= -\sum_v \left(\sum_j P_{vj}\right) \ell n\left(\sum_j P_{vj}\right) \\ \langle S_R \rangle_V &= -\sum_j \left(\sum_v P_{vj}\right) \ell n\left(\sum_v P_{vj}\right). \end{aligned} \tag{39}$$

Figure 5 illustrates these three entropies at the energies 0.33, 0.36, and 0.40 eV. Since each type of entropy for these three energies shows similar behavior, we will not consider their energy dependence, but instead will emphasize the general features of each entropy.

Looking first at $\langle S_V \rangle_R$, we see that in asymptotic reactants there is zero entropy because only v=0 is open. But as s=0 is approached, this entropy rapidly grows and then falls off to a nonzero value for s>1.5. This shows both the short-lived excitation in the transition state due to the participation in the scattering of asymptotically closed vibrational levels, and the uncertainty of the final vibrational state of products. The nonzero value at large product separation simply reflects the partitioning of amplitude between v′=2 and v′=3. Considering next the $\langle S_R \rangle_V$ plot, we notice that in reactants there is a small (compared to products) rotational entropy due to mixing between j′=0 and j′=2. Note that just before s=0 the entropy curves nearly reach zero. Referring back to Fig.3 , it can be seen that almost all

the flux flows through the lowest ($j'=0$) adiabatic bending channel in this region. However, due to the large number of available open rotational channels in products, $\langle S_R \rangle_V$ becomes quite large for $s>1.0$.

The S_T curves contain features of both $\langle S_V \rangle_R$ and $\langle S_R \rangle_V$: nonzero entropy in reactants and products with the entropy in products greater than in reactants, and a peak near $s=0$.

This concludes our analysis of the translational wavefunctions and their associated average energies and entropies. We have focused attention on the flow of amplitude through the individual channels as functons of both the system energy and reaction coordinate.

D. Integrated Density vs Reaction Coordinate

We acquire an additional perspective on the collision process by compressing information from the wavefunction probability density. Integration of the total density within planes of constant s then allows construction of an interesting plot of the integrated density as a function of the translational coordinate s. The integrated density is defined by the equation

$$I(s) = \omega \iint \Psi^*(n,m;s)\, \Psi(n,m;s)\, dn\, dm \qquad (40)$$

The factor ω appears in Eq. (40) to prevent the density from decaying asymptotically as $1/R^2$. Fig.6, illustrates the s-dependence of the integrated density for the energies 0.33, 0.36 and 0.40 eV. The oscillations in the densities are caused by interference between all locally open channels. The frequency of the oscillations can be correlated to some degree with the fact that available translational energy increases with increasing total energy. The decrease in magnitude of the densities past about $s=-0.1$ is a consequence

of the considerable amount of nonreactive flux in this reaction. The resonant curve (the 0.36 eV density) reaches a maximum before s=0, and then decreases as the system moves into the product region. Thus we might call this v′=2 resonance an "entrance channel resonance". The vibrational distributions have mostly settled down by s=0.5, and only the rotational populations show much change after this region of s.

V. Conclusions

The quantum dynamics of the three-dimensional $F+H_2$ reaction has been analyzed for three total energies, and for total angular momentum J=0. The energy 0.36 eV is of special significance, since this is close to the J=0 resonance energy for the process $F+H_2(v=0) \rightarrow H+HF(v'=2)$. The computational methods used to obtain the scattering wavefunction required for the dynamical analysis in the region of the collision complex have been presented. This has been prefaced by a brief review of the coordinates, Hamiltonian, basis sets, and boundary conditions used in the NCC approach to the reaction dynamics.

In the dynamical analysis, emphasis was placed on graphical methods for illustrating the variation with s of the translational wavefunctions, vibrotor energies, vibrational, rotational and total entropies, and the total density in planes perpendicular to the reaction coordinate. We will briefly summarize some of the results from this analysis. In Fig. 6 the translational wavefunctions $f_{vj}(s)$ are shown for the j=0-6 rotational states associated with the v=0-2 vibrational manifolds. In the $F+H_2$ reactant tube, the translational wavefunction f^{α}_{02} has an amplitude which is at most one half of f^{α}_{00}. Near s=0, there is a small amount of excitation into the lower rotational levels of the v=0 and 1 manifolds. In the H+HF product arrangement, f^{β}_{00} decays almost completely by $s=+1.0\ a_0$, while amplitude builds up in the j=4-6 rotational levels of the v=0 and 1 manifolds. However, the most dramatic effect in the product region is the relatively rapid buildup between s=0.5 and s=1.5 of amplitude in the j=4-6 rotational levels of the v=2 manifold. This rotational excitation occurs on the final part of the turn into the product valley (see Fig. 4).

The oscillations seen in Fig. 7 of the average vibrational energy $\langle E_V \rangle$ and the average rovibrational energy $\langle E_V + E_R \rangle$ as s goes from reactants to products are associated with interference effects among the vibrational channels. Of more interest than these average energies are the average and total entropies shown in Fig. 8. In reactants, the rotationally averaged vibrational entropy is zero (only v=0 is populated), but the vibrationally averaged rotational entropy is nonzero (j=0-2 are populated). Near s=0, the rotational entropy is lower than in reactants or products because of the strong propensity for the lowest bending state of the complex. In products, the vibrational entropy is about half the peak value in the collision complex, because flux is leaking out of the temporarily excited virtual states (primarily) into the v=2 manifold. Also, the rotational entropy in products is large (about twice the vibrational entropy), due to the relatively diffuse rotational excitation through many rotational channels (but primarily j=4-6).

The variation with s of the total wavefunction density, shown in Fig. 9, measures the net tendency of probability to accumulate at position s. This quantity, I(s), is computed as an integral over a plane of constant s of the local probability density. The most interesting features of this quantity are found to be: the oscillations in reactants due to interference between incoming and outgoing waves, and the factor of 10-100 drop in I(s) on turning the corner into the product valley. However, when comparing plots of I(s) at the three energies considered in this paper, the region between $s=-0.5\ a_0$ (near the entrance channel barrier) and s=0 is especially significant. On resonance (0.36 eV), the density in this regon is about a factor of two or more larger than for the other two energies, which lie above and below the resonance energy. The resonance is associated with buildup of

amplitude between the entrance channel barrier and the turn into products; thus it is termed an "entrance channel resonance".

In part II of this series[30], density and flux maps obtained from the total scattering wavefunction will be shown in planes perpendicular to the reaction coordinate and in planes for bent geometries (m>0) parallel to the collinear plane. Emphasis will be placed on the behavior of these quantities as the system goes through resonance.

REFERENCES

1. J.C. Polanyi and J.L. Schreiber, Faraday Disc. Chem. Soc. 62, 267 (1977).

2. J. B. Anderson, in "Advances in Chemical Physics", Vol. XLI, I. Prigogine and S. A. Rice, eds., Wiley, New York, 1980, p 229.

3. J.T. Muckermann, in "Theoretical Chemistry", Vol. 6A, H. Eyring and D. Henderson, eds., Plenum, New York, 1981, p 1.

4. S.F. Wu, B.R. Johnson, and R. Levine, Mol. Phys. 25, 839 (1973).

5. G.C. Schatz, J.M. Bowman, and A. Kuppermann, J. Chem. Phys. 63, 674 (1975).

6. J.N.L. Conner, W. Jakubetz, and J. Manz, Mol. Phys. 29, 347 (1975).

7. C.H. Zuhrt, T. Kamal, and L. Zulicke, Chem. Phys. Lett. 36, 396 (1975).

8. S.L. Latham, J.F. McNutt, R.E. Wyatt, and M.J. Redmon, J. Chem. Phys. 69, 3746 (1978).

9. J.N.L. Connor, Comp. Phys. Comm. 17, 117 (1979).

10. E.F. Hayes and R.B. Walker, J. Phys. Chem. 86, 85 (1982).

11. A. Kafri, Y. Shimoni, R.D. Levine, and S. Alexander, Chem. Phys. 13, 323 (1976).

12. Y. Shan, B.H. Choi, R.T. Poe, and K.T. Tang, Chem. Phys. Lett. 57, 379 (1978).

13. S.H. Suck, Chem. Phys. Lett. 77, 390 (1980).

14. S.H. Suck and R.W. Emmons, Chem. Phys. Lett. 79, 93 (1981).

15. J. Jellinek, M. Baer, V. Kahre, and D.J. Kouri, Chem. Phys. Lett. 75, 460 (1980).

16. J. Jellinek, M. Baer, and D.J. Kouri, Phys. Rev. Lett. 22, 1588 (1981).

17. M. Baer, J. Jellinek, and D.J. Kouri, submitted to J. Chem. Phys.

18. M.J. Redmon and R.E. Wyatt, Int. J. Quantum Chem. S9, 403 (1975).

19. M.J. Redmon and R.E. Wyatt, Int. J. Quantum Chem. S11, 343 (1977).

20. M.J. Redmon, Int. J. Quantum Chem. S13, 559 (1979).

21. M.J. Redmon and R.E. Wyatt, Chem. Phys. Lett. 63, 209 (1979).

22. R.E. Wyatt, J.F. McNutt, and M.J. Redmon, to appear in Ber. Bun.-Gesell. fur Physik. Chimie.

23. M.J. Redmon and R.E. Wyatt, to be published.

24. J.F. McNutt, M.J. Redmon, and R.E. Wyatt, to be published.

25. J.M. Bowman, K.-T. Lee, and G.-Z. Ju, Chem. Phys. Lett. 86, 384 (1982).

26. R.K. Sparks, C.C. Hayden, K. Shobatake, D.M. Neumark, and Y.T. Lee, in "Horizons in Quantum Chemistry", K. Fukui and B. Pullman, eds., Reidel, Dordrecht, 1980, p 91.

27. R.E. Wyatt and M.J. Redmon, to be published.

28. Y.T. Lee, personal communication.

29. N.C. Blais and D.G. Truhlar, to appear in J. Chem. Phys.

30. J.F. McNutt, R.E. Wyatt, and M.J. Redmon (following paper, II).

31. R.A. Marcus, J. Chem. Phys. 49, 2610 (1968).

32. S.H. Harms and R.E. Wyatt, J. Chem. Phys. 57, 2722 (1972); R.E. Wyatt, ibid, 56, 390 (1972).

33. R.E. Wyatt, in "Atom-Molecule Collision Theory - A Guide for the Experimentalist", R.B. Bernstein, ed., Plenum, New York, 1979, p 567.

34. J.T. Muckermann, J. Chem. Phys. 56,2997 (1972); the M5 parametrization varies from the ones reported in this reference, and the values can be found in Ref. 5.

35. S.H. Harms and R.E. Wyatt, J. Chem. Phys. 62, 3162 (1975).

36. S.H. Harms, A.B. Elkowitz, and R.E. Wyatt, Mol. Phys. 31, 177 (1976).

37. J.C. Light and R.B. Walker, J. Chem. Phys. 65, 1598 (1976).

38. J.C. Light and R.B. Walker, J. Chem. Phys. 65, 4272 (1976).

39. B. Nobel, "Applied Linear Algebra", Prentice Hall, New Jersey, 1969, p 314.

40. A.B. Elkowitz and R.E. Wyatt, J. Chem. Phys. 63, 702 (1975).

41. D.J. Zvijac and J.C. Light, Chem. Phys. 12, 237 (1976).

FIGURE CAPTIONS

1. Natural collision coordinates for 3-D reactive scattering. Z_r and z_r are the components of the mass scaled F-H_2 and HH relative separations on the body-fixed Z-axis. Z_p and z_p (not shown) are the components of the corresponding product separations on the BF Z-axis. Nonlinear geometries are measured with m; the m=0 plane is the collinear plane. The reaction coordinate s is measured along the reference curve RC. In the reactant and product Cartesian regions, planes of constant s lie perpendicular to Z_r and Z_p, respectively, while in the polar region constant s planes intersect the collinear plane on lines connecting the turning center TC and the reactant or product Z-axes. The floating origin[40] FO for r and γ varies with s and is introduced to simplify terms in the rotational Hamiltonan. The TC is located at (7.000, 2.579), and the radius of the circular reference curve is 1.563. The cartesian-polar boundaries are at s=-1.904 and s=+1.740 in reactants and products, respectively. At large to moderate separations, γ is the geometric angle between the molecule and atom-molecule vectors.
2. Adiabatic energy correlation diagrams (energies in eV). (a) vibrational energies E_v ; (b) vibrational energies plus the translational potential V_{tr} ; (c) hindered asymmetric top energies W_j for J=0; (d) the sum of the translational potential, lowest vibrational energy, and top energies.

3. (a)-(f) The real part of the diabatic translational wavefunctions at the total energies 0.33, 0.36, and 0.40 eV. Only four vibrotor TW in each of the v=0,1 and 2 manifolds for the 60 channel basis are shown. (a)-(c) are reactant tube TW; (d)-(f) are product tube TW.
4. (a) The average vibrational energy and (b) the average rovibrational energy. The average energy curves are shown with dots, and the background curves are the vibrational energy levels.
5. Entropies as a function of s for the three system energies considered (units are k, Boltzmann's constant).
6. A semi-log plot of the integrated s-plane wavefunction densities for the total energies 0.33, 0.36, and 0.40 eV.

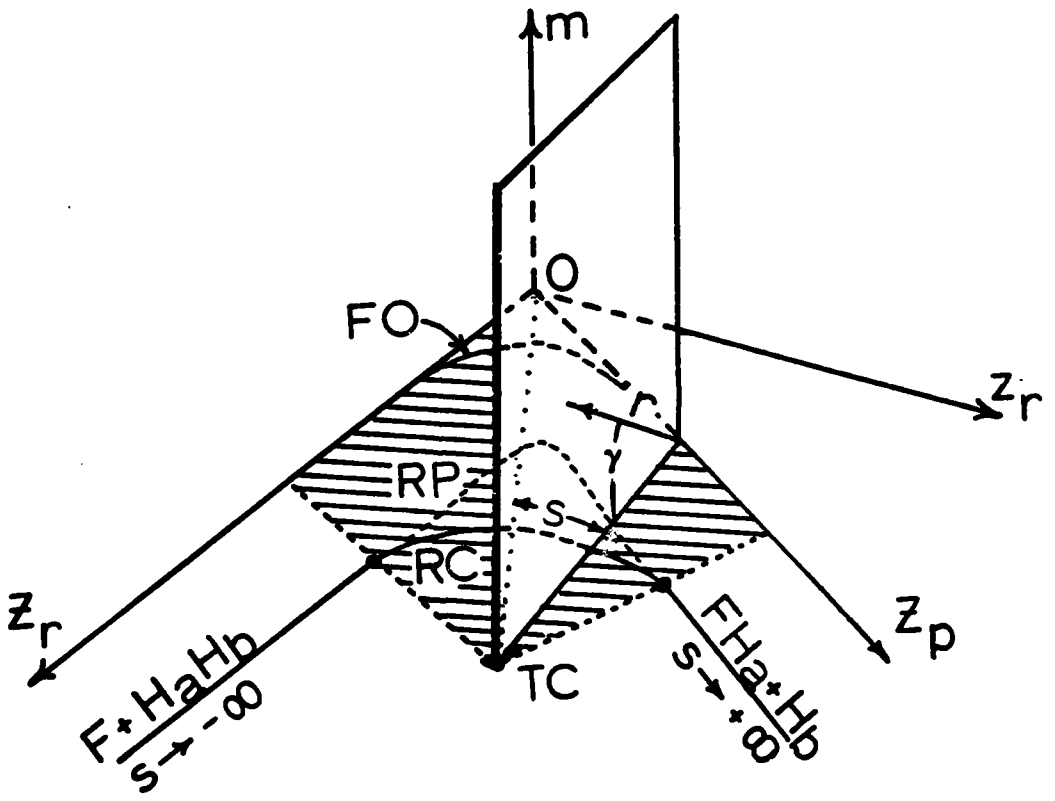

Figure 1

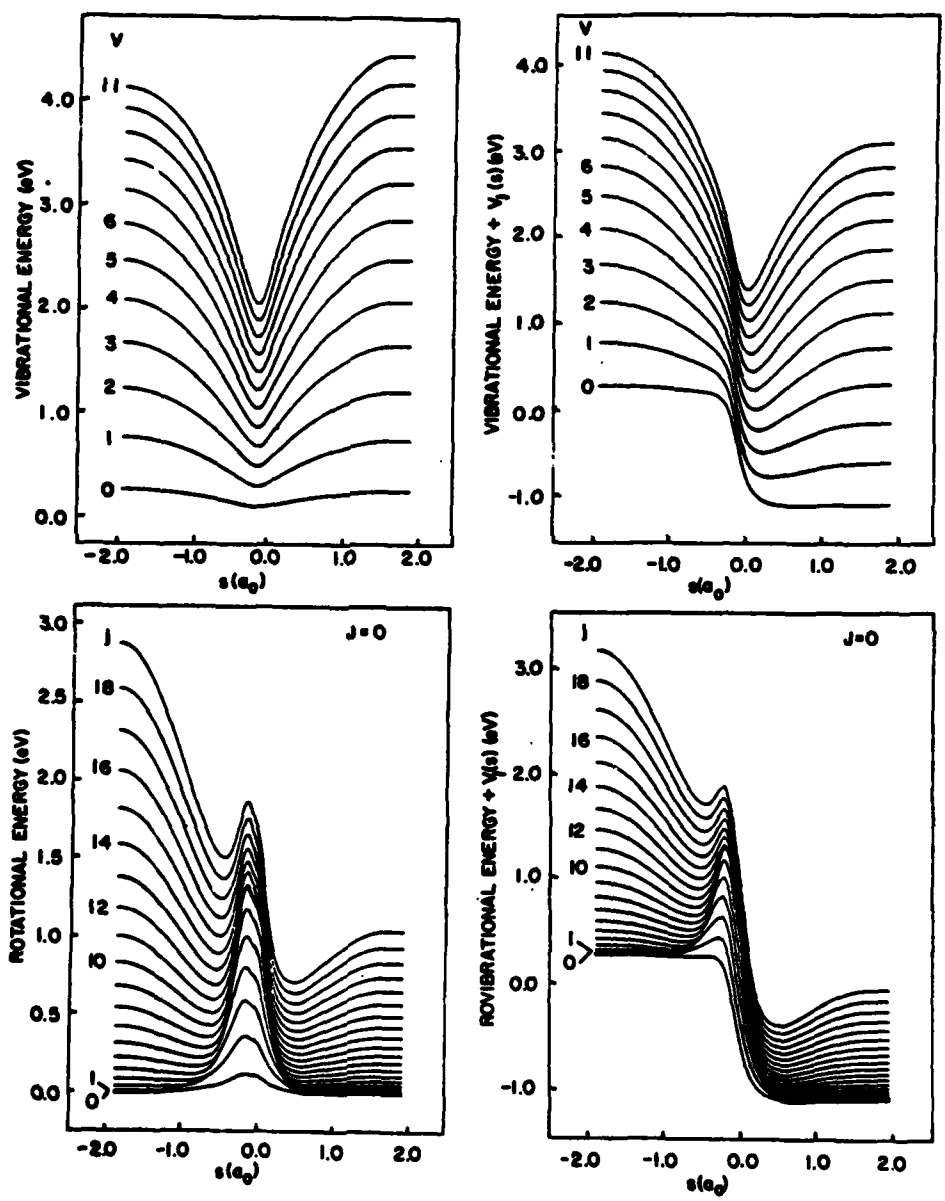
V
11
6
5
4
3
2
1
0
VIBRATIONAL ENERGY (eV)
VIBRATIONAL ENERGY + V_J (s) (eV)
s(a_0)
J
J=0
ROTATIONAL ENERGY (eV)
ROVIBRATIONAL ENERGY + V_J(s) (eV)

Figure 2

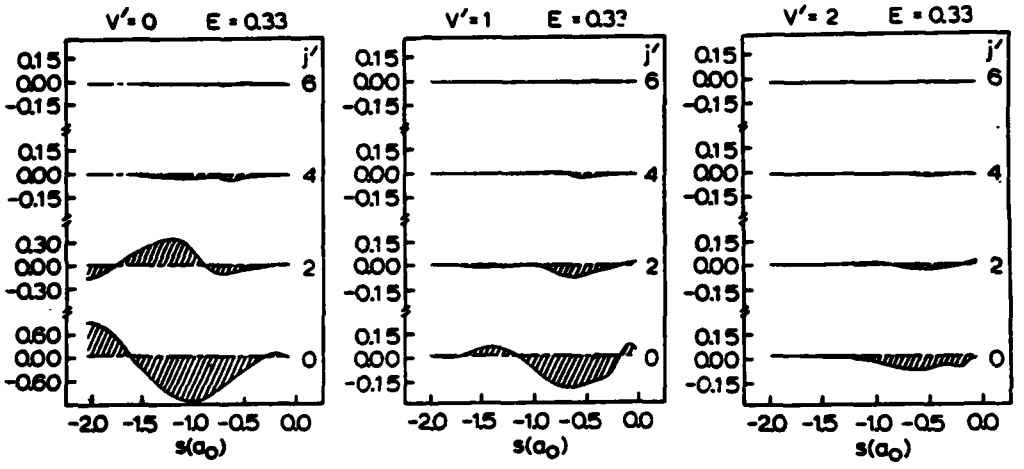
V'= 0 E = 0.33
V'= 1 E = 0.32
V'= 2 E = 0.33
j'
6
4
2
0
0.15
0.00
-0.15
0.30
-0.30
0.60
-0.60
-2.0 -1.5 -1.0 -0.5 0.0
s(a0)

Figure 3a

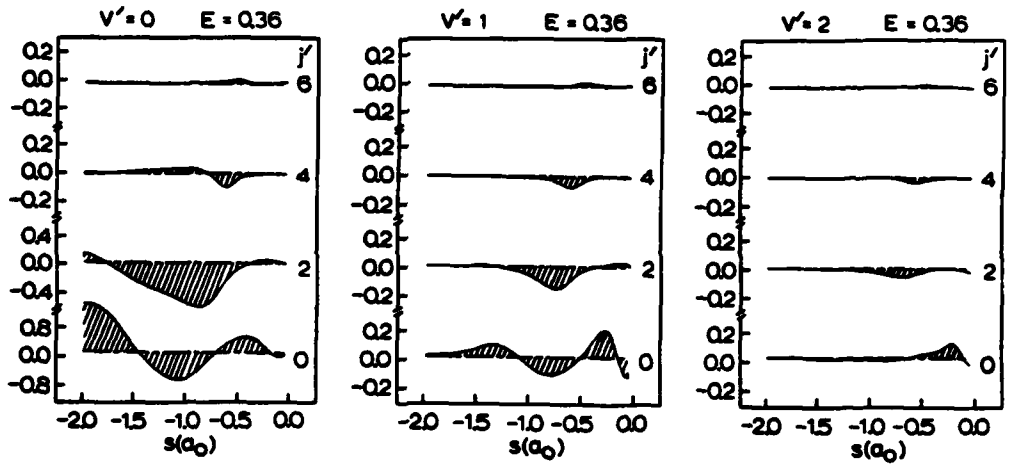
V'=0 E=0.36
V'=1 E=0.36
V'=2 E=0.36
j'
6
4
2
0
0.2
0.0
-0.2
0.4
-0.4
0.8
-0.8
-2.0 -1.5 -1.0 -0.5 0.0
s(a0)

Figure 3b

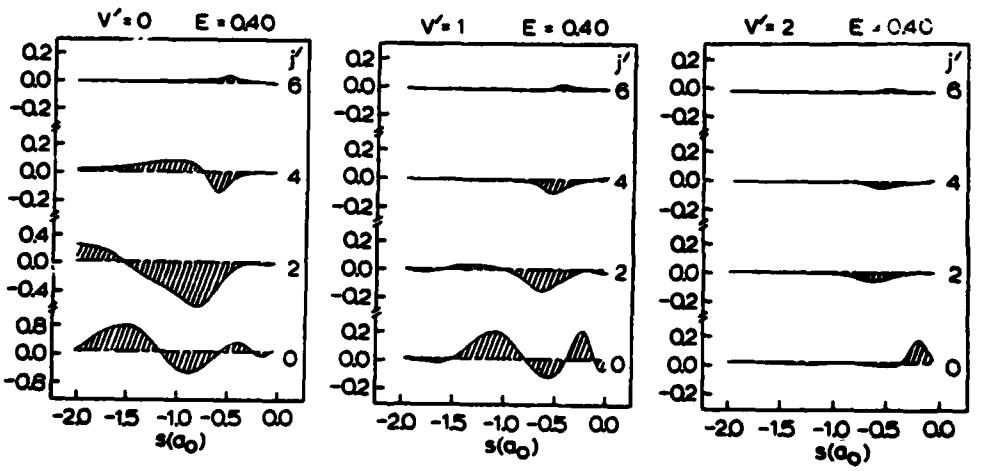
V'=0 E=0.40
V'=1 E=0.40
V'=2 E=0.40
j'
6
4
2
0
0.2
0.0
-0.2
0.4
-0.4
0.8
-0.8
-2.0 -1.5 -1.0 -0.5 0.0
s(a0)

Figure 3c

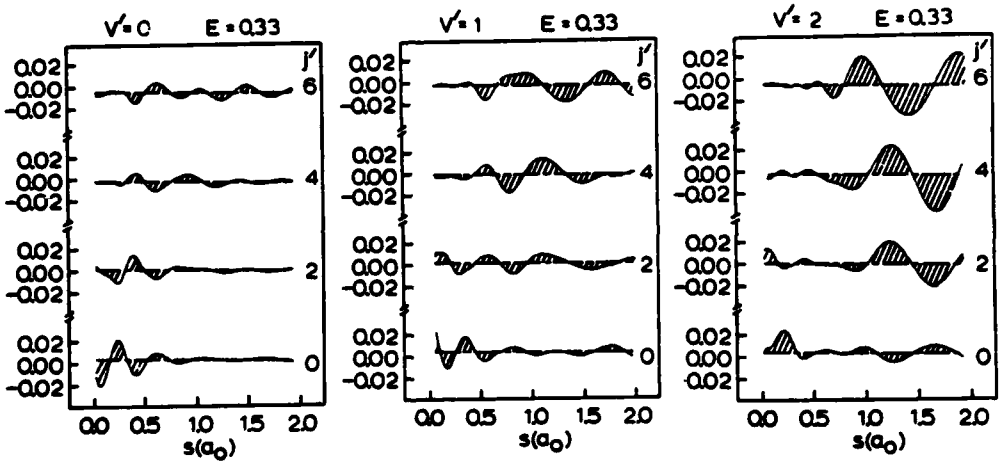

Figure 3d

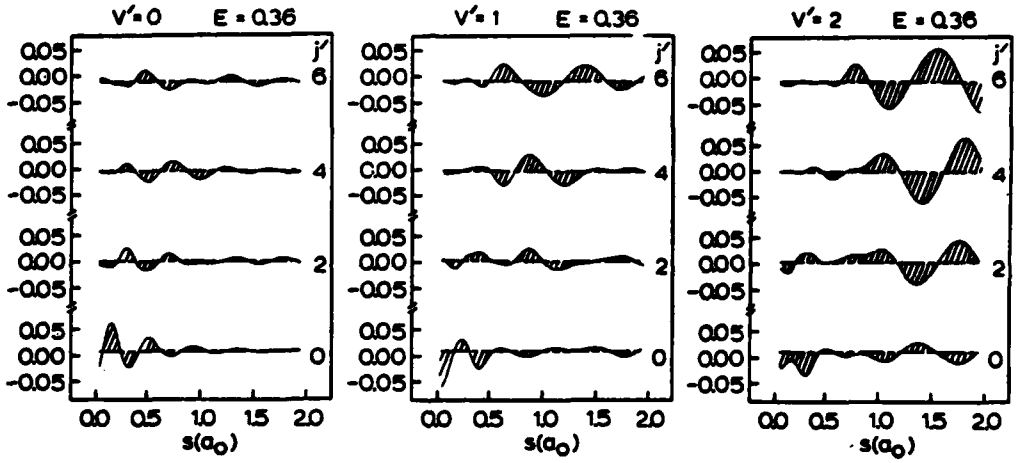

Figure 3e

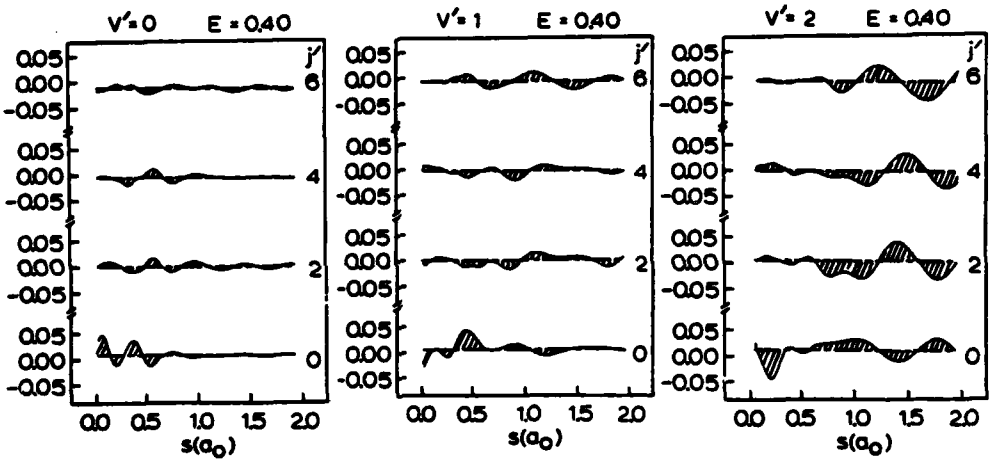

Figure 3f

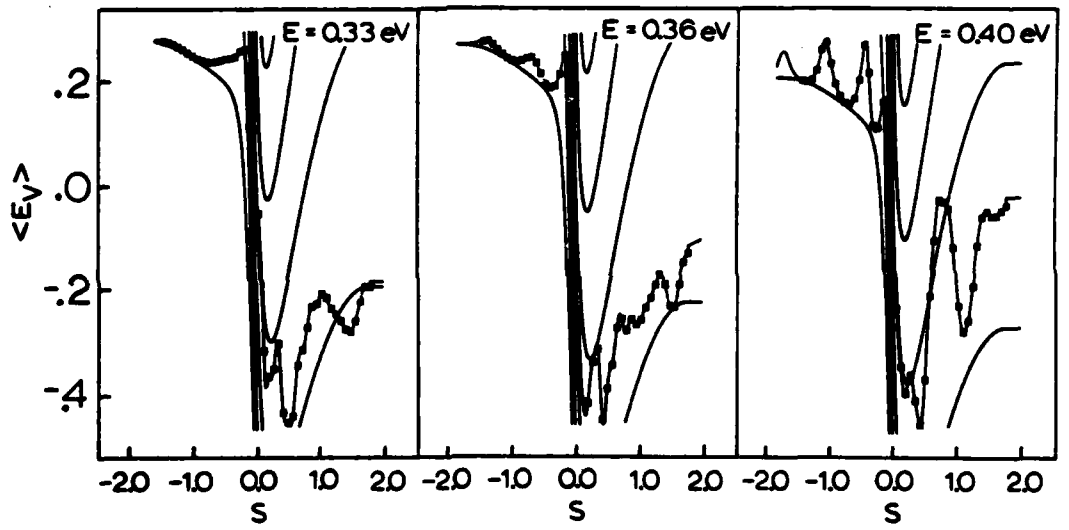

Figure 4a

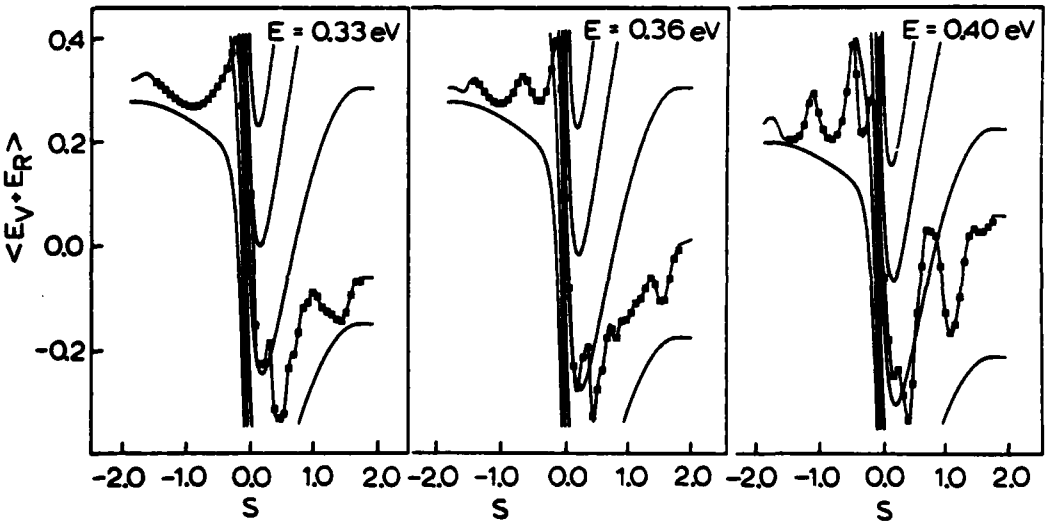

Figure 4b

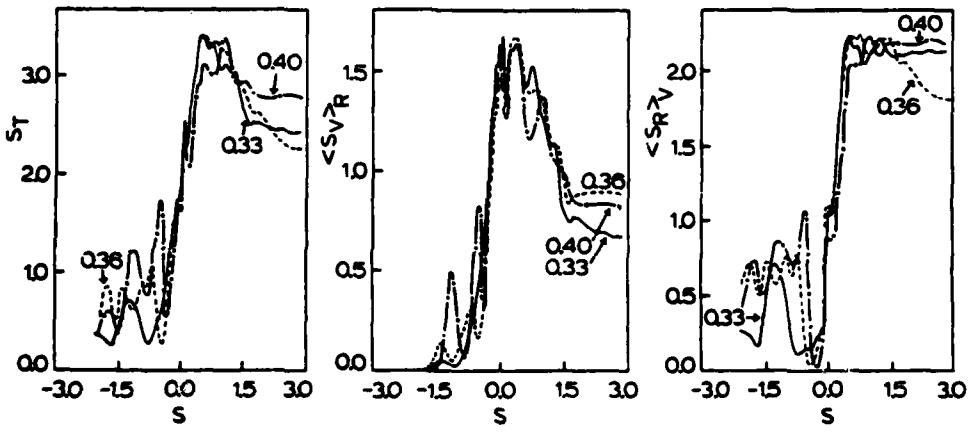
s_T
3.0
2.0
1.0
0.0
0.40
0.33
0.36
-3.0 -1.5 0.0 1.5 3.0
s
$\langle s_V \rangle_R$
1.5
1.0
0.5
0.0
0.36
0.40
0.33
-3.0 -1.5 0.0 1.5 3.0
s
$\langle s_R \rangle_V$
2.0
1.5
1.0
0.5
0.0
0.40
0.36
0.33
-3.0 -1.5 0.0 1.5 3.0
s

Figure 5

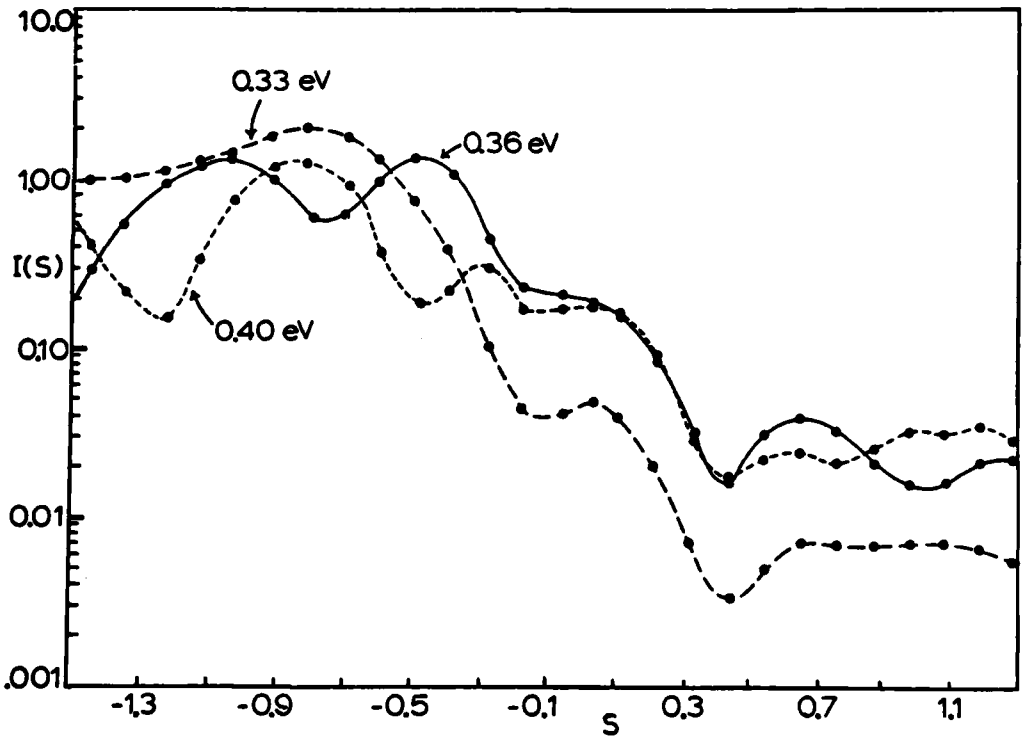

Figure 6

APPENDIX B

Quantum Mechanical Differential Reaction Cross Sections for the $F+H_2$ Reaction

DRAFT

Quantum Mechanical Differential Reaction Cross Sections for the $F+H_2(v=0) \rightarrow FH(v'=2)+H$ Reaction*

by

Robert E. Wyatt

Department of Chemistry
The University of Texas
Austin, Texas 78712

and

Michael J. Redmon

Chemical Dynamics Corporation
1550 W. Henderson Road
Suite N-140
Columbus, Ohio 43220

ABSTRACT

Velocity-scattering angle intensity maps for the $F+H_2(v=0,j=0) \rightarrow FH(v'=2,j')+H$ reaction are predicted from quantum mechanical J_z-conserving calculations. The shift in the angular distribution from backscattering at 1.8 kcal/mole to sideways scattering (intensity peak at 100°) at 3.0 kcal/mole is in quantitative agreement with recent high resolution crossed molecular beam experiments.

*Supported in part by the National Science Foundation and the Robert A. Welch Foundation, and by the Air Force Office of Scientific Research, U.S. Air Force (AFSC), under contract number F49620-81-C-0046.

Quantum mechanical resonance structure in the collinear[1] $F+H_2(v=0) \rightarrow FH(v'=2)+H$ reaction was predicted in 1973 and in the three-dimensional reaction[2] in 1979. In order to illustrate their results, Redmon and Wyatt plotted the reaction probability surface for $v=0 \rightarrow v'=2$ reaction. This is a surface of total probability for the reaction $(v=0,j=0) \rightarrow (v'=2,\Sigma j')$, plotted vs. total energy E and total angular momentum J (since j=0 in reactants, $J=\ell$, where ℓ is the atom-molecule relative orbital angular momentum; ℓ is related to the impact parameter, $\mu vb \approx \ell h$). This reaction probability surface is shown in Figure 1; as E is increased at each value of J, the reaction probability suddenly increases, reaches a peak at the resonance energy $E_r(J)$, and then declines onto a shoulder at higher energy. The "resonance ridge" of high reactivity moves to higher E as J increases. (The J dependence of E_r is remarkably well predicted by a new semiclassical model based upon resonant periodic orbits[3]). Up to 0.35 eV, the reaction probability declines monotonically with J. However, for $E \lesssim 0.37$ eV, the peak reactivity is reached for a nonzero value of J (e.g., at 0.40 eV, the peak reactivity occurs at about J=10). By way of contrast, the $0 \rightarrow 3$ reaction probability surface decreases monotonically with increasing J, for $E \lesssim 0.50$ eV. The purpose of this Letter is to show that these quantum mechanical results also predict that the $0 \rightarrow 2$ differential reaction cross section undergoes a dramatic change when the energy is increased from 0.35 to 0.40 eV.

In their 1979 crossed molecular beam studies of the $F+H_2$ reaction, Sparks et al.[4] found results which are qualitatively consistent with the quantum mechanical reaction probability surfaces. When the product in-

tensity was plotted in terms of velocity-scattering angle intensity maps, then at a mean relative collision energy of 2.0 kcal/mole, the product molecules for v'=1, 2, and 3 were all scattered predominately in the $\theta = 180°$ backward direction (i.e, back in the direction from which F approached the H_2 molecule.) However, when the mean collision energy was increased slightly to 3.2 kcal/mole, the peak in the v'=2 product distribution moved to a smaller angle - extensive sideways scattering occurred. By way of contrast, the v'=1 and 3 distributions remained primarily back-scattered at the higher energy. On the basis of the reaction probability surfaces, and the new quantum results reported here, we interpret the shift to sideways scattering in the HF(v'=2) product distribution as a direct manifestation of the quantum resonance.

Before presenting results for the $F+H_2$ reaction, we will briefly review the relevant theory[5]. In an atom-diatom collision at total angular momentum J, if we were following the close-coupling (CC) procedure, the total scattering wavefunction would be expanded in products of local vibrational and rotational basis functions. In our approach, the rotational basis functions are hindered asymmetric top states[7], which are labeled by the asymptotic quantum numbers j and ℓ. Here j is the rotational quantum number of the diatom and ℓ denotes the atom-molecule relative (orbital) angular momentum quantum number. The triangle inequality limits the range of allowed values for ℓ: $|J-j| \leq \ell \leq J+j$ (parity selection rules further limit the number of ℓ's in this interval). Except for very low energies, the number of vibration-rotation channels ($vj\ell$) in a close-coupling calculation at energy E and total angular momentum J is so huge that we are

prevented from obtaining "exact" solutions of the CC equations. For this reason, we are forced to use a channel reduction scheme to cut the total number of channels down to a workable level. In our version of the J_z-conserving approximation[8], which was used in all calculations for $J > 0$, we use only one asymmetric top function in the wavefunction expansion for each value of J and j. This special value of ℓ (denoted L) is selected automatically[8] such that these asymmetric top states produce a maximum concentration of amplitude for near-collinear geometries in the collision complex. The procedure is called "J_z-conserving" because the asymmetric top states which are used always concentrate amplitude in the FHH K=0 bending states (K is the angular momentum quantum number for twist about the z-axis of the complex). Solution of the reduced set of CC equations then leads to S-matrix elements (amplitudes for outgoing waves) which are labeled $S^J_{v_o j_o L_o \to vjL}$, or since we are interested here in reactions initiated from the ground state of $H_2(v=0,j=0)$, we will use a shortened notation for the S-matrix elements: S^J_{vjL} (where L is determined uniquely by J and j).

Once the S-matrix elements have been computed, we can use them to construct both differential and total reaction cross sections. The differential reaction cross section is computed from the helicity amplitude:

$$h_{vj}(\theta;E) = (\sqrt{2}\, k_o)^{-1} \sum_{J=0}^{\infty} (2J+1)^{\frac{1}{2}}\, \bar{P}_J(\theta) S^J_{vjL}(E), \qquad (1)$$

where k_o is the reactant channel translational wavenumber ($E_{trans} = \hbar^2 k_o^2 / 2\mu_r$, $\mu_r = m_A(m_B+m_C)/(m_A+m_B+m_C)$), and where $\bar{P}_J(\theta)$ is a normalized Legendre polynomial. The angle θ is defined so that $\theta = 180°$ corresponds to "backscattering" of FH in the direction from which F approached the H_2 molecule. The differential reaction cross section is then

$$\sigma_{vj}(\theta;E) = |h_{vj}(\theta;E)|^2. \tag{2}$$

Finally, the total reaction cross section is given by

$$\sigma_{vj}(E) = \int_0^{\pi} \sin\theta d\theta \int_0^{2\pi} d\phi \; \sigma_{vj}(\theta,E)$$

$$= \frac{\pi}{k_o^2} \sum_{J=0}^{\infty} (2J+1) |S^J_{vjL}|^2. \tag{3}$$

The S-matrix elements are complex numbers whose magnitude and phase enters the computation of $\sigma_{vj}(\theta;E)$, while only magnitudes enter the total cross section. Equation (3) is the same one that we previously used to obtain total cross sections from the S-matrix[2].

The J_z-conserving calculations[9] were performed at two total energies (measured from the bottom of the F+H_2 entrance valley; E_{trans} = E-0.27 eV), 0.35 and 0.40 eV, which correspond to relative collision energies of 1.8 and 3.0 kcal/mole, respectively. At each energy, J_z-conserving calculations were performed for each value of J between 0 and 18. The basis sets always employed 10 vibrational manifolds, with the following rotor distributions:

16/14/12/12/6/2/2/2/2/2, 0.35 eV;

18/18/18/16/14/12/6/4/2/2, 0.40 eV.

This notation means that a total of 16 hindered rotor states were used in the v=0 manifold at 0.35 eV, etc. In spite of the fact that a larger basis was used at the higher energy (110 channels, vs. 70 at the lower energy), the results at 0.40 eV are less converged than at 0.35 eV. Particularly for $J \gtrsim 10$, the S-matrices are not fully converged with respect to shifting rotor basis functions from one manifold to another. In spite

of this, we believe that the results presented here have at least "semi-quantitative" validity.

It was mentioned earlier that the helicity amplitude (and hence the differential cross section) depends upon both mangitudes and phases of individual S-matrix elements. Lack of convergence in the S-matrix elements (particularly the phases) can lead to artificial wiggles in the computed differential cross sections. In order to avoid artificial oscillations in the cross sections, we carefully examined the "smoothness" of both the magnitudes and phases of all S-matrix elements, at both energies. Plots were made of $|S^J_{vjL}|$ vs. J at each value of j for v=2. In addition, if ϕ^J_{vjL} denotes the phase of an S-matrix element, plots were made of ϕ^J_{vjL} and $(\phi^{J+1}_{vjL} - \phi^J_{vjL})$ vs. J (again, for each j at each E). In some cases (usually higher J values), magnitudes and phases were adjusted "by eye" to produce smooth looking plots. In spite of the somewhat subjective character in this procedure, we felt that it compensated to some extent for convergence errors in the S-matrices.

The differential cross sections for the $F+H_2(v=0,j=0) \rightarrow FH(v'=2,j')+H$ reaction at 0.35 and 0.40 eV are shown in Figures 2 and 3, respectively. The results are shown as intensities $I(V,\theta)$ on velocity-angle maps, where "velocity" refers to the recoil speed of FH and H in the v'j' final channel, and where "angle" refers to the reactive scattering angle θ in Eqs. (1) and (2). A contour map, with cross-hatched maxima, is shown in the left panel of each figure, and a more dramatic perspective plot (viewed from the "forward" direction) is shown in the right panel. Of course, only specific final speeds (radii) corresponding to v'j'=(2,0), (2,1), ... are possible,

but the contour and perspective routines automatically fill in other values to make continuous functions for plotting. Looking first at Figure 2, the intensity is clearly peaked at $\theta = 180°$ (backscattering), and the dominant rotor distribution is for $j'=4-5$. There is a smooth, monotonic decline in $I(V,\theta)$ as θ moves to the forward direction; practically no intensity is found in the forward hemisphere. Turning now to Figure 3, we note the dramatic qualitative change in the intensity. The intensity has now shifted so that it now peaks at $\theta = 100°$, a full 80° off the backward direction, with $I(V, 100°)/I(V, 180°) \sim 2$. In addition, the rotor distribution peaks at $j'=3$; the cross-hatched peaks lie at slightly smaller radii (speeds) than the outer limiting circle (corresponding to $v'=2$, $j'=0$). (The rotational distribution peaks at higher j' values for calculations with other basis sets; this point is under investigation). Also apparent in Figure 3 is the small backward peak at $\theta = 180°$; unlike the major peak near $\theta = 100°$, the height of this peak is particularly sensitive to <u>phases</u> of the S-matrix elements. At this point, we cannot say definitively that there is really a small ripple in $I(V,\theta)$ in the backward direction. We are much more confident in claiming that the large peak near 100° is a reflection of the dynamics and the underlying potential surface.

The sideways shift in the $v'=2$ quantum mechanical product intensity map is in agreement with intensity maps from crossed molecular beam experiments. In recent high resolution $F+H_2$ experiments[10] (which came several years after the 1979 results that were reported in ref. 4) in which the most probable collision energy was 3.1 kcal/mole, with a FWHM of only 0.04 kcal/mole, the product intensity for $v'=2$ peaked at about 100°, with a most probable rotational quantum number of about $j'=7$. In addition, the $v'=2$ intensity near 100° is about a factor of 1.7 higher than in the backward direction. Al-

though our current calculations underestimate the extent of rotational excitation in the v'=2 manifold, the shift of the intensity peak as the collision energy is increased from 2 to 3 kcal/mole is in quantitative agreement with the high resolution beam results!

Comparisons of these results with other theoretical predictions are of interest. First, quasiclassical trajectory calculations on the Muckerman V potential surface, even at a collision energy of 5 kcal/mole, fail to predict sideways scattering of the HF(v=2) molecules[11]. Classical mechanics completely misses the sideways shift in the v'=2 intensity that occurs between 0.35 and 0.40 eV! Turning to quantum calculations, IOS calculations[12] have been performed at selected energies between 0.31 and 0.50 eV on the Muckerman V potential surface. The v=2 differential reaction cross section at 0.36 eV is backpeaked, but shows a slight shoulder between 80° and 120°. When the energy is increased to 0.423 eV, the differential reaction cross section has about the same values at 85° and 180°, but is 10% lower at 140°, and declines rapidly for $\theta \lesssim 70°$. At 0.50 eV, there is a slight sideways peak at $\theta = 40°$; the height at 40° is 40% higher than at 180°. There is clearly a trend toward sideways scattering at higher energies in the IOS results, but the extent of the angular shift between 0.35 and 0.40 eV that appears in both the J_z-conserving calculations, and in the experimental results, is not quantitatively predicted. This is probably due to an important difference between the J_z-conserving and the IOS reaction probabilities; in the J_z-conserving case, for $E \gtrsim 0.37$ eV, the peak reaction probability in v'=2 occurs for $J > 0$ (resonance ridge in Figure 1), while the IOS calculations predict flat reaction probabilities between J=0 and J_{max} ($J_{max} = 10$ at 0.423 eV). Another approximate quantum procedure for generating differential cross sections has recently been proposed[13]. S-matrix

elements for $v \rightarrow v'$ collinear reactions were used (at shifted energies to account for both centrifugal effects and the bending energy of the complex) in Eq. (2) to generate "rotationally summed" cross sections. In going from E_{trans} = 1.0 up to 2.9 kcal/mole, $\sigma_{0\rightarrow 2}$ shifts from backpeaked to sidepeaked, with a maximum near 165°. In addition, the ratio $\sigma_{0\rightarrow 2}(165°)/\sigma_{0\rightarrow 2}(180°)$ is about 2.5 at the higher energy. In this model, the $0 \rightarrow 2$ reaction probability, when plotted vs. J, peaks at J=12 at 2.9 kcal/mole, but monotonically declines from its value of J=0 at the lower energy. These trends are in qualitative agreement with our J_z-conserving results. Finally, DWBA differential reaction cross sections[14] have been computed at several total energies between 0.31 and 0.57 eV. Comparing results at 0.37 eV and 0.57 eV, the peak in $\sigma_{0\rightarrow 2}$ moves forward from 180° to 110°. Again, we see a trend to sidepeaking, but neither the onset nor the extent of sideways scattering is as abrupt as in both the J_z-conserving results and the experimental beam results.

In summary, from quantum mechanical calculations within the J_z-conserving approximation, product intensity maps have been generated for the $F+H_2(v=0,j=0) \rightarrow FH(v'=2,j')+H$ three-dimensional reaction. The extent of the sideways shift in the angular distribution is in quantitative agreement with recent high resolution crossed molecular beam results. We believe that this sideways shift is a direct manifestation of a quantum mechanical resonance in the FHH collision complex. The nature of this resonance (including scattering wavefunction density and flux maps in the transition state region, entropy and vibrotational energy analysis along the reaction coordinate, Argand diagrams showing the energy dependence of selected S-matrix elements, phase shift analysis, time-delays computed from the energy derivatives of the S-matrix phases, and a kinematic model for the sideways shift in the angular distribution) is explored in more detail elsewhere[15].

Figure Captions

1. Quantum mechanical reaction probability surface for the F+H(v=0, j=0) → FH(v'=2,Σj')+H reaction (adapted from ref. 2). J is the same as ℓ, the atom-molecule orbital angular momentum quantum number. E_{TOT} is the total energy, measured from the bottom of the entrance valley.

2. Product intensity for v'=2 in velocity-scattering angle variables. The energy is 0.35 eV (the total v=0 → v'=2 reaction cross section is $1.2a_o^2$). The left panel shows a contour map of the intensity, with cross hatched maxima. The right panel shows a perspective view of the intensity, viewed from 45° off the forward direction.

3. Product intensity for v'=2 in velocity-scattering angle coordinates. The energy is 0.40 eV. At this energy, the total v=0 → v'=2 cross section is $2.5a_o^2$. See the caption to Figure 2 for further details.

References

1. S. F. Wu, B. R. Johnson, and R. D. Levine, Mol. Phys. 25, 839 (1973); G. C. Schatz, J. M. Bowman, and A. Kuppermann, J. Chem. Phys. 58, 4023 (1973), 63, 674 (1975).

2. M. J. Redmon and R. E. Wyatt, Chem. Phys. Lett. 63, 209 (1979).

3. E. Pollak and R. E. Wyatt, to be published.

4. R. K. Sparks, C. C. Hayden, K. Shobatake, D. M. Neumark, and Y. T. Lee, in K. Fukui and B. Pullman (eds.), "Horizons of Quantum Chemistry," (Reidel, Dordrecht, 1980), p. 91.

5. J. F. McNutt, M. J. Redmon, and R. E. Wyatt, to be published.

6. R. E. Wyatt, in R. B. Bernstein (ed.) "Atom-Molecule Collision Theory: A Guide for the Experimentalist" (Plenum, N.Y., 1979), Ch. 9a.

7. S. H. Harms, A. B. Elkowitz, and R. E. Wyatt, Mol. Phys. 31, 177 (1976).

8. A. B. Elkowtiz and R. E. Wyatt, Mol. Phys. 31, 189 (1976).

9. The Muckerman V potential surface was used (see J. T. Muckerman in D. H. Henderson (ed.), "Theoretical Chemistry: Advances and Perspectives," 6A, (Academic, N.Y., 1981), p. 1) with a modified bending potential (see J. F. McNutt and R. E. Wyatt in D. G. Truhlar (ed.), "Potential Energy Surfaces and Dynamics Calculations" (Plenum, N.Y., 1981), p. 495. This potential surface has some well known inadequacies; see the first of refs. 12.

10. C. C. Hayden and Y. T. Lee, private communication, Dec. 1981. We gratefully thank these authors for their many helpful comments.

11. N. C. Blais and D. G. Truhlar, J. Chem. Phys. 76, 449 (1982).

12. M. Baer, J. Jellinek, and D. J. Kouri, J. Chem. Phys., to be published; J. Jellinek, M. Baer, and D. J. Kouri, Phys. Rev. Lett. 47, 1588 (1981).

13. J. M. Bowman, K. T. Lee, and G. Z. Ju, Chem. Phys. Lett. 86, 384 (1984).

14. S. H. Suck, Chem. Phys. Lett. 77, 390 (1980); S. H. Suck and R. W. Emmons, Chem. Phys. Lett. 79, 93 (1981); S. H. Suck and R. W. Emmons, Phys. Rev. A24, 129 (1981).

15. R. E. Wyatt, J. F. McNutt, and M. J. Redmon, Ber. der Bun.-Gesell. für Physik. Chemie, 86, (1982).

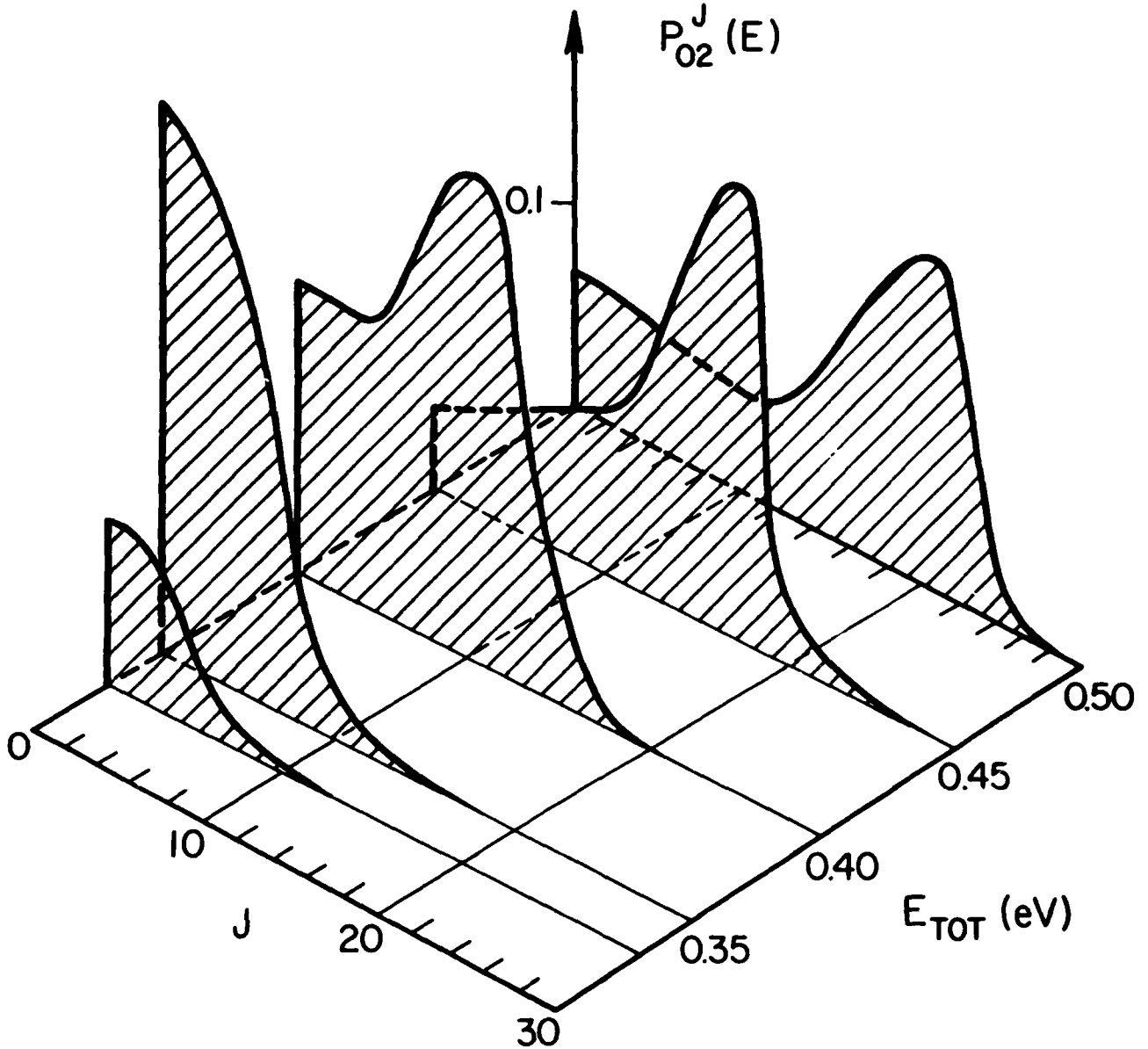
$P_{02}^{J}(E)$
0.1
0
10
J
20
30
0.35
0.40
0.45
0.50
E_{TOT} (eV)

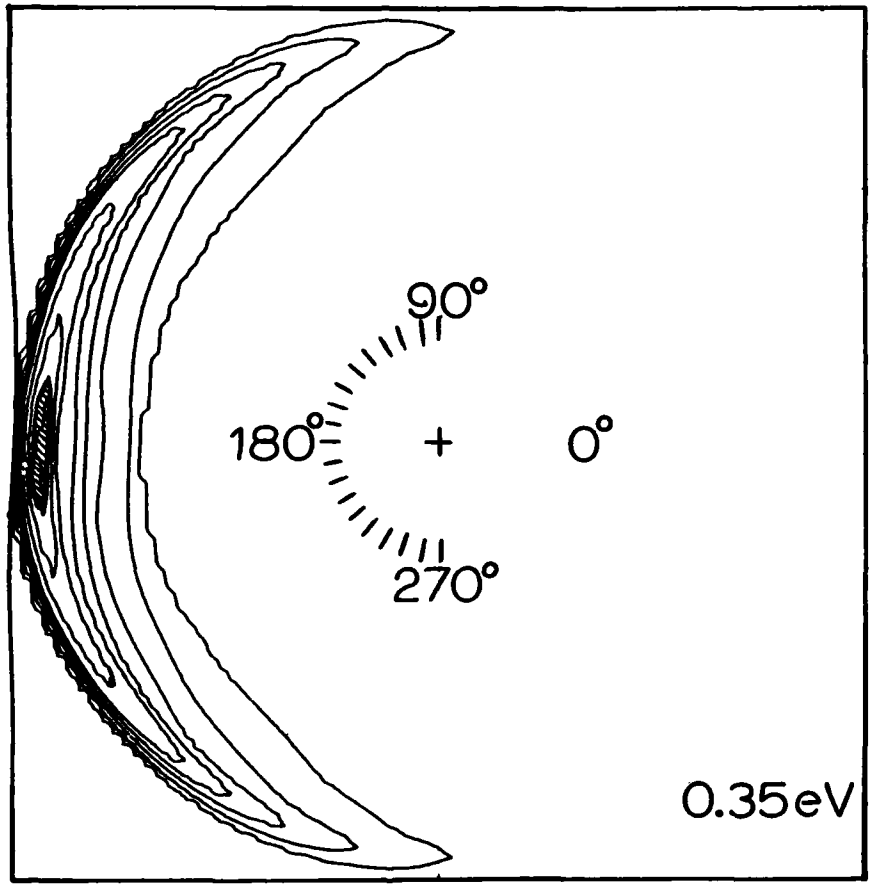
90°
180°
0°
270°
0.35eV

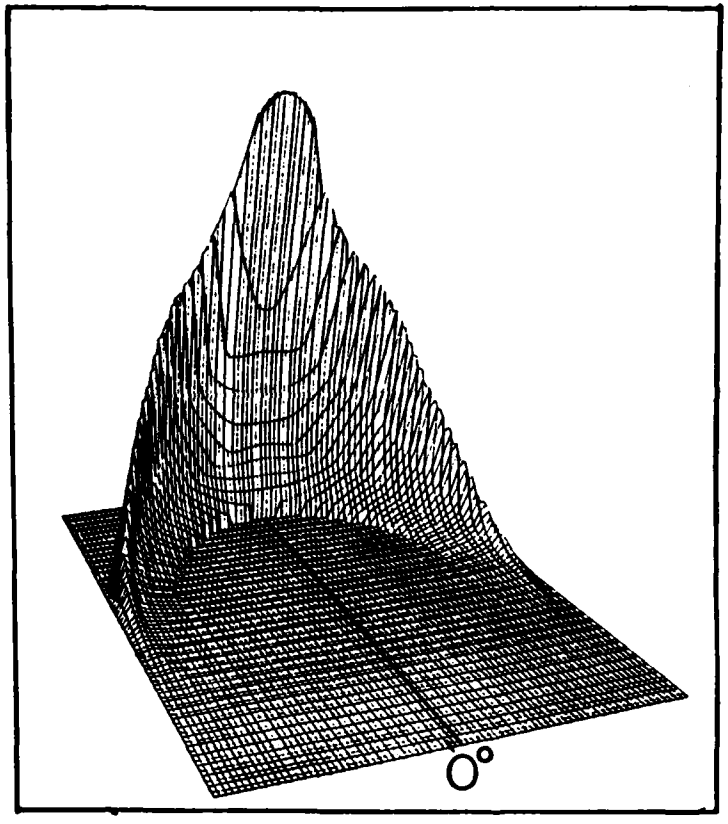
0°

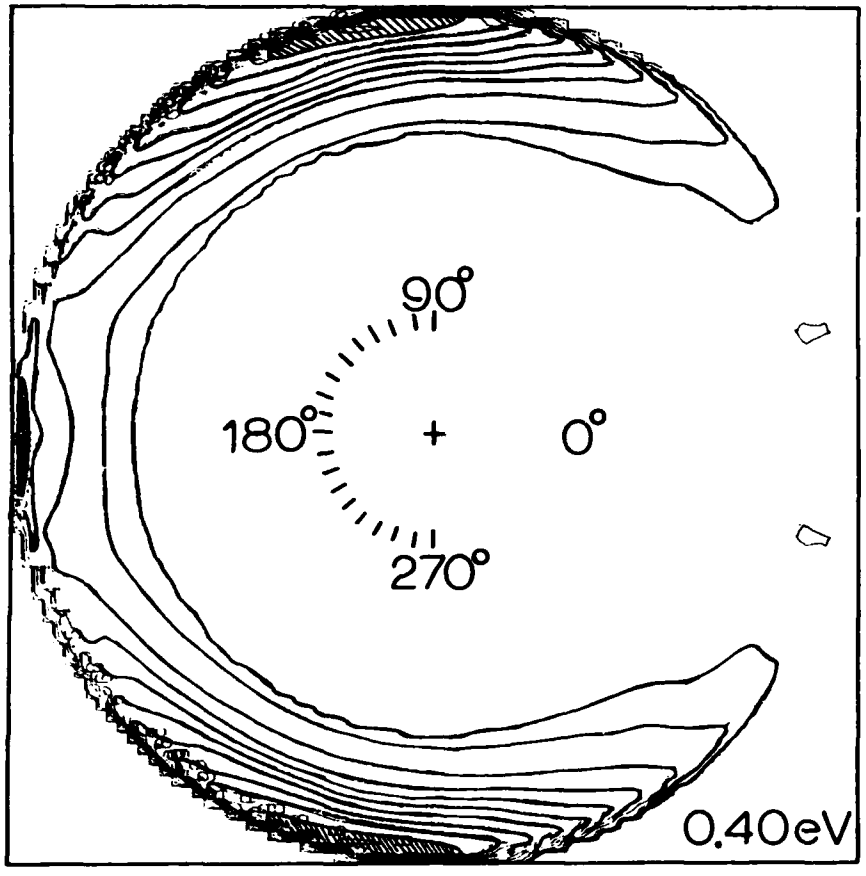
90°
180°
0°
270°
0.40eV

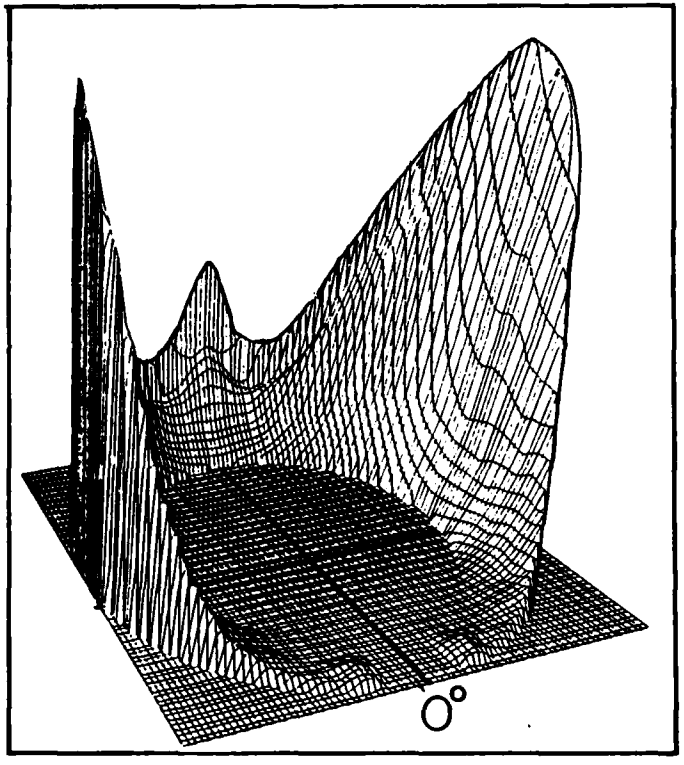
0°

APPENDIX C

The Quenching of $Na(3^2P)$ by H_2: A Quantal IOS Calculation of Electronic-to-Vibrational Energy Transfer

DRAFT

The Quenching of $Na(3^2P)$ by H_2: A Quantal IOS Calculation of Electronic-to-Vibrational Energy Transfer *

Bruce C. Garrett and Michael J. Redmon

Chemical Dynamics Corporation, 1550 W. Henderson Rd., Columbus, OH 43220

Donald G. Truhlar

Department of Chemistry, University of Minnesota, Minneapolis, MN 55455

* Supported by the Air Force Office of Scientific Research, U.S. Air Force (AFSC), under contract number F49620-81-C-0046.

I. Introduction

The quenching of electronically excited Na by H_2 is a prototype for electronic-to-vibrational energy transfer in molecular collisions. This process has been widely studied both experimentally[1-5] and theoretically.[6-11] The theoretical interpretation of the quenching process has focused upon the states of $^2A'$ symmetry; the lowest $^2B_2$ state has a well and exhibits an avoided crossing with the ground state surface. Previous dynamical studies indicate that these two electronic states can qualitatively describe the quenching process.[6,10] A quantitative description of this process requires accurate ab initio potential energy surfaces for the electronic states of importance and the nonadiabatic coupling terms between these electronic states. Ab initio calculations of the $^2A'$ states have been made;[7-9] however, the nonadiabatic coupling terms have not been reported.

Recently a diatomics-in-molecules (DIM) potential energy surface has been presented for the three lowest-energy potential energy surfaces of NaH_2.[10,11] The two lowest-energy surfaces agree well with the work of Botschwina and Meyer.[7,9] A major advantage to using the DIM formalism is that it provides a global representation of the potential energy surfaces and the couplings between the surfaces.

There has been a large amount of work on developing methods for the quantum mechanical treatment of electronic transitions in atom-molecule collisions.[12-17] The early work of Zimmermann and George[12] compared the use of diabatic and adiabatic representations. In the adiabatic representation coupling between different electronic states introduces first-derivative terms in the coupled-channel equations. Zimmermann and George solved the adiabatic coupled-channel equations by transforming the N second-order differential equations into a set of 2N first-order

differential equations. Baers approach[13] to the problem sought to obtain coupled channel equations that could be solved using the efficient computational algorithms developed for second-order differential equations. In his approach a transformation is made from the adiabatic representation to a diabatic representation in which all coupling arises through off diagonal elements of the potential matrix. This approach has been applied to collinear atom-diatomic collisions but is limited to systems in which only two electronic states are important. More recently Rebentrost and Lester[14] have used a similar diabatic transformation to treat the nonreactive F + H_2 problem in three dimensions.

The previous quantum mechanical calculation on Na + H_2 by McGuire and Bellum[6] used the two lowest-energy adiabatic potential energy surfaces as an approximation to the diagonal diabatic potential energy surfaces. The off-diagonal terms of the diabatic potential were modelled as gaussian terms centered on the location of the minimum of the energy difference on the crossing seam. Cross sections were caluclated within the Infinite-Order-Sudden (IOS) approximation;[18] however, the integral over the IOS angle was approximated using only the 90 degree approach of the Na to the H_2 molecule.

In the present calculation we describe a new method for calculating electronic transition cross sections using adiabatic potential energy surfaces and the nonadiabatic coupling terms as input. In this approach we use a mixed adiabatic-diabatic representation in which the motion in the diatomic internuclear distance is treated diabatically and the motion in the Na to center-of-mass of H_2 distance is treated adiabatically. We use the IOS approximation and converge the calculations with respect to the numerical integral over IOS angles.

In section II we present the details of the new theoretical method and in section III we present details of the computational procedure. Section IV contains results of the calculations and section V presents a discussion.

II. Theory

We consider the collision of an atom A with a diatomic molecule BC, where R is the distance from A to the center of mass of BC, r is the BC internuclear distance, and γ is the angle between the R and r vectors. Within the IOS approximation the total Hamiltonian is given by[19]

$$H_{IOS}^{j,\ell} = -\frac{h^2}{2\mu R}\frac{\partial^2}{\partial R^2}R + \frac{h^2\ell(\ell+1)}{2\mu R^2} + H_{int}^{j} \qquad (1)$$

where μ is the reduced mass for the R motion. The Hamiltonian for the internal motion is given by

$$H_{int}^{j} = -\frac{h^2}{2\mu_{BC} r}\frac{\partial^2}{\partial r^2}r + \frac{h^2 j(j+1)}{2\mu_{BC} r^2} + H_{el} \qquad (2)$$

where μ_{BC} is the reduced mass for the r motion. The Born-Oppenheimer electronically adiabatic wavefunctions are eigenfunctions of the electronic Hamiltonian H_{el}

$$H_{el}\,\phi_n^{aA}(\underline{x},r,R,\gamma) = V_n^{aA}(r,R,\gamma)\phi_n^{aA}(\underline{x},r,R,\gamma) \qquad (3)$$

where $\underline{x}$ is the collection of electronic coordinates and $V_n^{aA}(r,R,\gamma)$ is the electronically adiabatic potential energy surface for electronic state n. Within the IOS formalism the internal and orbital angular momenta, j and ℓ, are constants and are not coupled with the electronic angular momenta.

The total wavefunction for an initial state α_0 is expanded in eigenfunctions of the internal Hamiltonian

$$\psi^{J\ell}_{\alpha_o}(\underline{x},r,R,\gamma) = R^{-1}\sum_{\alpha}\psi^{J}_{\alpha}(\underline{x},r,R,\gamma)\ \chi^{J}_{\alpha\alpha_o}(R,\gamma) \tag{4}$$

where

$$H^{J}_{int}\ \psi^{J}_{\alpha}(\underline{x},r,R,\gamma) = E^{J}_{\alpha}(R,\gamma)\ \psi^{J}_{\alpha}(\underline{x},r,R,\gamma) \tag{5}$$

The wavefunctions for the internal degrees of freedom ($\underline{x}$ and r) are obtained as follows. For a fixed R and γ a transformation is made to a representation which is P-diabatic[17] with respect to the r motion

$$\phi^{dA}_{n'}(\underline{x},R,\gamma) = \sum_{n''} u^{dA}_{nn'}(r,R,\gamma)\ \phi^{aA}_{n}(\underline{x},r,R,\gamma) \tag{6}$$

This transformation is defined by

$$\frac{\partial}{\partial r}\, u_{nn'}(r,R,\gamma) = -\sum_{n''} f^{aA}_{nn''}(r,R,\gamma)\ u_{n''n'}(r,R,\gamma) \tag{7}$$

where

$$f^{aA}_{nn'}(r,R,\gamma) = \langle \phi^{aA}_{n}(\underline{x},r,R,\gamma) \left| \frac{\partial}{\partial r} \right| \phi^{aA}_{n'}(\underline{x},r,R,\gamma) \rangle_{\underline{x}} \tag{8}$$

and the subscript on the matrix element denotes the variables integrated over. The internal wavefunctions $\psi_{\alpha}(\underline{x},r,R,\gamma)$ are expanded in this P-diabatic basis

$$\psi^{J}_{\alpha}(\underline{x},r,R,\gamma) = r^{-1}\sum_{nv} \phi^{dA}_{n}(\underline{x},r,R,\gamma)\ \rho_{v}(r)\ C^{J}_{nv,\alpha}(R,\gamma) \tag{9}$$

where $\rho_v(r)$ is a vibrational basis function. Substituting (9) into (5) and closing from the left with $\int d\underline{x} \int dr\, r^2\, r^{-1}\, \phi_n^{dA^*}(\underline{x},R,\gamma)\, \rho_v^*(r)$ yields the eigenvalue equation

$$\underline{H}^J(R,\gamma)\, \underline{C}^J(R,\gamma) = \underline{C}^J(R,\gamma)\, \underline{E}^J(R,\gamma) \tag{10}$$

where the matrix elements of the internal Hamiltonian are given by

$$H^J_{nv,n'v'}(R,\gamma) = \int dr\, \rho_v^*(r) \left\{ \left[-\frac{h^2}{2\mu_{BC}} \frac{\partial^2}{\partial r^2} + \frac{h^2 j(j+1)}{2\mu_{BC} r^2} \right] \delta_{nn'} + V^{dA}_{nn'}(r,R,\gamma) \right\} \rho_{v'}(r) \tag{11}$$

and the potential matrix $V_{nn'}^{dA}$ is given by

$$\underline{V}^{dA}(r,R,\gamma) = \underline{u}^T(r,R,\gamma)\, \underline{V}^{aA}(r,R,\gamma)\, \underline{u}(r,R,\gamma) \tag{12}$$

The close coupling equations for a fixed γ are given by

$$\int d\underline{x} \int dr\, r^2\, \psi^{J^*}_{\alpha'}(\underline{x},r,R,\gamma) \left[H^{J\ell}_{IOS} - E \right] \Psi^{J\ell}_{\alpha_o}(\underline{x},r,R,\gamma) = 0 \tag{13}$$

Substituting equations (1) and (4) into (13) gives

$$\sum_\alpha \left\{ \left[-\frac{h^2}{2\mu} \frac{\partial^2}{\partial R^2} + \frac{h^2 \ell(\ell+1)}{2\mu R^2} + E^J_\alpha(R,\gamma) - E \right] \delta_{\alpha'\alpha} - \frac{h^2}{\mu} F^J_{\alpha'\alpha}(R,\gamma) \frac{\partial}{\partial r} - \frac{h^2}{2\mu} G^J_{\alpha'\alpha}(R,\gamma) \right\} \chi^{J\ell}_{u\alpha_o}(R,\gamma) = 0 \tag{14}$$

The coupling terms are defined by

$$F^J_{\alpha'\alpha}(R,\gamma) = \langle \psi^J_{\alpha'}(\underline{x},r,R,\gamma) \mid \frac{\partial}{\partial R} \mid \psi^J_\alpha(\underline{x},r,R,\gamma) \rangle_{\underline{x},r} \tag{15}$$

$$G^J_{\alpha'\alpha}(R,\gamma) = \langle \psi^J_{\alpha'}(\underline{x},r,R,\gamma) \mid \frac{\partial^2}{\partial R^2} \mid \psi^J_\alpha(\underline{x},r,R,\gamma) \rangle_{\underline{x},r} \tag{16}$$

Using equation (9) these can be rewritten as

$$F^{J}_{\alpha',\alpha}(R,\gamma) = \sum_{nvn'} C^{J}_{nv,\alpha'}(R,\gamma) \left[F^{J}_{nn'}(R,\gamma)\, C^{J}_{n'v,\alpha}(R,\gamma) + \delta_{nn'} \frac{\partial}{\partial R} C_{n'v,\alpha}(R,\gamma) \right] \tag{17}$$

where

$$F^{dA}_{nn'}(R,\gamma) = \langle \phi^{dA}_{n}(\underline{x},R,\gamma) \mid \frac{\partial}{\partial R} \mid \phi^{dA}_{n'}(\underline{x},R,\gamma) \rangle_{\underline{x}} \tag{18}$$

and

$$G^{J}_{\alpha',\alpha}(R,\gamma) = \sum_{nvn'} C^{J}_{nv,\alpha'}(R,\gamma) \left[G^{dA}_{nn'}(R,\gamma)\, C^{J}_{n'v,\alpha}(R,\gamma) + 2\, F^{dA}_{nn'} \frac{\partial}{\partial R} C^{J}_{n'v,\alpha}(R,\gamma) + \delta_{nn'} \frac{\partial^2}{\partial R^2} C^{J}_{n'v,\alpha}(R,\gamma) \right] \tag{19}$$

where

$$G^{dA}_{nn'}(R,\gamma) = \langle \phi^{dA}_{n}(\underline{x},R,\gamma) \mid \frac{\partial^2}{\partial R^2} \mid \phi^{dA}_{n'}(\underline{x},R,\gamma) \rangle_{\underline{x}} \tag{20}$$

The radial wavefunctions $\chi^{J\ell}_{\alpha\alpha_o}(R,\gamma)$ are subject to the standard boundary conditions[19]

$$\chi^{J\ell}_{\alpha\alpha_o}(R,\gamma) \mid_{R=0} = 0 \tag{21}$$

and

$$\chi^{J\ell}_{\alpha\alpha_o}(R,\gamma) \xrightarrow[R\to\infty]{} k^{-\frac{1}{2}}_{J\alpha} \left\{ \delta_{\alpha\alpha_o} \exp\left[-i(k_{J\alpha}R - \ell\pi/2)\right] - S^{J\ell}_{\alpha\alpha_o}(\gamma) \exp\left[i(k_{J\alpha}R - \ell\pi/2)\right] \right\} \tag{22}$$

where the asymptotic wavenumber is defined by

$$k_{J\alpha} = \frac{2\mu}{\hbar^2} \left[E - E^{J}_{\alpha}(R,\gamma) \right] \mid_{R\to\infty} \tag{23}$$

Opacity functions can be defined for each value of j and ℓ

$$P^{j\ell}_{\alpha\alpha_o} = \int d\gamma \sin\gamma \; | \; \delta_{\alpha\alpha_o} - S^{j\ell}_{\alpha\alpha_o}(\gamma) \; |^2 \tag{24}$$

and the total cross section for transition from initial state j, to final state α_o summed over all final j's is[19]

$$\sigma^{j}_{\alpha\alpha_o} = \frac{\pi}{2k^2_{j\alpha}} \sum_{\ell} P^{j\ell}_{\alpha\alpha_o} \tag{25}$$

III. Calculational details

A. Vibrational basis functions

The vibrational basis functions are chosen to be eigenfunctions of the asymptotic diatomic Hamiltonian. For the Na + H_2 system, all of the electronic states considered correlate asymptotically with H_2 in its ground electronic state. Within the DIM formalism, all electronic coupling vanishes for Na infinitely separated from H_2 and therefore the asymptotic diatomic Hamiltonian is simply that for a vibrating, rotating diatomic molecule. The vibrational basis function are defined by

$$\left[-\frac{h^2}{2\mu_{BC}} \frac{\partial^2}{\partial r^2} + \frac{h^2 j(j+1)}{2\mu_{BC} r^2} + V_{BC}(r) \right] \rho_v(r) = \rho_v \varepsilon_v(r) \tag{26}$$

where $V_{BC}(r)$ is the asymptotic BC vibrational potential. The basis functions are expanded in a harmonic oscillator basis, $\{h_k(r)\}$,

$$\rho_v(r) = \sum_k h_k(r) \, a_{kv} \tag{27}$$

All integrals over r are done by Gauss-Hermite quadrature; both for the

integrals necessary to define $\rho_v(r)$ and the integrals necessary in computing $\psi_\alpha(\underline{x},r,R,\gamma)$. The numerical values of the vibrational basis functions are stored on the grid of quadrature points $\{r_m\}_{m=1}^{M}$ to be used in subsequent numerical integrals.

B. P-diabatic transformation

Equation (7) for the transformation matrix $\underline{u}$ is solved by the Magnus method.[17] The transformation matrix is only needed at the Gaussian quadrature points and we approximate it as follows

$$\underline{u}(r_{m+1},R,\gamma) = \exp\left\{-(r_{m+1}-r_m)\,\underline{f}^{aA}\left[\tfrac{1}{2}(r_{m+1}+r_m),R,\gamma\right]\right\}\underline{u}(r_m,R,\gamma) \qquad (25)$$

The choice of $\underline{u}$ at the first grid point is arbitrary and the final results of the calculations are independent of this choice. The exponential of a matrix is evaluated by the method of ref. 20.

C. R-matrix propagation

Equation (14) is not solved directly for the radial wavefunctions, instead we use the R-matrix propagation method[21] to obtain a global R matrix for relating the radial wavefunction and its derivative a large R values. The S matrix is then obtained from the R matrix. The method for treating electronic transitions within the R-matrix propagation method when the input is in an adiabatic representation has been previously presented.[17] In brief review, the internal basis functions $\psi_\alpha(\underline{x},r,R,\gamma)$ are chosen to be independent of the radial coordinate R within each sector. Propagation across a sector can be easily expressed in terms of the eigenvalues of the internal Hamiltonian, $E_\alpha^j(R,\gamma)$. The coupling between the internal states arises at the sector boundaries in transforming from the internal basis functions in one sector to those in the adjacent sector. It is the defintion of this sector transformation matrix which is the most

difficult aspect of applying the R-matrix propagation method.

The transformation matrix from sector i to sector i+1 is defined by

$$T_{\alpha\alpha'}^{i,i+1}(\gamma) = \langle \psi_\alpha^j(\underline{x},r,R_C^i,\gamma) \mid \psi_{\alpha'}^j,(\underline{x},r,R_C^{i+1},\gamma) \rangle_{\underline{x},r} \tag{29}$$

where $R_C^{\,i}$ is the center of sector i. It has been shown that this can be approximated by

$$T_{\alpha\alpha'}^{i,i+1}(\gamma) \simeq \exp\left\{(R_C^{i+1} - R_C^i)\, F_{\alpha\alpha'}^j\left[\tfrac{1}{2}(R_C^i + R_C^{i+1}),\gamma\right]\right\} \tag{30}$$

where $\underline{F}(R,\gamma)$ is defined in eq. (17). We use an alternate method to obtain $T_{\alpha\alpha'}^{i,i+1}(\gamma)$. Substituting eq. (9) into eq.(30)

$$T_{\alpha\alpha'}^{i,i+1}(\gamma) = \sum_{n\nu n'\nu'} C_{n\nu,\alpha}^j(R_C^i,\gamma) \int dr\, \rho_\nu^*(r) \int d\underline{x}\ \phi_n^{dA^*}(\underline{x},r,R_C^j,\gamma)$$
$$\phi_{n'}^{dA}(\underline{x},r,R_C^{i+1},\gamma)\, \rho_{\nu'}(r)\, C_{n'\nu',\alpha'}^j(R_C^{i+1},\gamma) \tag{31}$$

However, the P-diabatic basis functions $\phi_n^{dA}(\underline{x},R,\gamma)$ are, by definition, independent of r. Using this fact and substituting eq. (6) we obtain

$$T_{\alpha\alpha'}^{i,i+1}(\gamma) = \sum_{n\nu n'} C_{n\nu,\alpha}^j(R_C^i,\gamma) \sum_{mm'} u_{mn}(r,R_C^i,\gamma)\, \tau_{mm'}^{i,i+1}(r,\gamma)$$
$$u_{m'n'}(r,R_C^{i+1},\gamma)\, C_{n'\nu,\alpha'}^j(R_C^{i+1},\gamma) \tag{32}$$

Since the l.h.s. of eq. (32) is independent of r we can choose any value for r in the r.h.s. of this equation. We use eq. (32) where we approximate the overlap of the adiabatic electronic state between sectors by

$$\tau_{nn'}^{i,i+1}(r,\gamma) = \langle \phi_n^{aA}(\underline{x},r,R_C^i,\gamma) \mid \phi_{n'}^{aA}(\underline{x},r,R_C^{i+1},\gamma) \rangle_{\underline{x}} \tag{33}$$

$$\tau_{nn'}^{i,i+1}(r,\gamma) \simeq \exp\left\{(R_C^{i+1} - R_C^i)\, F_{nn'}^{\alpha A}\left[r, \tfrac{1}{2}(R_C^i + R_C^{i+1}), \gamma\right]\right\} \qquad (34)$$

1. J. A. Silver, N. C. Blais, and G. H. Kwei, J. Chem. Phys. 71, 3412 (1979).

2. E. A. Gislason, A. W. Kleyn, and J. Los, Chem. Phys. 59, 91 (1981).

3. I. V. Hertel, Advan. Chem. Phys. 45, 341 (1981).

4. I. V. Hertel, Advan. Chem. Phys., edited by K. Lawley, to be published.

5. J. L. Magee and T. Ri, J. Chem. Phys. 9, 639 (1941); K. J. Laidler, J. Chem. Phys. 10, 34 (1942).

7. P. McGuire and J. C. Bellum, J. Chem. Phys. 71, 1975 (1979).

6. P. Botschwina, Ph.D. thesis, Uiversity of Kaiserslautern, 1980.

8. P. Habitz, Chem. Phys. 54, 131 (1980).

9. P. Botschwina, W. Meyer, I. V. Hertel, and W. Reiland, J. Chem. Phys. 75, 5438 (1981).

10. D. G. Truhlar, J. W. Duff, N. C. Blais, J. C. Tully, and B. C. Garrett, J. Chem. Phys., in press.

11. N. C. Blais, D. G. Truhlar, and B. C. Garrett, J. Chem. Phys., in press.

12. I. H. Zimmerman and T. F. George, Chem. Phys. 7, 323 (1975); I. H. Zimmerman and T. F. George, J. Chem. Phys. 63, 2109 (1975).

13. M. Baer, Chem. Phys. Lett. 35, 112 (1975).

14. F. Rebentrost and W. A. Lester, Jr., J. Chem. Phys. 63, 3737 (1975); 64, 3879, 4223 (1976); 67, 3367 (1977).

15. P. L. DeVries and T. F. George, J. Chem. Phys. 67, 1293 (1977).

16. D. L. Miller and R. E. Wyatt, J. Chem. Phys. 67, 1302 (1977).

17. B. C. Garrett and D. G. Truhlar, Theor. Chem. Adv. Perspectives 6A, 215 (1981); B. C. Garrett, M. J. Redmon, D. G. Truhlar, and C. F. Melius, J. Chem. Phys. 74 , 412 (1981).

18. For example see, R. T Pack, J. Chem. Phys. 60 , 633 (1974). 19. G. A. Parker and R. T Pack, J. Chem. Phys. 68 , 1585 (1978).

20. E. Dalgaard and P. Jorgensen, J. Chem. Phys. 69 , 3833 (1978).

21. J. C. Light and R. B. Walker, J. Chem. Phys. 65, 4272 (1976).

Figure Captions

1. Potential energy contours for the three lowest adiabatic potential energy surfaces $V_n^{aA}(r,R,\gamma)$ of NaH_2; parts (a), (b), and (c) are for n = 1, 2, and 3, respectively. The energy contours are plotted as a function of the H_2 internuclear distance r and the distance from Na to the center of mass of H_2 R, for a fixed angle, γ = 90 degrees. The contours are evenly spaced at 0.2eV.
2. Adiabatic potential energy curves $V_n^{aA}(r,R,\gamma)$ and diabatic potential energy curves $V_{nm}^{dA}(r,R,\gamma)$ for NaH_2. The curves are plotted as a function of the H_2 distance r for fixed Na-to-H_2 distance R and for fixed angle γ = 75 degrees. The diabatic potential curves are defined by eq. (12) and are diabatic only in the r motion. For parts (a) and (d) R = $3a_0$, for parts (b) and (e) R = $4a_0$, and for parts (c) and (f) R = $5a_0$. Parts (a) - (c) show the three lowest adiabatic curves (solid lines) and the three diagonal diabatic potential curves (dashed lines). Parts (d) - (f) show the off-diagonal diabatic potential coupling curves: 1,2 (solid); 1,3 (short dashed); and 2,3 (long dashed).

AD-A125 135 COMPUTATIONAL STUDY OF NONADIABATIC EFFECTS IN ATOM-MOLECULE REACTIVE SCATTERING(U) CHEMICAL DYNAMICS CORP COLUMBUS OH B C GARRETT ET AL. 15 NOV 82 2/2

UNCLASSIFIED AFOSR-TR-83-0002 F49620-81-C-0046 F/G 7/4 NL

END

FILMED

DTIC

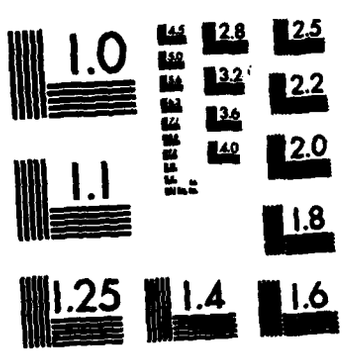

Figure Captions

1. Potential energy contours for the three lowest adiabatic potential energy surfaces $V_n^{aA}(r,R,\gamma)$ of NaH_2; parts (a), (b), and (c) are for n = 1, 2, and 3, respectively. The energy contours are plotted as a function of the H_2 internuclear distance r and the distance from Na to the center of mass of H_2 R, for a fixed angle, γ = 90 degrees. The contours are evenly spaced at 0.2eV.
2. Adiabatic potential energy curves $V_n^{aA}(r,R,\gamma)$ and diabatic potential energy curves $V_{nm}^{dA}(r,R,\gamma)$ for NaH_2. The curves are plotted as a function of the H_2 distance r for fixed Na-to-H_2 distance R and for fixed angle γ = 75 degrees. The diabatic potential curves are defined by eq. (12) and are diabatic only in the r motion. For parts (a) and (d) R = $3a_0$, for parts (b) and (e) R = $4a_0$, and for parts (c) and (f) R = $5a_0$. Parts (a) - (c) show the three lowest adiabatic curves (solid lines) and the three diagonal diabatic potential curves (dashed lines). Parts (d) - (f) show the off-diagonal diabatic potential coupling curves: 1,2 (solid); 1,3 (short dashed); and 2,3 (long dashed).

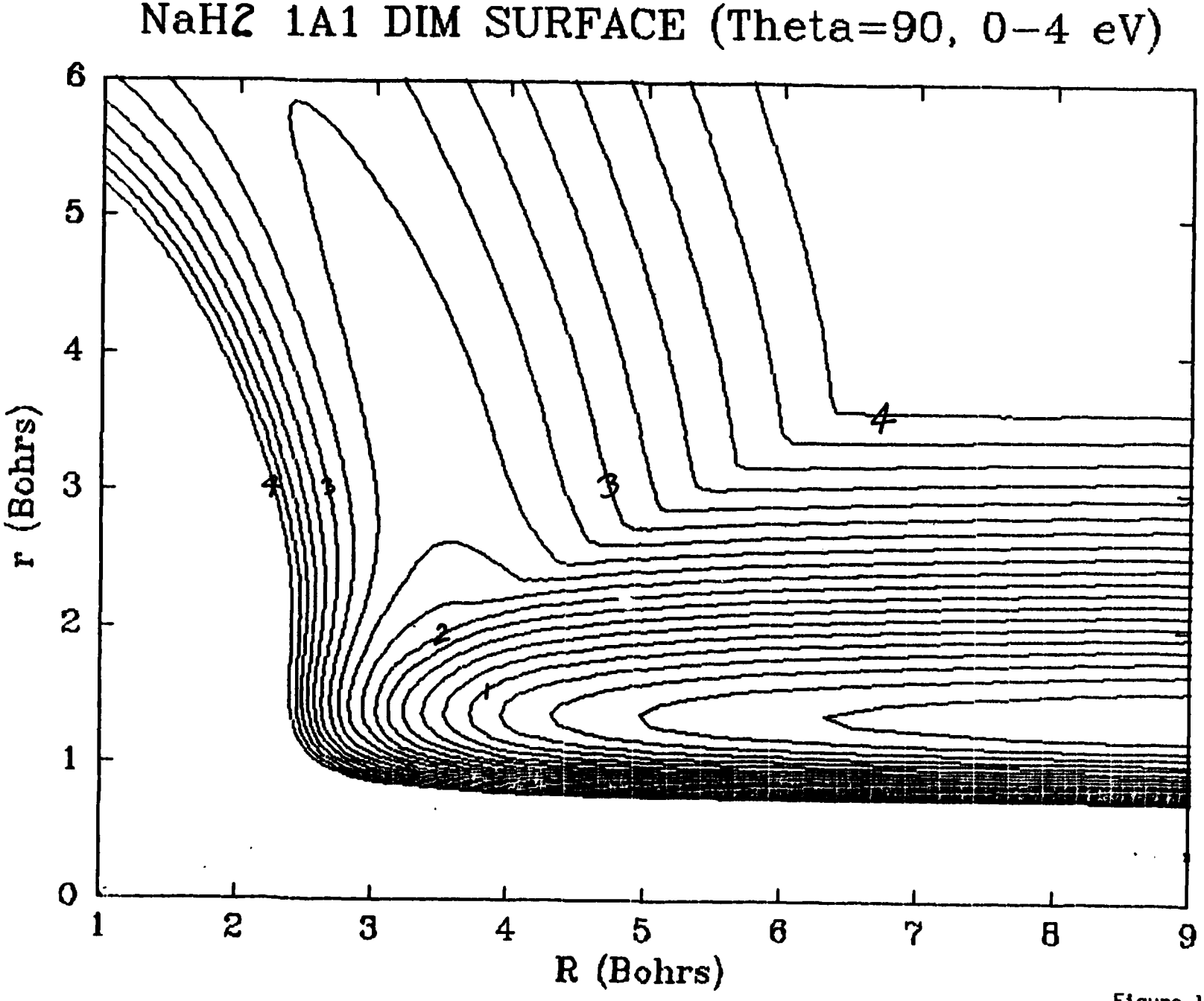
NaH2 1A1 DIM SURFACE (Theta=90, 0-4 eV)
r (Bohrs)
R (Bohrs)
0
1
2
3
4
5
6
7
8
9
1
2
3
4

Figure 1(a)

NaH2 1B2 DIM SURFACE (Theta=90, 1.6-4 eV)
r (Bohrs)
R (Bohrs)
0
1
2
3
4
5
6
7
8
9
4
3
2

Figure 1(b)

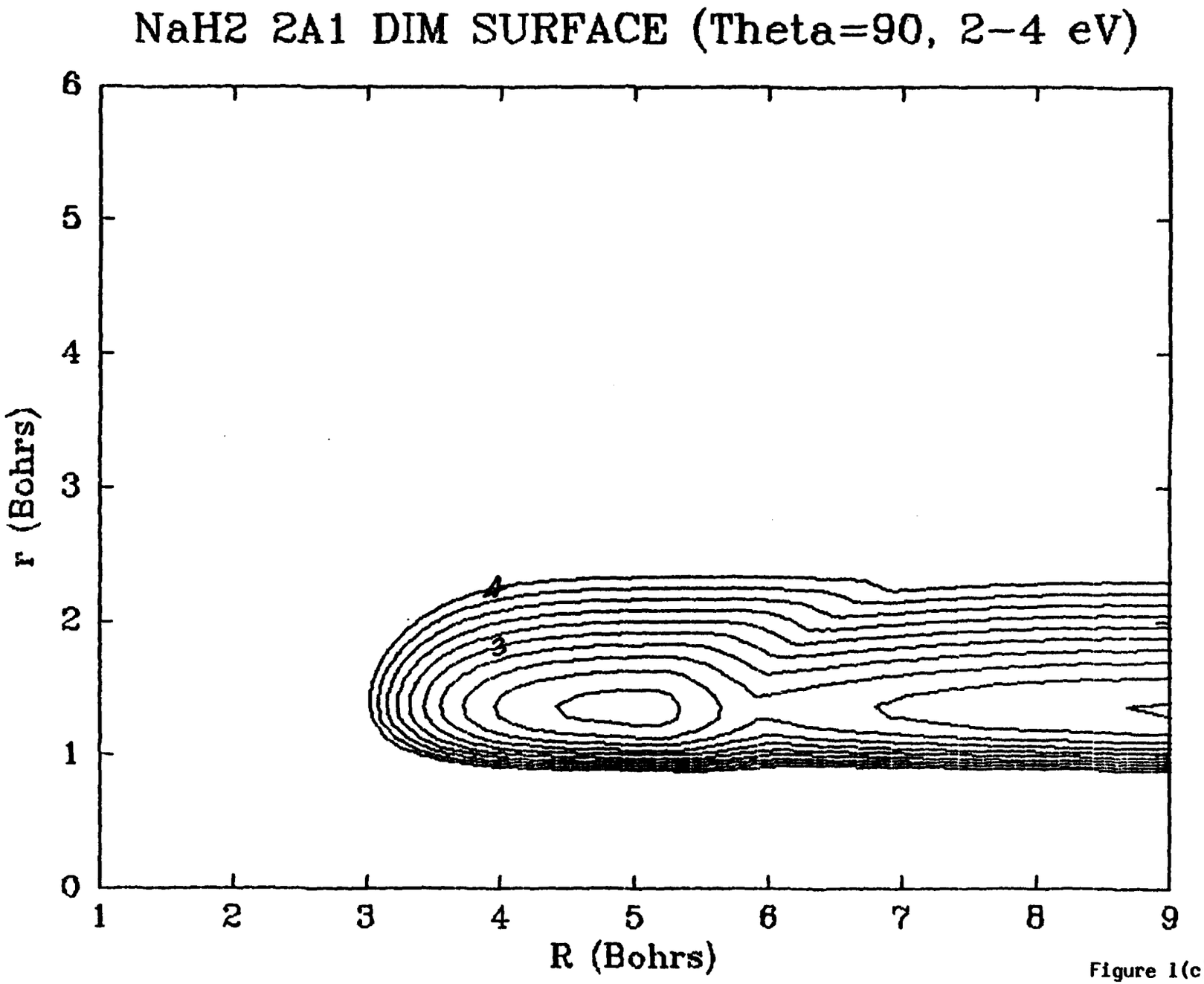
NaH2 2A1 DIM SURFACE (Theta=90, 2-4 eV)
r (Bohrs)
R (Bohrs)
0
1
2
3
4
5
6
7
8
9
4
3

Figure 1(c)

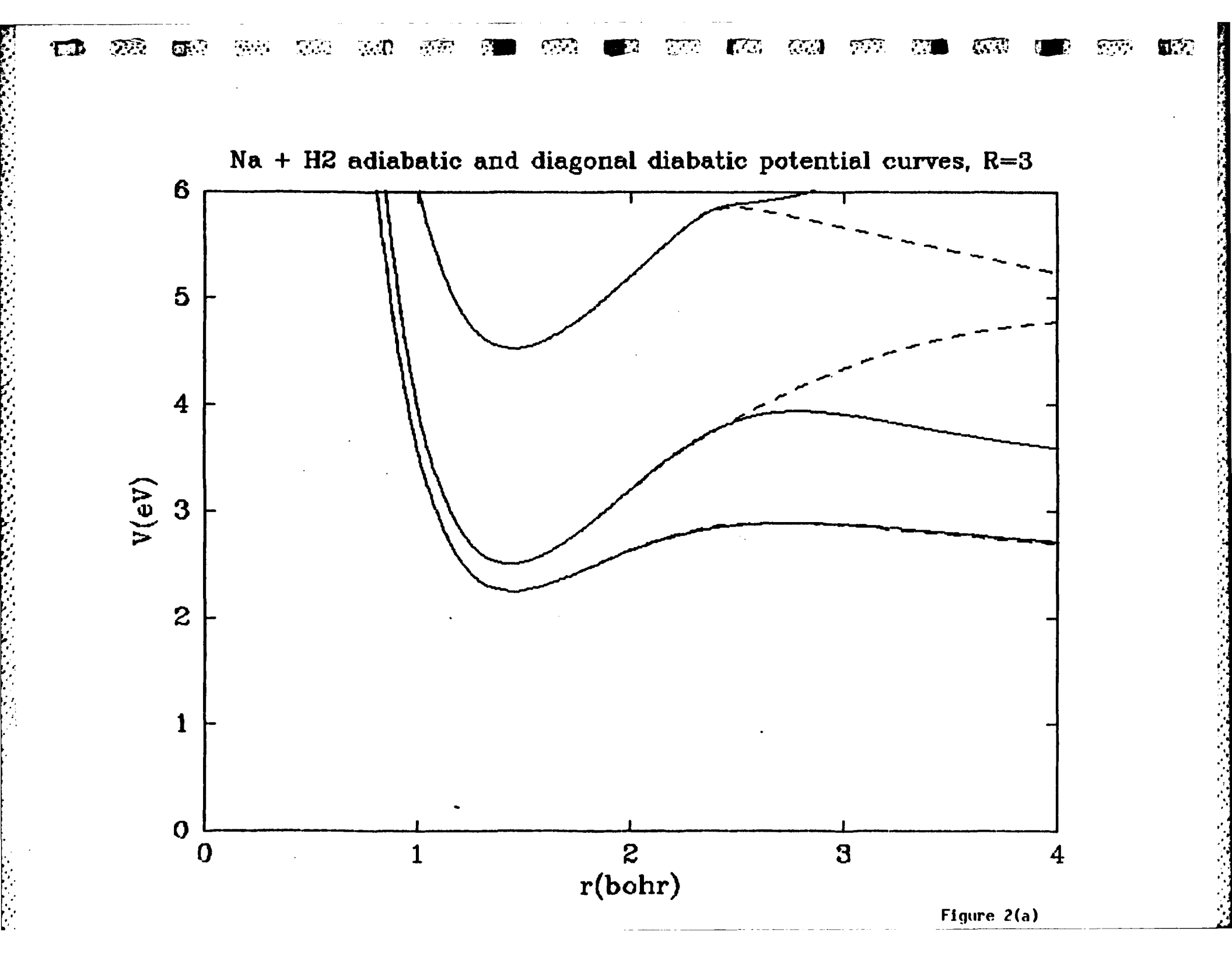
Na + H2 adiabatic and diagonal diabatic potential curves, R=3
V(eV)
r(bohr)
0
1
2
3
4
5
6

Figure 2(a)

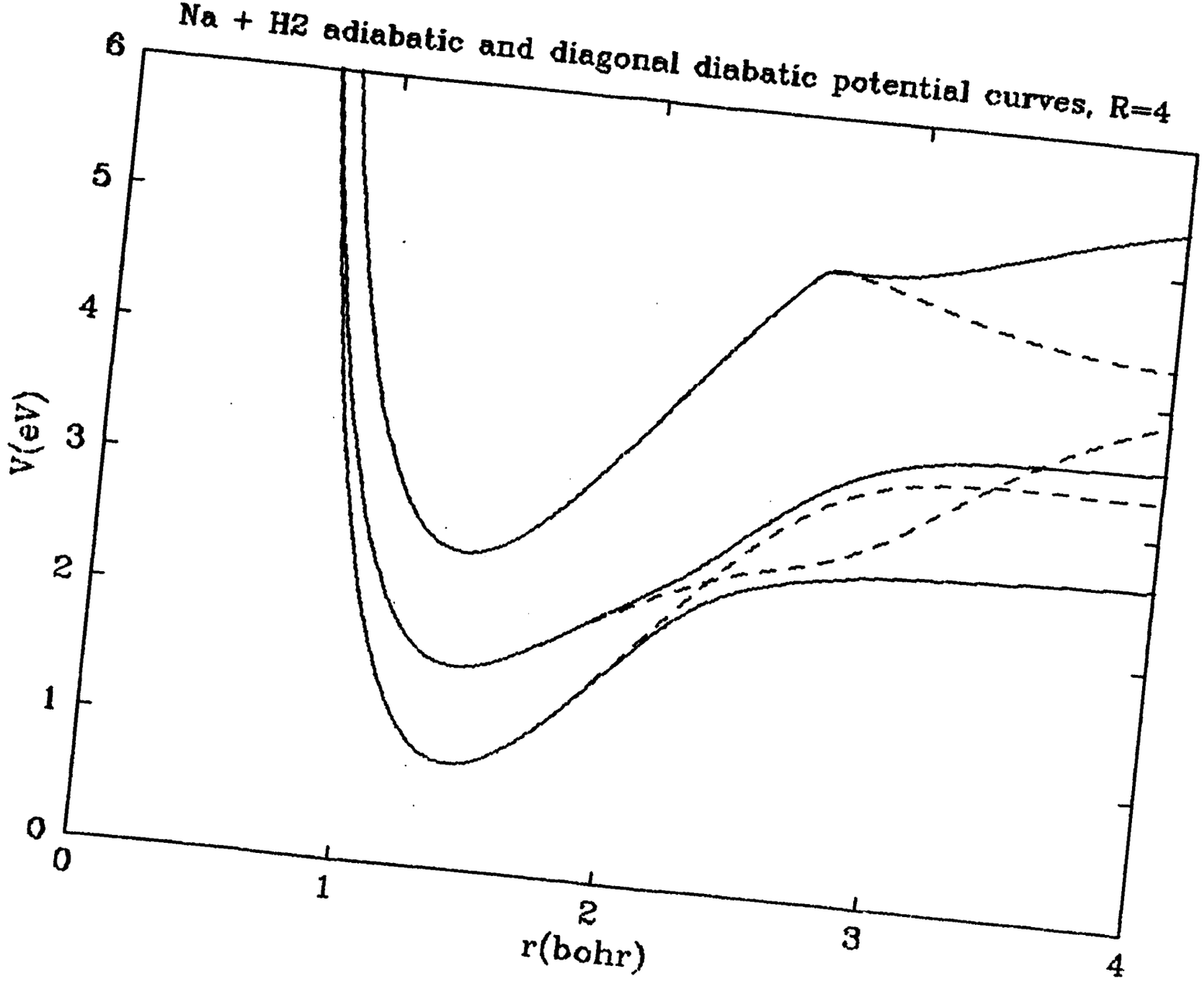
Na + H2 adiabatic and diagonal diabatic potential curves, R=4
V(eV)
r(bohr)
0
1
2
3
4
5
6

Figure 2(b)

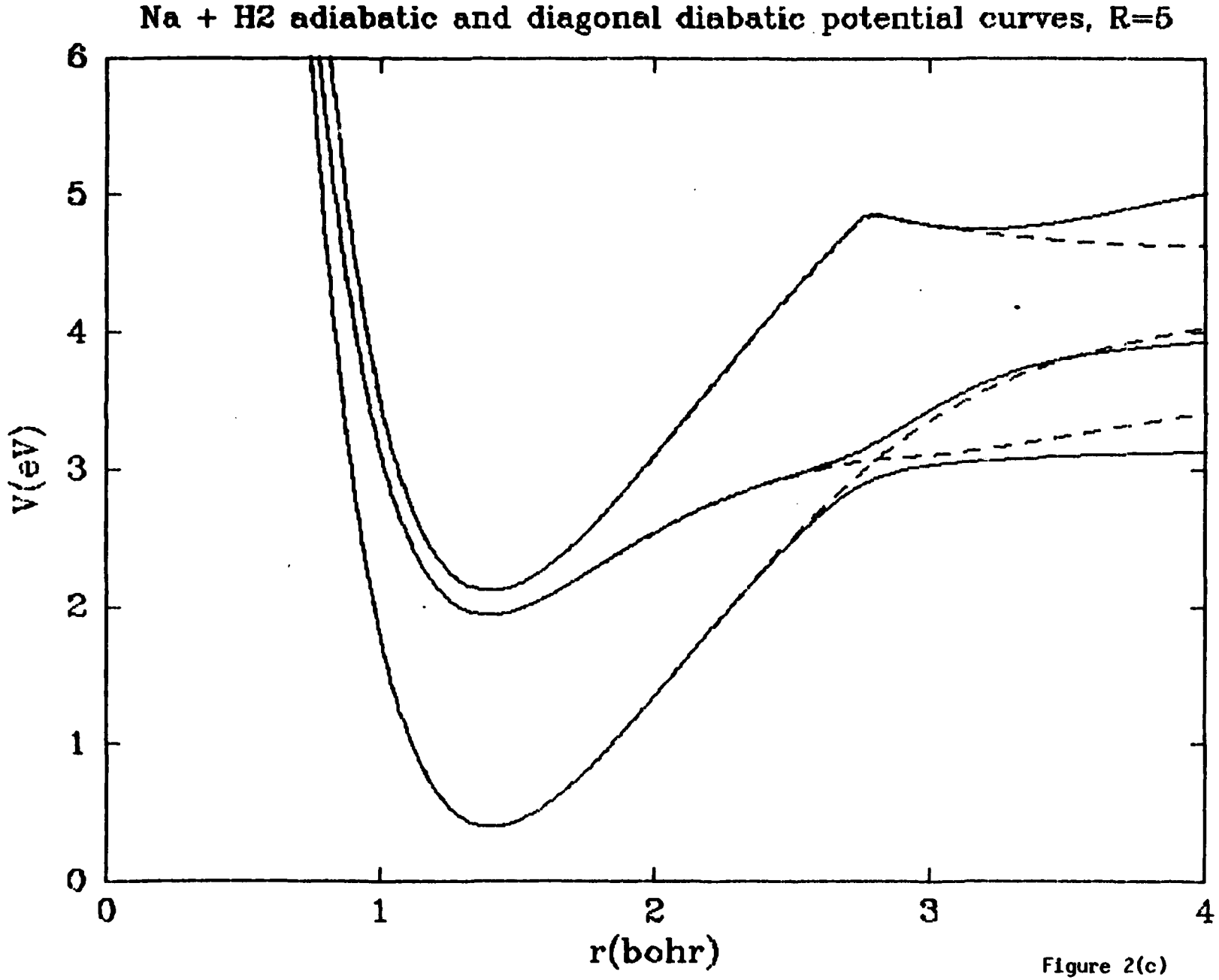
Na + H2 adiabatic and diagonal diabatic potential curves, R=5
V(eV)
r(bohr)
0
1
2
3
4
5
6

Figure 2(c)

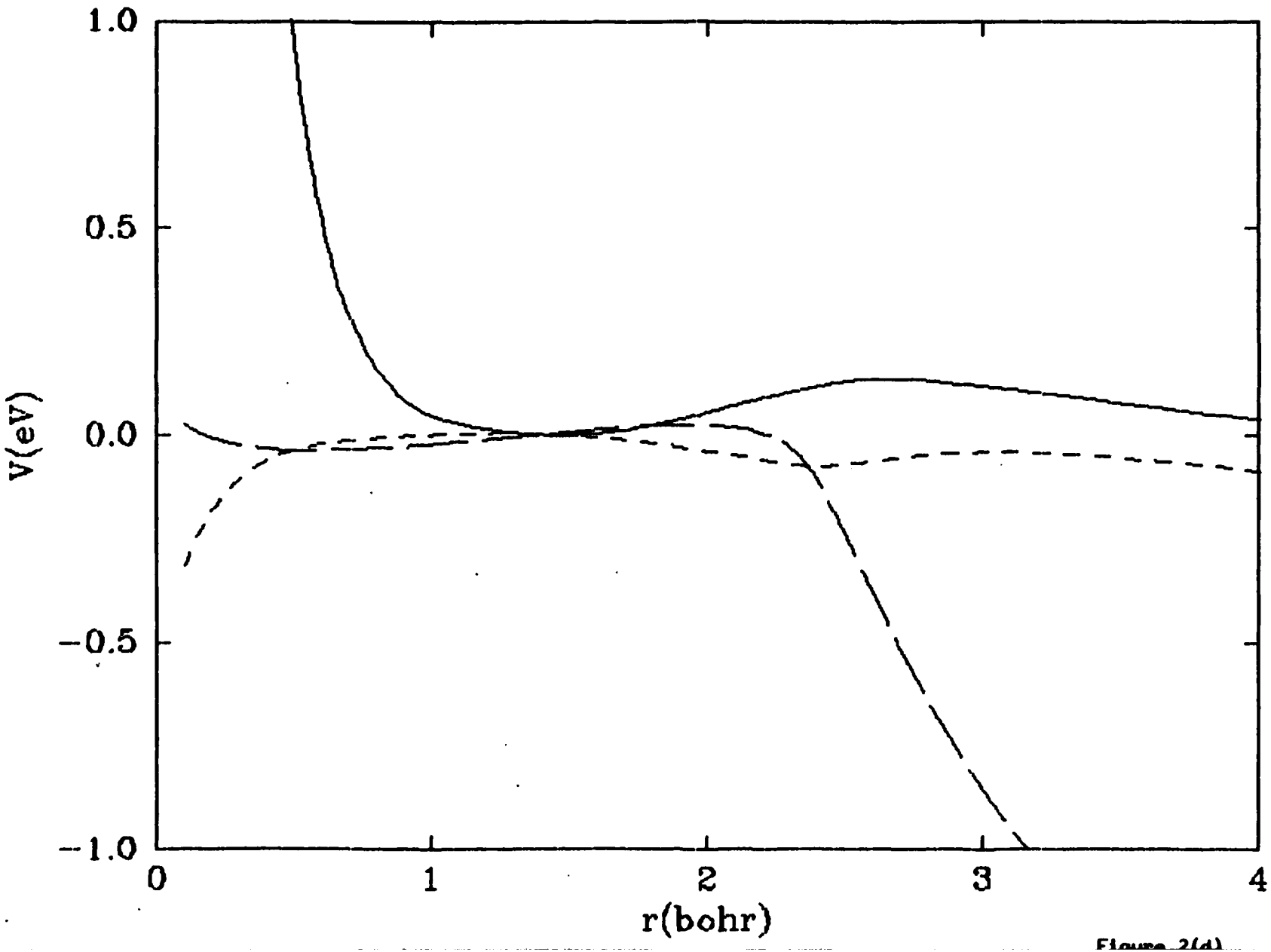
Na + H2 off-diagonal diabatic potential curves, R=3
1.0
0.5
0.0
−0.5
−1.0
V(eV)
0
1
2
3
4
r(bohr)

Figure 2(d)

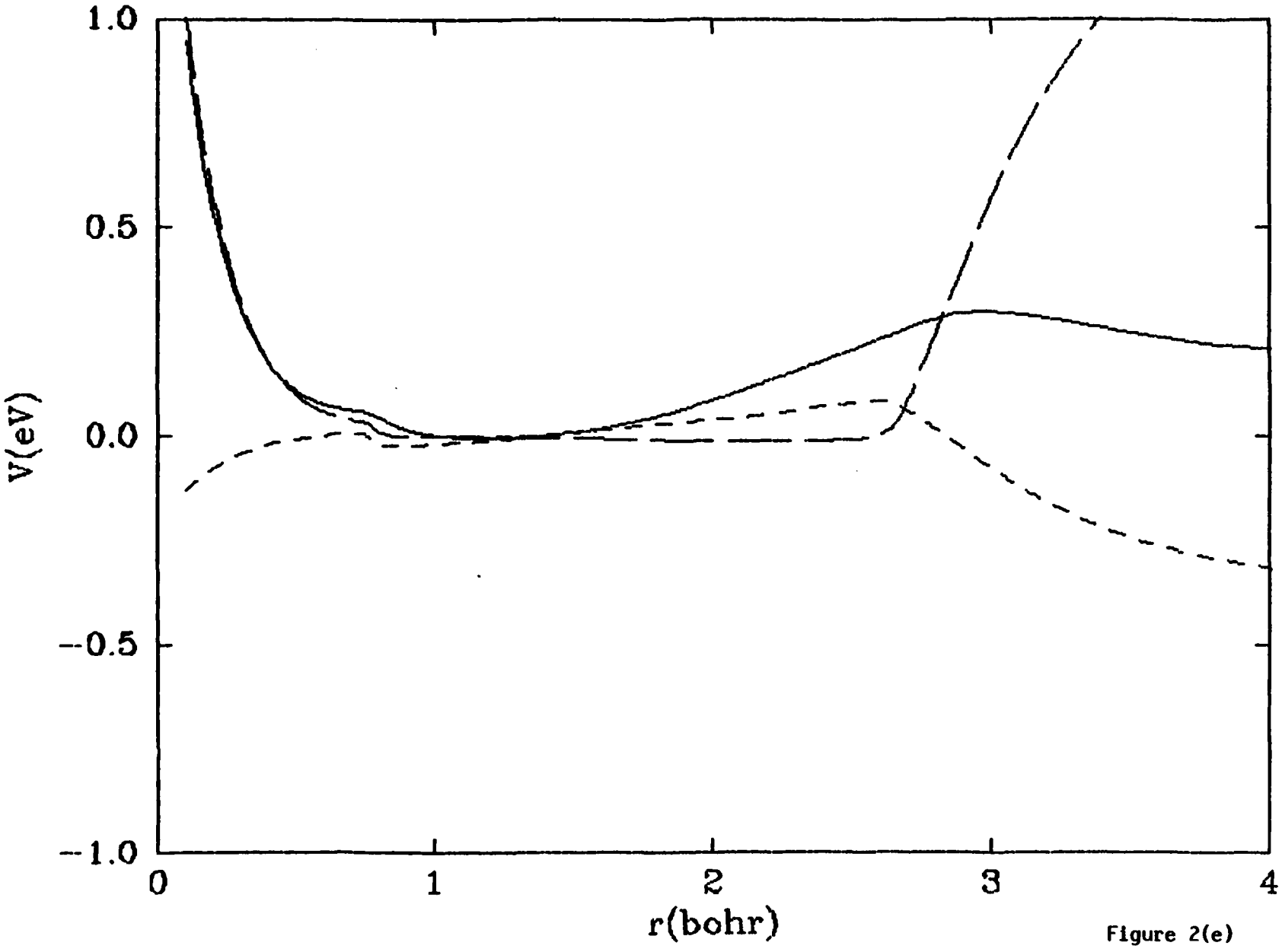
Na + H2 off-diagonal diabatic potential curves, R=4
1.0
0.5
0.0
-0.5
-1.0
V(eV)
0
1
2
3
4
r(bohr)

Figure 2(e)

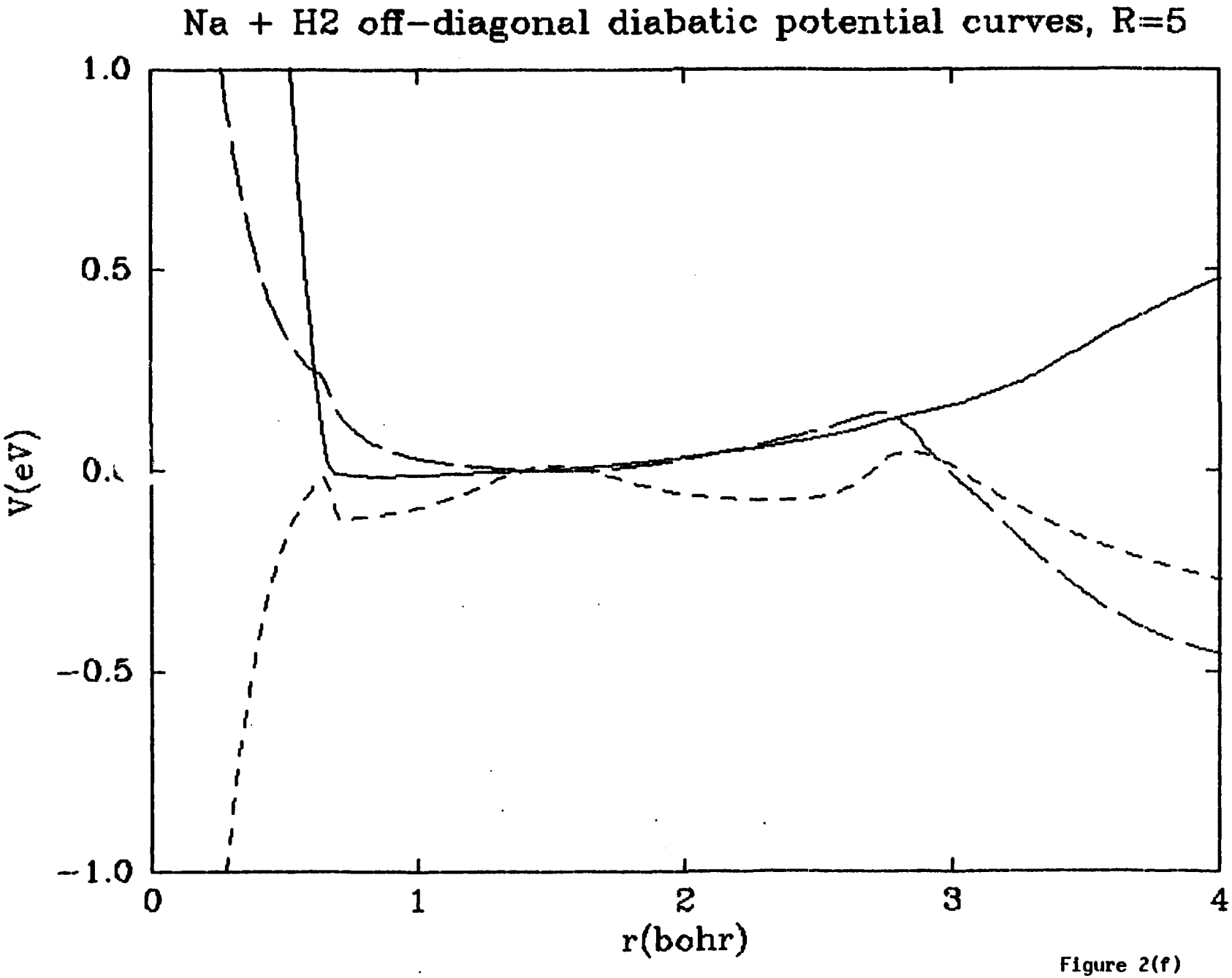
Na + H2 off−diagonal diabatic potential curves, R=5
1.0
0.5
0.
−0.5
−1.0
V(eV)
0
1
2
3
4
r(bohr)

Figure 2(f)

APPENDIX D

An Iterative Approach to Reactive Scattering

AN ITERATIVE APPROACH TO REACTIVE SCATTERING

This appendix presents the results of research to extend the iterative-variational method[1,2] to reactive atom-molecule collisions. The rationale for this work is the following:

- The standard reactive scattering methods limited in the number of coupled equations they can handle (<200), thus limiting accurate close-coupling treatments to nearly thermoneutral reactions involving hydrogen abstraction.
- The standard reaction coordinate methods are limited by the use of mass-weighted coordinates, and hence are difficult to apply to small skew-angle systems. This comment does not apply to so-called hyperspherical coordinate schemes, although the limitation to systems of the order of 100-200 channels does.
- The standard close-coupling theory (using Cartesian coordinates) contains nonlocal potentials to account for rearrangement. These nonlocal potentials arise in the same manner regardless of whether the exchange involves electrons or nuclei.
- Iterative methods have been very successful in treating nonlocal potentials that arise in electron scattering theory. A similar iterative method has also been successful in solving large (>500) sets of coupled equations for inelastic atom-molecule scattering.

These observations suggest that an iterative method might form the basis for a theoretical approach to reactive scattering that can be applied to a much wider class of problems than can refinements of current reaction-coordinate methods. The rest of this section presents a discussion of our preliminary research in this area.

B.1 INELASTIC SCATTERING

This section describes unpublished extensions to the iterative method as it applies to inelastic scattering. Consider an atom A colliding with a target molecule BC, with the Hamiltonian (refer to Figure 1)

$$H = -\frac{\hbar^2}{2\mu}\nabla_R^2 - \frac{\hbar^2}{2m}\nabla_r^2 + V(R,r,\gamma) \qquad (1)$$

where the coordinates $\vec{r}$ and $\vec{R}$ correspond to the BC internuclear vector and the vector from A to the BC center-of-mass, respectively. γ is the angle subtended by $\vec{R}$ and $\vec{r}$. The reduced masses are given by

$$m = \frac{m_B\, m_C}{m_B + m_C} \tag{2}$$

and

$$\mu = \frac{m_A\, m_B\, m_C}{m(m_A + m_B + m_C)} \tag{3}$$

H is more convenient when the potential is partitioned into a term corresponding to the BC molecule and an interaction term

$$V_{BC} = \lim_{R\to\infty} V(R,r,\gamma) \tag{4}$$

$$V_{int} = V - V_{BC} \tag{5}$$

so that the moleculear and total Hamiltonians are

$$H_{BC} = -\frac{\hbar^2}{2m}\nabla_r^2 + V_{BC} \tag{6}$$

$$H = -\frac{\hbar^2}{2\mu}\frac{1}{R}\frac{\partial^2}{\partial R^2}R + \frac{\hat{L}^2(\hat{R})}{2\mu R^2} + H_{BC} + V_{int} \tag{7}$$

where $L(\hat{R})$ is the orbital angular momentum operator. We now seek solutions for a specific total angular momentum of the form

$$\Psi^f(J,M) = \sum_{i=1}^{N_c} \chi_i(\vec{r}.\hat{R})\,\frac{U_{if}(R)}{R} \tag{8}$$

where $i\equiv\{n,j,\ell\}$ and $f\equiv\{n',j',\ell'\}$. χ_i are chosen to be eigenfunctions of H_{BC} and of total and orbital angular momentum.

A variational principle is used to obtain the coupled equations

$$I = \int d\vec{r}\, d\hat{R}\ \Psi^{f*}(H-E)\ \Psi^{f} \tag{9a}$$

$$= \int dR \sum_i -\frac{\hbar^2}{2\mu} U^*_{if} U''_{if} + \int dR \sum_{ij} U^*_{if} W_{ij}(R)\, U_{jf} \tag{9b}$$

$$= \int dR \sum_i \frac{\hbar^2}{2\mu} U^{*\prime}_{if} U'_{if} + \int dR \sum_{ij} U^*_{if} W_{ij}(R)\, U_{jf} - \frac{\hbar^2}{2\mu} U^*_{if} U'_{if} \Big|_0^\infty \tag{9c}$$

where

$$W_{ij}(R) = \frac{\hbar^2}{2\mu}\left[\frac{\ell_i(\ell_i+1)}{R^2} + (\varepsilon_i^{BC} - E)\right]\delta_{ij} + \int d\vec{r}\, d\hat{R}\ \chi_i^*\ V_{int}\ \chi_j \tag{10}$$

The best solution, the one that leaves I stationary with respect to arbitrary variations in U_{if} (endpoints held fixed), is given by the solutions to the differential equations

$$U''_{if}(R) = \frac{2\mu}{\hbar^2} \sum_j W_{ij}(R)\, U_{jf}(R) \tag{11}$$

which can be solved by a large variety of numerical methods, provided the number of coupled equations is limited to less than approximately 200. We proceed now to cast these equations into a set of algebraic equations, to dramatically increase the number of equations that can be simultaneously solved. We introduce a basis for the radial functions, i.e.

$$U_{if}(R) = \sum_{\alpha=1}^{N_g} \phi_{i\alpha}(R)\, C_{i\alpha} \tag{12}$$

The variation principle then leads to a set of algebraic equations for the

coefficients $C_{i\alpha}$. By virtue of equation (9c) the basis functions $\phi_{i\alpha}$ need only belong to the class of continuous functions and need not have continuous first derivatives; i.e. the basis may be peicewise analytic. This last observation suggests that the finite element method[3] can be used to advantage in solving these equations. We divide the range of R into a grid $\{ R_1 < R_2 <...< R_N \}$ and choose the $\phi_{i\alpha}$ such that

$$\phi_{i\alpha}(R) = \begin{cases} 0 & R \leq R_{\alpha-1} \\ 1 & R = R_\alpha \\ 0 & R \geq R_{\alpha+1} \end{cases} \tag{13}$$

With this choice $C_{i\alpha} = U_{if}(R_\alpha)$. Holding the endpoints fixed, the variation principle gives the $N_c \times (N_g-2)$ algebraic equations

$$\sum_{j=1}^{N_c} \sum_{\beta=1}^{N_g} K_{i\alpha,j\beta} C_{j\beta} = 0 \qquad \alpha = 2,3, \cdots N_g-1 \tag{14}$$

where

$$K_{i\alpha,j\beta} = \int dR \frac{\hbar^2}{2\mu} \phi^{*\prime}_{i\alpha} \phi'_{j\beta} \delta_{ij} - \int dR \, \phi^*_{i\alpha} W_{ij} \phi_{j\beta} \tag{15}$$

$\underset{\sim}{K}$ is a symmetric, banded supermatrix (Figure 2) because of our definition of the $\phi_{i\alpha}$ in Eq. (13). Each block labeled by (α,β) is of dimensions $N_c \times N_c$.

Since the solution must be regular at the origin, we know that $C_{i1} = 0$. For any choice of C_{iN_g} these equations may then be solved.

It is important to stress that it is the banded symmetric form of $\underset{\sim}{K}$ that makes this approach attractive. All data may be processed sequentially, thus avoiding the heavy use of direct access I/O that characterizes the previous implementation of the iterative method. Therefore, even when $\underset{\sim}{K}$ is too large to fit in core, the solution of Eq. (14) is of comparable effort to a single

numerical integration of Eq. (11).

Additional attractive properties of this approach are 1) there are no stability problems, even for solutions beginning with incorrect boundary conditions at $U_{if}(R_{N_g})$ and 2) with a judicious choice of $\phi_{i\alpha}(R)$, as discussed below, the number of grid points N_g can be considerably reduced over the number required for standard numerical integration. Thus this approach shares a desirable trait of the more popular invarient-embedding methods in molecular scattering theory[4].

The C_{iN_g} are, of course, not known in advance. However, they can be expressed in terms of the others

$$C_{iN_g} \equiv U_{if}(R_{N_g}) = \varepsilon_i^* \delta_{if} - \varepsilon_i S_{if} \tag{16}$$

where

$$\varepsilon_i = k_i^{-\frac{1}{2}} \exp\left[i\left(k_i R_N - \frac{\ell_i \pi}{2}\right)\right] \tag{17a}$$

and

$$k_i^2 = \frac{2\mu}{\hbar^2}\left(\varepsilon_i^{BC} - E\right) \tag{17b}$$

The S-matrix elements can be expressed as

$$S_{if} = S_{if}^0 + \left(\frac{i}{2}\right)\left(\frac{2\mu}{\hbar^2}\right)\sum_{jj'}\int \chi_{ji}\, W_{jj'}^1\, U_{j'f}\, dR \tag{18}$$

where

$$\underset{\sim}{W} = \underset{\sim}{W}^0 + \underset{\sim}{W}^1 \tag{19}$$

$$\underset{\sim}{\chi}'' = \frac{2\mu}{\hbar^2}\, \underset{\sim}{W}^0\, \underset{\sim}{\chi} \tag{20}$$

and

$$\chi_{if}(R_{N_g}) = \varepsilon_i^* \delta_{if} - \varepsilon_i S_{if}^0 \tag{21}$$

Substituting Eq.(18) and Eq.(21) into Eq.(16) leads to

$$\sum_{j=1}^{N_c}\sum_{\beta=1}^{N_g} B_{iN_g,j\beta}\, C_{j\beta} = \chi_{if}(R_{N_g}) \tag{22}$$

where

$$B_{iN_g,j\beta} = \left(\frac{1}{2}\right)\left(\frac{2\mu}{\hbar^2}\right)\varepsilon_i \sum_{j'}\int \chi_{j'i}\, W^1_{j'j}\, \Phi_{j\beta}\, dR + \delta_{iN_g,j\beta} \tag{23}$$

Eqs.(14) and (22) together result in a set of $N_c\times(N_g-1)$ equations for $N_c\times(N_g-1)$ unknowns

$$\underset{\sim}{K}'\,\vec{C} = \vec{e} \tag{24}$$

where

$$e_{j\beta} = \delta_{\beta N_g}\,\chi_{jf}(R_{N_g}) \tag{25}$$

and $\underset{\sim}{K}'$ has the structure shown in Fig. 3.

Eq.(24) can in principle be solved directly for S_{if} in a noniterative fashion. However, such a solution is unrealistic for large N_c because Eq.(22) destroys the banded symmetric nature of $\underset{\sim}{K}$. Therefore, we introduce the following iterative procedure: Let

$$\underset{\sim}{K}' = \underset{\sim}{K}^0 + \underset{\sim}{K}^1 \tag{26}$$

where $\underset{\sim}{K}^0$ is banded symmetric and $\underset{\sim}{K}^1$ is zero everywhere except in the last block of rows (iN_g). Let

$$\underset{\sim}{K}^0\,\underset{\sim}{G}^1 = \vec{e} \tag{27a}$$

and

$$\underset{\sim}{K}^0\,\vec{G}^n + \underset{\sim}{K}^1\,\vec{G}^{n-1} = \vec{e} \tag{27b}$$

Let

$$\vec{C}^n = \sum_{i=1}^{n} d_i\,\vec{G}^i \tag{28}$$

We choose the d_i by minimizing

$$I' = \left|\underset{\sim}{K}'\,\vec{C}^n - \vec{e}\right|^2 \tag{29}$$

subject to the renormalization constraint

$$\sum_i \phi_i = 1 \tag{30}$$

This leads to

$$d_i = \frac{d_i'}{\sum_i d_i'} \tag{31}$$

where

$$d_i' = \sum_j (\underset{\sim}{J}^{-1})_{ij} \tag{32}$$

$$J_{ij} = \vec{\Delta}^{i*} \cdot \vec{\Delta}^{j} \tag{33}$$

and

$$\vec{\Delta}^{i} = \underset{\sim}{K}^{i} (\vec{G}^{i} - \vec{G}^{i-1}) \tag{34}$$

Equations (27) through (34) are iterated until convergence is achieved.

An excellent choice of basis functions $\phi_{i\alpha}$ is obtained by using eigenfunctions of the equations

$$\phi_{i\alpha}''(R) = \frac{2\mu}{\hbar^2} W_{ii}(R)\, \phi_{i\alpha}(R) \tag{35}$$

These equations are solved and the integrals, Eq.(15), are evaluated numerically by a suitable quadrature. With this choice, our basis functions always have the correct local behavior, thus improving convergence, and go to the proper asymptotic limit when

$$W_{ij} = 0 \qquad i \neq j \tag{36}$$

This means that at long range the grid spacings may be much larger than the local wavelength, and that R_{N_g} may be kept relatively small, even in the presence of coulomb interactions.

B.2 REACTIVE SCATTERING

We now consider an extension of the iterative method described above to three-atom rearrangements A + BC → AB + C but exclude breakup A + BC → A +B +C since we are still limited by Lippmann-Schwinger boundary conditions. We expand our solutions as[5]

$$\psi^{\beta f}(J,M) = \sum_{\alpha=a,bc}\sum_{i=1}^{N_{\alpha c}} \chi_{\alpha i}(\vec{r}_\alpha,\hat{R}_\alpha)\ \frac{U_{\alpha i,\beta f}(R_\alpha)}{R_\alpha} \tag{37}$$

where the arrangements a,b, and c are shown in Fig. 4. The radial functions have the boundary conditions

$$\lim_{R_\alpha\to\infty} U_{\alpha i,\beta f}(R_\alpha) = \epsilon^{*}_{\alpha i}\ \delta_{if}\delta_{\alpha\beta} - \epsilon_{\alpha i}\delta_{\alpha i}\delta_{\beta f} \tag{38}$$

Again, we expand in a peicewise analytic basis, $\phi_{\alpha i\sigma}$,

$$U_{\alpha i,\beta f}(R_\alpha) = \sum_{\sigma=1}^{N_{\alpha g}} \phi_{\alpha i\sigma}(R_\alpha)\ C_{\alpha i\sigma} \tag{39}$$

Variation of the $C_{\alpha i\sigma}$ will lead to the set of equations

$$\sum_{\beta j\rho} K_{\alpha i\sigma,\beta j\rho}\ C_{\beta j\rho} = 0 \qquad \sigma = 2,3,\cdots N_{\alpha g}-1 \tag{40}$$

We use integral expressions for the S-matrix elements to provide an additional equation for each arrangement channel. The resulting algebraic equations will be solved iteratively as in Eqs. (27)-(34).

The method discussed for inelastic scattering in the previous section can be taken over without alteration to the reactive case. There are differences in application, however, that will now be considered.

First, the matrix elements $K_{\alpha i\sigma,\beta j\rho}$ will now form a supermatrix of supermatrices, the block structure being shown in Fig. 5. The diagonal blocks

with $\alpha = \beta$ contain identical integrals to the inelastic case in Eq.(15). The elements of the off-diagonal blocks are more complex, involving overlaps of the nonorthogonal functions $\chi_{\alpha i}(\vec{r}_\alpha, \hat{R}_\alpha)$ and $\chi_{\beta j}(\vec{r}_\beta, \hat{R}_\beta)$. These blocks are not banded, since the functions $\phi_{\alpha i\sigma}(R_\alpha)$ will in general have nonzero overlaps with functions for other arrangements. The off-diagonal blocks are obviously the exchange interactions and are matrix elements of the nonlocal exchange kernals[5]. The associated expressions for the S-matrix elements are consequently more complex than Eqs.(18)-(21).

In addition, the matrix $\underset{\sim}{K}^1$ of Eq.(26) no longer consists simply of the boundary condition Eq.(22). Since $\underset{\sim}{K}^1$ is no longer banded, $\underset{\sim}{K}^0$ can be chosen by constructing parallel lines to the diagonal as indicated by the dashed lines in Fig. 5. The bandwidth can be chosen consistent with the speed and size of the computer being used. $\underset{\sim}{K}^0$ will include everything inside the band. $\underset{\sim}{K}^1$ will include everything outside the band in addition to the rows coming from the boundary conditions Eq.(22). It is this aspect of $\underset{\sim}{K}^1$ which simultaneously includes the boundary value problem of inelastic scattering and the nonlocal potential problem of rearrangement scattering that allows its treatment within a single iterative procedure. Although is more complicated in the reactive case, the iterative procedure still retains its sequential processing property. This is extremely important for the development of a computationally tractable method on the new generation of supercomputers, with their enormous fast-core memories and core-like (fast) online storage, and vector processors. These extremely large and fast machines will enable an iterative sequential-access procedure such as discussed here to handle thousands of coupled equations, which, particularly with decoupling techniques, will open up a large number of processes to theoretical investigation that are beyond the consideration of any existing method.

REFERENCES

1. L. D. Thomas, "Solution fo the Coupled Equations of Atom-Molecule Inelastic Scattering for a Single Initial State", J. Chem. Phys. 70, 2979 (1979).
2. L. D. Thomas, "Solution of the Coupled Equations of Inelastic Atom-Molecule Scattering for a Single Initial State.II. Use of Nondiagonal Matrix Green Functions.", J. Chem. Phys.76, 4925(1982).
3. G. Strang and G. Fix, An Analysis of the Finite Element Method (Prentice Hall, New Jersey, 1973).
4. L. D. Thomas, M. H. Alexander, B. R. Johnson, W. A. Lester Jr., J. C. Light, K. D. McLenithan, G. A. Parker, M. J. Redmon, T. G. Schmalz, D. Secrest, and R. B. Walker, "Comparison of Numerical Methods for Solving the Second-Order Differential Equations of Molecular Scattering Theory", J. Comp. Phys. 41, 407 (1981).
5. W. H. Miller, J. Chem. Phys. 50, 407 (1969).

FIGURE CAPTIONS

1. Coordinate system for three-atom nonreactive scattering. The origin of $\vec{R}$ is the center-of-mass of the BC molecule.
2. Schematic representation of the banded supermatrix $\underset{\sim}{K}$.
3. Schematic representation of the matrix $\underset{\sim}{K}^1$.
4. Coordinate system appropriate for rearrangement scattering. The center-of-mass of each diatomic fragment is the origin of the corresponding vector to the colliding atom in that channel.
5. Schematic representation of the supermatrix occuring in the extension of the iterative method to reactive scattering. Each diagonal block is identical to the corresponding block of the inelastic case. The inelastic $\underset{\sim}{K}^1$ block is replaced by the region inside the heavy dashed diagonal lines and outside the banded region, and is chosen as appropriate for the problem at hand and the available computer resources.

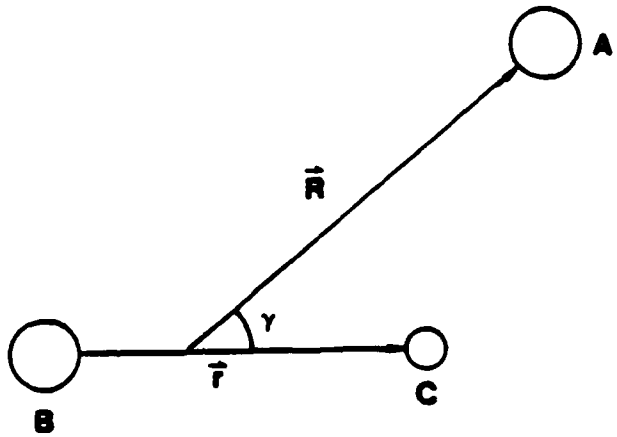

Figure 1

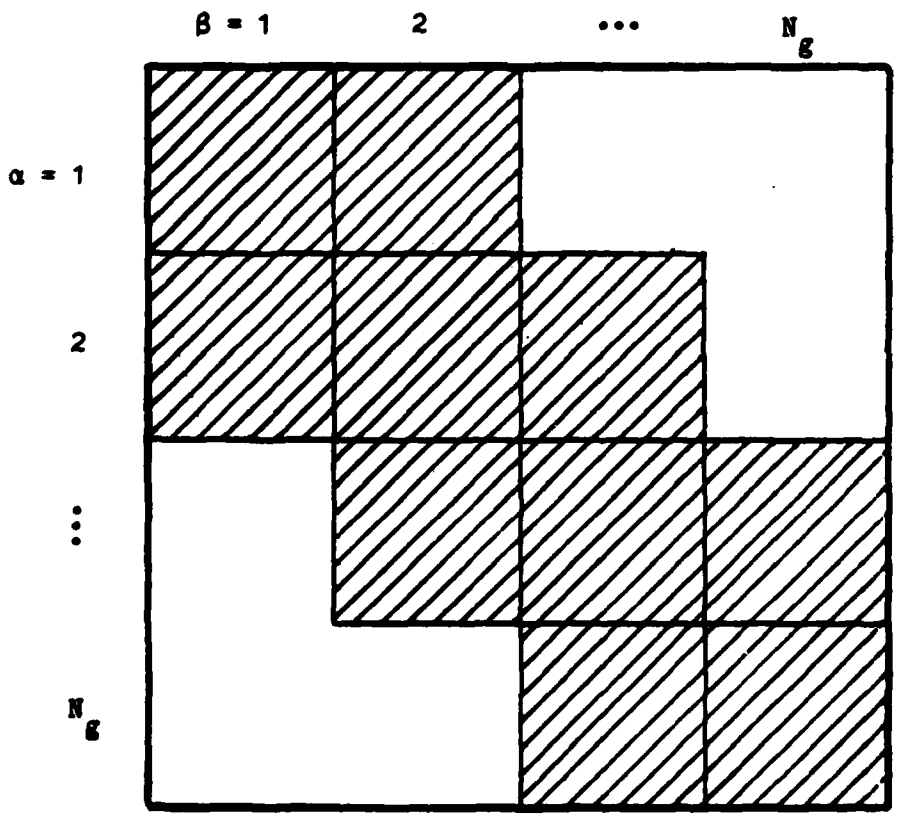

Figure 2

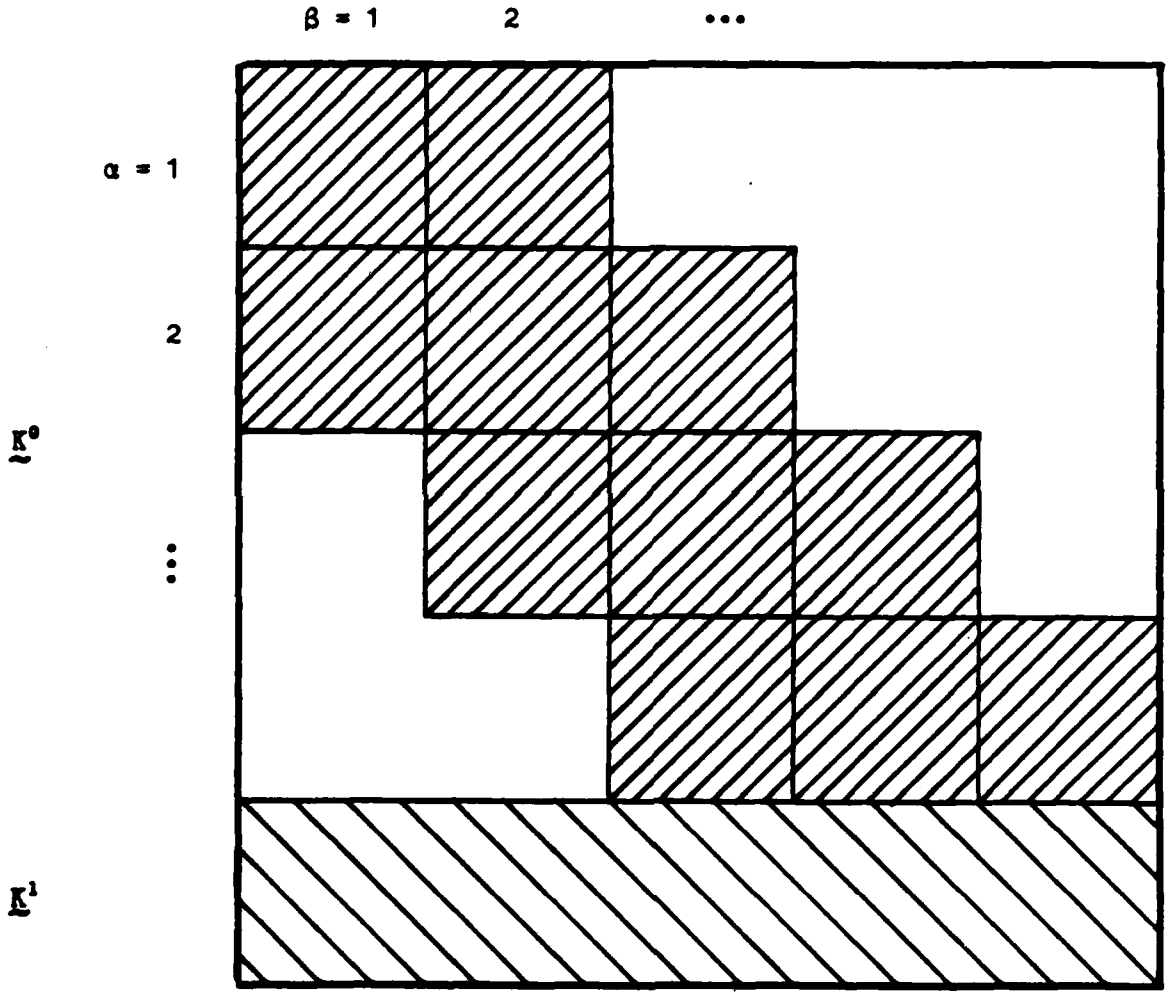

Figure 3

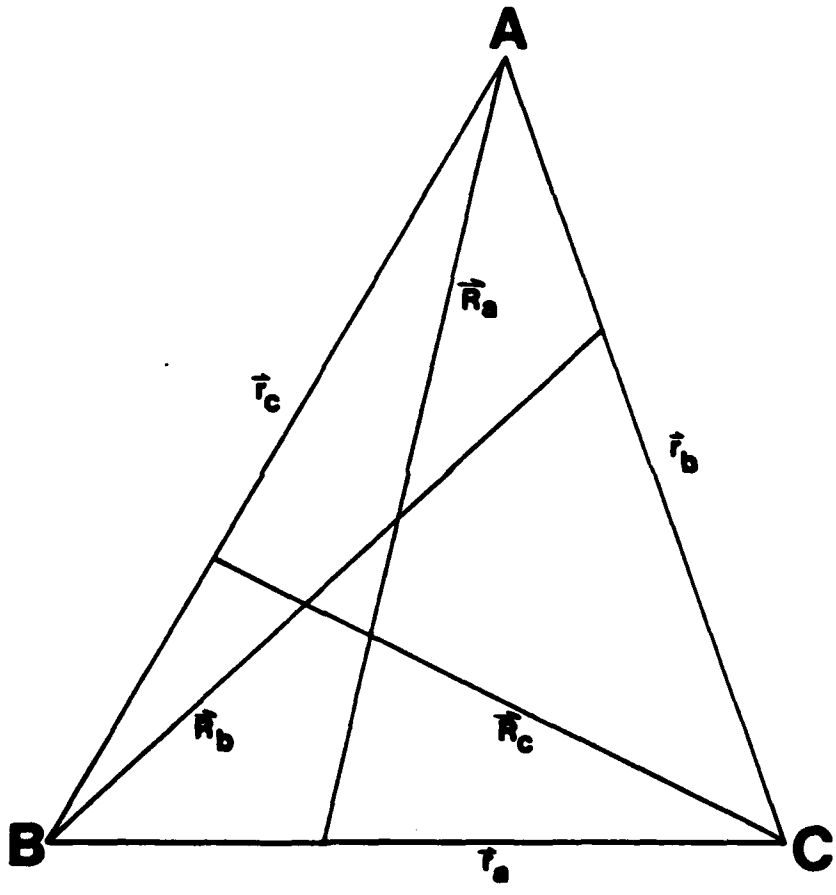

Figure 4

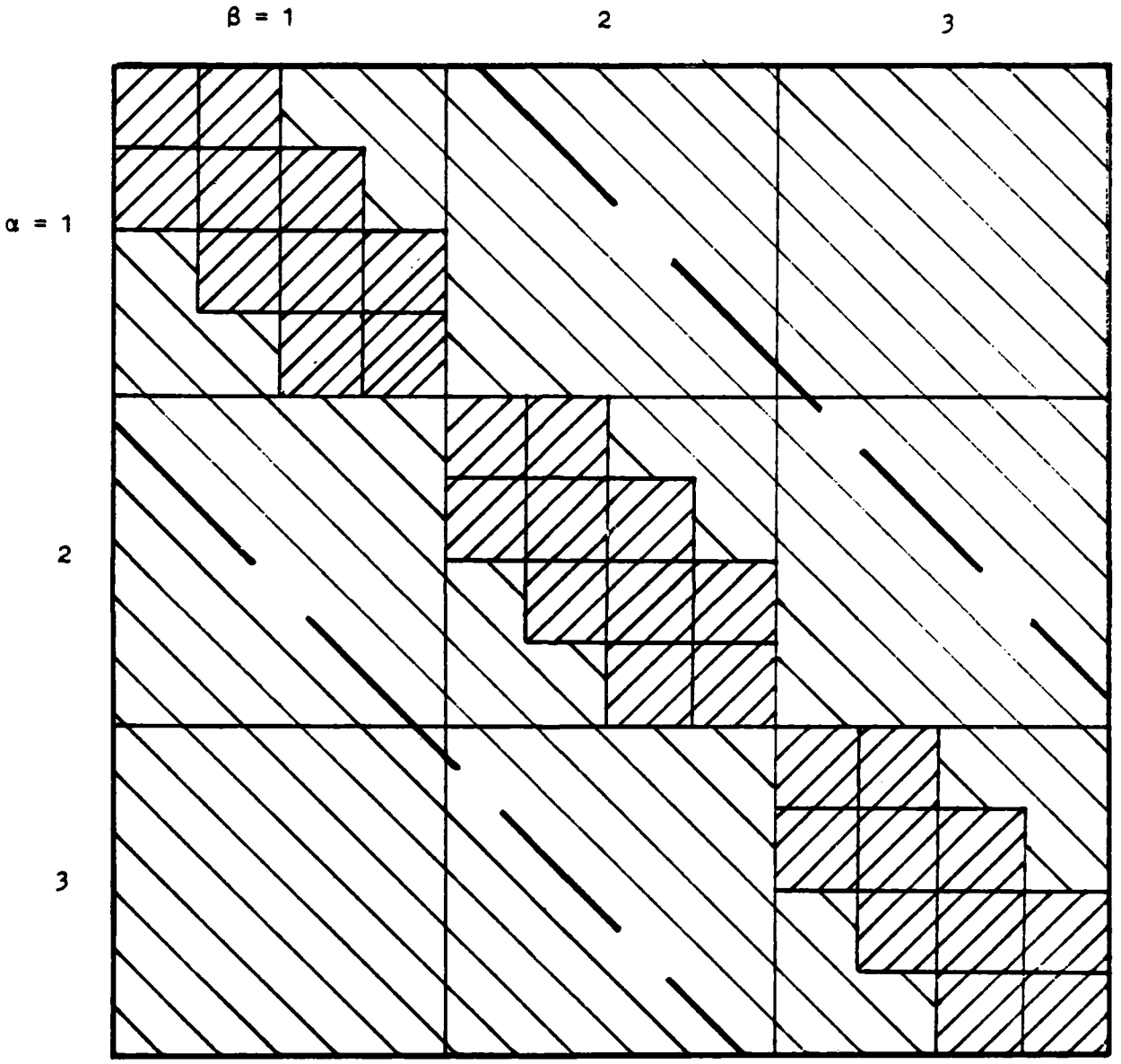

Figure 5

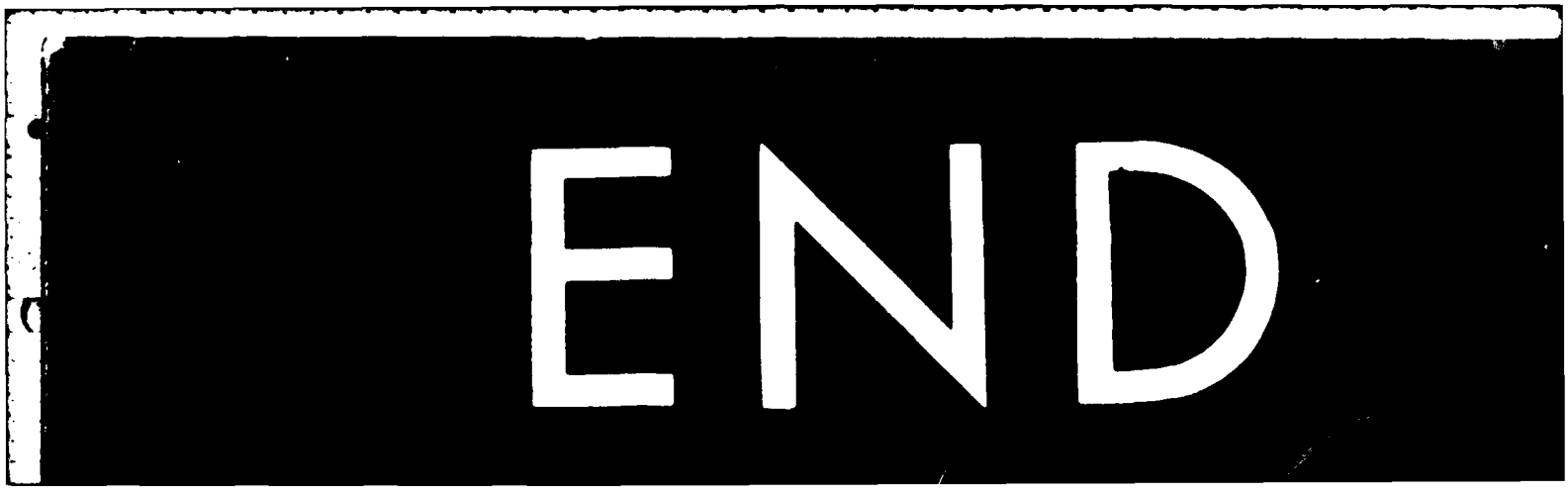
END